REPORT DOCUMENTATION PAGE

Form Approved OMB NO. 0704-0188

1. REPORT DATE (DD-MM-YYYY)	2. REPORT TYPE	3. DATES COVERED (From - To)
28-10-2015	Ph.D. Dissertation	-

4. TITLE AND SUBTITLE
Vibrational Spectroscopy of Laser Cooled CaH+

5a. CONTRACT NUMBER
W911NF-14-1-0378

5b. GRANT NUMBER

5c. PROGRAM ELEMENT NUMBER
611103

6. AUTHORS
Ncamiso Khanyile

5d. PROJECT NUMBER

5e. TASK NUMBER

5f. WORK UNIT NUMBER

7. PERFORMING ORGANIZATION NAMES AND ADDRESSES
University of California - Los Angeles
Office of Contract and Grant Administration
11000 Kinross Avenue, Suite 211
Los Angeles, CA 90095 -1406

8. PERFORMING ORGANIZATION REPORT NUMBER

9. SPONSORING/MONITORING AGENCY NAME(S) AND ADDRESS (ES)
U.S. Army Research Office
P.O. Box 12211
Research Triangle Park, NC 27709-2211

10. SPONSOR/MONITOR'S ACRONYM(S)
ARO

11. SPONSOR/MONITOR'S REPORT NUMBER(S)
65311-PH-MUR.1

12. DISTRIBUTION AVAILIBILITY STATEMENT
Approved for public release; distribution is unlimited.

13. SUPPLEMENTARY NOTES
The views, opinions and/or findings contained in this report are those of the author(s) and should not contrued as an official Department of the Army position, policy or decision, unless so designated by other documentation.

14. ABSTRACT
Cold molecules and molecular ions are leading to a renaissance in the field of molecular spectroscopy just as laser-cooled atoms resulted in a renaissance of atomic physics. Cold molecules enable the performance of spectroscopy with unprecedented precision. Spectroscopy with cold molecules is driven by many of its modern ap- plications such as precision measurements, cold chemistry and quantum information. Molecular ions trapped in RF Paul traps and sympathetically-cooled with laser-cooled atomic ions have been shown to be a great platform to measure spectroscopic transi- tions lines at a precision beyond traditional methods, where high ion density is neces- sary but

15. SUBJECT TERMS
molecular ion spectroscopy, vibrational spectroscopy, CaH+

16. SECURITY CLASSIFICATION OF:			17. LIMITATION OF ABSTRACT	15. NUMBER OF PAGES	19a. NAME OF RESPONSIBLE PERSON
a. REPORT	b. ABSTRACT	c. THIS PAGE			Eric Hudson
UU	UU	UU	UU		19b. TELEPHONE NUMBER 310-825-5224

Report Title

Vibrational Spectroscopy of Laser Cooled CaH+

ABSTRACT

Cold molecules and molecular ions are leading to a renaissance in the field of molecular spectroscopy just as laser-cooled atoms resulted in a renaissance of atomic physics. Cold molecules enable the performance of spectroscopy with unprecedented precision. Spectroscopy with cold molecules is driven by many of its modern ap- plications such as precision measurements, cold chemistry and quantum information. Molecular ions trapped in RF Paul traps and sympathetically-cooled with laser-cooled atomic ions have been shown to be a great platform to measure spectroscopic transi- tions lines at a precision beyond traditional methods, where high ion density is neces- sary but difficult to achieve with the classical preparations. In this thesis, we perform vibrational spectroscopy on the ?? = 10??=0 and ?? = 9 ? ? = 0 overtone of a trapped and sympathetically-cooled 40CaH+ molecular ion using a resonance- enhanced two-photon dissociation scheme. Our experiments are motivated by theo- retical work that proposes comparing the vibrational overtones of 40CaH+ with elec- tronic transitions in atoms to detect possible time variation of in the mass ratio of the proton-to-electron. Due to a lack of experimental data, we start the search using a broadband femtosecond Ti:Sapph laser and the guidance of theoretical calculations. Our initial spectroscopy opens the path for more precise measurements to detect the variation of proton-to-electron mass ratio and to search for astrophysical presence of 40CaH+. Our method fits a wide range of molecular ions that can be co-trapped and efficiently cooled by atomic ions and is the first step to higher precision mea- surements. This enabled us to measure high-order vibrational overtones of a molecule using only less than 300 molecules for the entire spectrum. High precision measurements on 40CaH+ are enhanced by cooling down the motional temperature ion down to the motional ground state. Future high precision measurements will be conducted on narrow transitions using techniques that transforms the internal state changes into changes in temperature of the ions of 40CaH+.

VIBRATIONAL SPECTROSCOPY OF SYMPATHETICALLY LASER-COOLED CaH^+

A Thesis
Presented to
The Academic Faculty

by

Ncamiso B. Khanyile

In Partial Fulfillment
of the Requirements for the Degree
Doctor of Philosophy in the
School of Chemistry and Biochemistry

Georgia Institute of Technology
August 2015

VIBRATIONAL SPECTROSCOPY OF SYMPATHETICALLY LASER-COOLED CaH^+

Approved by:

Professor David S. Sherrill,
Committee Chair
School of Chemistry and Biochemistry
Georgia Institute of Technology

Professor Paul L. Houston
School of Chemistry and Biochemistry
Georgia Institute of Technology

Professor Kenneth R. Brown, Advisor
School of Chemistry and Biochemistry
Georgia Institute of Technology

Professor Michael S. Chapman
School of Physics
Georgia Institute of Technology

Professor Thomas M. Orlando
School of Chemistry and Biochemistry
Georgia Institute of Technology

Date Approved: 28 April 2015

To my late parents

Hezekiel H. K. Khanyile and Chatherine K. Dlamini

PREFACE

Everything that is living can be understood in terms of the jiggling and wiggling of atoms– R. Feynman

ACKNOWLEDGEMENTS

First and foremost, I would like to thank Dr. Kenneth Brown who allowed me into his research group and showed great patience and understanding over the course of my graduate career. Not only did Dr. Brown produce a conducive work environment, he also engineered a great social culture in the group, which made coming to work more pleasant.

I would also like to thank my committee members, Dr. David Sherrill, Dr. Thomas Orlando, Dr. Paul Houston and Dr. Michael Chapman who accepted to join the committee at a short notice. I gained much valuable insight from your discussions.

I would like to thank my lab members for making graduate life more enjoyable and scientific exploration much more undemanding. These include former members, Ricardo Viteri, Craig Clark, James Goeders, Grahame Vitorini, True Merrill, and Yu Tomita. Current members, Gang Shu, Chingiz Kabtayev, Mauricio Guietterez, Rene Rugango, Colin Trout, and Smitha Janadran. Also the many undergraduates that worked with us over the years. I would also like to express my gratitude to the GTRI-QIS group for their continued immeasurable support of the Brown group.

I would like to thank my family away from home in Atlanta that ensured I was well looked after. These include Sthokozile Katongera and Gogo Katongera, Muzi Ginindza, Njabulo Dlamini, Thembi Mdluli, Ngoni Hwata, and many countless friends that had a positive impact in my life. Skeem sami; Thokozani, Sihle, Nhlonipho, Wandile, Sandile, Phila, Samkeliso, Sebentile, Lungile, and many more.

I would also like to thank my family in Swaziland. Without them, I am nothing. Special thanks to my brothers, Sabelo and Alfred, my cousins, Gcinile and Ncamisile

who held the fort down at home. My siblings, Gugu, Linda, Alayna, Fatima, Nonceba, Melusi, Maphevu. My cousins, Sindi, Leo, Bongani, Wandie, Sipho, Madoda, Dingane, Bafana, Msizi, Lomakhosi, and Samkeliso. My nieces Philile and Wiyo. Humble gratitude and reverence is reserved for my aunts, Anti Lozitha, Make Matobhi, Anti Phopho, Anti Ntsontso, and Malume Mkhulu for filling in the vacant space left by parents. Mkhulu and Gogo Nkhosi. To those that passed away, I know that you were with me all the way. *Angihambi Ngedvwa!!* Khanyile, Langa, Mangwane, Macubaltfuli, Zulu!!!

Finally, I would like to thank the woman whose unwavering support over the years has been a constant source of strength over the years. Nokulunga Mavuso whose unconditional love, trust, patience, understanding, and faith cannot be found anywhere else. Words cannot capture the impact you have had in my life *make wa Luhlelo*. I love you and may God continue to bless us and keep us together.

TABLE OF CONTENTS

LIST OF TABLES

LIST OF FIGURES

SUMMARY

Cold molecules and molecular ions are leading to a renaissance in the field of molecular spectroscopy just as laser-cooled atoms resulted in a renaissance of atomic physics. Cold molecules enable the performance of spectroscopy with unprecedented precision. Spectroscopy with cold molecules is driven by many of its modern applications such as precision measurements, cold chemistry and quantum information. Molecular ions trapped in RF Paul traps and sympathetically-cooled with laser-cooled atomic ions have been shown to be a great platform to measure spectroscopic transitions lines at a precision beyond traditional methods, where high ion density is necessary but difficult to achieve with the classical preparations. In this thesis, we perform vibrational spectroscopy on the $\nu' = 10 \leftarrow \nu = 0$ and $\nu' = 9 \leftarrow \nu = 0$ overtone of a trapped and sympathetically-cooled $^{40}CaH^+$ molecular ion using a resonance-enhanced two-photon dissociation scheme. Our experiments are motivated by theoretical work that proposes comparing the vibrational overtones of $^{40}CaH^+$ with electronic transitions in atoms to detect possible time variation of in the mass ratio of the proton-to-electron. Due to a lack of experimental data, we start the search using a broadband femtosecond Ti:Sapph laser and the guidance of theoretical calculations. Our initial spectroscopy opens the path for more precise measurements to detect the variation of proton-to-electron mass ratio and to search for astrophysical presence of $^{40}CaH^+$. Our method fits a wide range of molecular ions that can be co-trapped and efficiently cooled by atomic ions and is the first step to higher precision measurements. This enabled us to measure high-order vibrational overtones of a molecule using only less than 300 molecules for the entire spectrum. High precision measurements on $^{40}CaH^+$ are enhanced by cooling down the motional temperature ion down

to the motional ground state. Future high precision measurements will be conducted on narrow transitions using techniques that transforms the internal state changes into changes in temperature of the ions of $^{40}CaH^{+}$.

CHAPTER I

INTRODUCTION

In the field of molecular spectroscopy, diatomic spectroscopy has yielded great dividends in our understanding of chemistry and physics. Because of the simple structure of diatomics, experimental manipulation and control is relatively easy compared to complex molecules. The study of diatomic spectra was encapsulated by Herzberg's seminal book, *Spectroscopy of Diatomic Molecules* in 1950, which summarized methods of electronic spectroscopy measurements of diatomics at the time [1]. The impact of the book has been far reaching, and it is considered a classic.

Diatomic molecules are attractive because relatively accurate solutions of the Schrödinger equation can be obtained without requiring expensive computational time. Diatomic spectroscopy is used as the basis for the determination of molecular structure and reaction dynamics. The simple nature of diatomic molecules allows for high precision *ab inititio* calculations because there are few electrons to worry about versus complex molecules. Improvements on experimental determination of molecular constants serves as a benchmark on which molecular theory can be refined.

Not only is the study of molecular spectra important in determining molecular structure, but it became apparent that diatomic molecules play an important role in the chemical and physical processes occurring in the interstellar medium. Diatomic molecules serve as the building blocks for larger molecules in the ISM. An example is the formation of the H_3^+ molecule, which is believed to be formed by reactive collisions between H_2^+ and H [2]. Recently, it has been suggested that some of the fundamental constants of nature such as the fine structure constant, α, and the proton-to-electron mass ratio, μ, may not be constant over cosmological time scales [3]. High precision

measurements on molecular spectra, can test the temporal variation of fundamental constants of nature. Diatomic molecules are posed as ideal candidates for the study of fundamental physics.

1.1 Diatomics in interstellar and precision measurements

Extraterrestrial spectroscopy traces its origins to German optician and physicist, Joseph von Fraunhofer, who constructed high quality lenses to make telescopes, which he used to observe dark lines of the solar spectrum in 1718 [4]. He invented a heliometer and a diffraction grating and studied lines previously noticed by W.H. Wollaston [5]. Years later, in 1769, G. R. Kirchhoff and R. W. Bunsen demonstrated that the comparison of laboratory spectra with emission spectra from stars was a useful tool for studying the cosmos [6]. This signified the power of spectroscopy as an instrument to study chemical and physical properties of interstellar processes and fundamental physics. The technique of matching laboratory spectra with absorption spectra from interstellar medium (ISM) is still being used today to characterize many lines from the ISM [7, 8]. While significant progress has been made to identify many emission lines, quite a number still remain uncharacterized, often referred to as "interstellar weeds". This presents great opportunities to study molecular spectra with applications to astrochemistry and astrophysics.

Research in interstellar chemistry started when the first molecules were detected in space in the 1930s [9]. The first one was the CH radical and sometime later the CH^+ ion and CN molecule [10, 11]. These had an electronic spectra in the region of the atmosphere that was transparent to the earth. The spectra from diffuse clouds is dominated by atomic species and diatomic molecules. Later discoveries of complex molecules indicated that diatomic molecules played an important role in the formation of those molecules. Since atomic hydrogen is the most abundant atom in space ($\approx$ 70%), it is no surprise that many molecules in the ISM are hydrides.

Hydride molecular ions are of great interest because many of their neutral counterparts have been discovered in regions that favor the formation of ions. Several hydride molecular ions have been detected in the solar photospheric spectrum including MgH^+, OH^+, SiH^+ and AlH^+ [12, 13]. These molecules are also present in comets, cool stellar atmospheres, and interstellar media. Due to the large ionization potential of these atoms, it is believed that these hydrides will be formed deep inside the solar atmosphere. These molecules become the basis of weak unresolved lines with enhanced opacities. Studies of collisional processes involving highly excited states of atomic ions such as Ca^+ and Mg^+ with H_2 in stellar atmospheres leads to the broadening of the spectra of these atomic ions in the resonance doublet solar spectrum. [14, 15]. The need for more investigations of molecular ions in the ISM was called for by Herzberg in his essay in the book *Molecular Ions: Spectroscopy, Structure, and Chemistry* when he said:

> Although the number of molecular ions observed in the interstellar medium is still small it is generally agreed, on the basis of the work by Herbst and Klemperer, Watson and others, that ions play a major role in the chemical reactions that take place in the interstellar medium. This is so largely because ion-molecule reactions are fast reactions; they have no activation energy.

The above statement highlights the general importance of molecular ions in driving the processes in the ISM while also lamenting on the lack of observed spectra [16].

Neutral CaH has been observed in sunspots where the temperatures are above the ionization potential of $I(\mathrm{Ca})= 6.113$ eV [17]. Furthermore, the observation of MgH^+ lines in the solar spectrum while Mg has an ionization potential of $I(\mathrm{Mg})= 7.646$ eV indicates that $^{40}CaH^+$ should be observed in the solar spectrum [18]. Ca^+ has been observed in the atmosphere where it is believed to be deposited by meteor ablation [19]. However, despite several calls for the spectra for $^{40}CaH^+$, there had not

been any experimental spectra of $^{40}CaH^+$. Few theoretical studies of $^{40}CaH^+$ exist, which form the basis of this experiment [17, 20–25].

1.2 Diatomics and fundamental physics

Temporal variations of fundamental constants such as α, the fine structure constant, and μ, the proton-to-electron mass ratio, are important in testing current physical theories and development of new theories such as supersymmetry. The local position invariance principle of the Einstein equivalence principle states that there should be no variance of fundamental constants of nature in time or position [26, 27]. However, proposed theories allow for the variation in space and time of fundamental constants [28]. These models deriving from string theory include space-time with extra dimensions where the geometry can vary as well as the the amplitude of light scalar fields that can couple to ordinary matter. These variations change the apparent values of constants [29]. These models are important in the bid to explain the dark energy in the universe. Testing these theories requires precision measurements of atomic and molecular spectra. Diatomic molecules have been proposed as ideal candidates to study the possible time variation of the proton-to-electron mass ratio, μ. Prior to high precision spectroscopy, the time variation of fundamental constants was determined by comparing red-shifted spectra from quasars and current laboratory spectra [30]. However, such measurements only have an accuracy of 10^{-6}, which is significantly lower than the needed accuracy for the detection of year-to-year variation.

Significant progress has been made in atomic spectroscopy to place an upper bound on the variation of α. Rosenband *et al.* compared the ratio of Al^+ to Hg^+ electronic transitions to an accuracy of 5.2×10^{-17}, and the change in α to be $(1.6\pm2.3)\times10^{-17}$ per year [31]. The time variation in μ cannot be easily detected in atomic ions because μ weakly depends on isotopic effects in atomic ions. On the other hand, the time

variation in μ scales with the transitions in molecules as $E_{el} : E_{vib} : E_{rot} \approx 1 : \mu^{-1/2} : \mu^{-1}$. Comparing the rovibrational spectra of molecules can offer great insight on the time variation of μ. There have been many proposals and experiments to determine the upper bound of μ [28, 29, 32, 33]. So far none of these experiments have been able to achieve the required precision of greater than 10^{-15} needed to detect the variation on a year-to-year basis. A recent experiment has been able to measure the mass of the electron by comparing the cyclotron frequency of a heavy-ion system to the frequency of the precision of the electron spin [34]. However, comparing the rovibrational spectra of molecules remains the best method to detect yearly variations in μ. For example, $^{40}CaH^+$ has been proposed to measure the temporal variation in fundamental constants [33].

1.3 Cold molecular ions

Despite the fact that many other molecular ions have been identified in the interstellar medium, research in molecular spectroscopy has largely favored neutral molecules over molecular ions. This is because traditional spectroscopy techniques require large molecular densities, $\approx 10^8$ molecules/cm^3 to obtain a good signal-to-noise ratio. This becomes difficult with ions because Coulombic repulsion between the ions limits ion density [35]. Furthermore, detection schemes used in neutral molecule studies requires the production of an ion, which can be detected as a result of probing a transition, are not very useful for molecular ions. Consequently, there are many unassigned lines in the interstellar spectrum [36]. Diatomic molecular ions could provide some solutions to the observed but unaccounted interstellar lines. To get around these limitations, ion trapping and Doppler cooling can perform high precision measurements on molecular ions, because it removes line broadening processes such as pressure and Doppler broadening.

Cold molecular ions have an advantage over neutral molecules because they can be

stored with a combination of RF and DC fields. This allows for longer interrogation times, Doppler free, and collision free measurements. In addition, by trapping ions as a linear crystal chain at the center of the RF null, the Stark shift can be reduced so that measurements can be done with an accuracy greater than 10^{-15} [29].

The combination of radio frequency traps and laser cooling seeks to overcome the challenges of measuring the spectra of molecular ions. In ion traps, the ions are confined in a specified region for a long time where lasers can address them repeatedly. Thus, the lack of density is no longer a problem since the position of the ion is exactly known, therefore, the density becomes effectively infinite [37]. In addition, removing the translational energy of the ion, i.e. laser cooling, removes the excess energy, which allows for weak transitions to be probed with a high signal-to-noise ratio. Because the ions are trapped in isolated environments with pressures lower than 10^{-9} torr, the collision and pressure broadening effects are avoided. The $^{40}CaH^{+}$ molecular ion could help characterize some of these interstellar weeds. While most diatomic molecular ions cannot be directly laser-cooled, they can be cooled through their Coulombic interaction with laser-cooled atomic ions in a trap, a process called sympathetic cooling [38].

1.4 Sympathetically-cooled molecular ions

The advent of laser cooling produced many possibilities for scientific research. However, not many ions can be directly laser-cooled because laser cooling requires closed optical cycles that can be pumped repeatedly without decay to other metastable states[1]. Other ions have, very deep UV regions for optical cycling, which becomes experimentally unfeasible. Many molecules have a similar fate; due to vibrational and rotational structure of molecules, direct laser cooling is not possible for most molecules.

[1] A recent paper [39] suggests that cooling can be achieved without spontaneous emission by restricting the atom-light interaction to a time short compared to the cycle of absorption followed by natural decay. The applicability of this method in trapped ions has not yet been demonstrated.

In order to directly cool molecules, the internal structure of the molecule needs strong Franck-Condon overlap to minimize decays to other rovibrational levels. This means that a molecule can be laser-cooled with few lasers. Neutral molecules such as SrF, YO, and CaF, have diagonal Franck-Condon overlap, which allows them to be laser-cooled [40–43]. For molecular ions, only a few candidates have similar Franck-Condon overlap to SrF that have been identified, AlH^+, BH^+ and SrO^+ [44, 45].

For most molecules, sympathetic cooling with a laser-cooled atomic ion remains the solution for reducing the motional energy and performing precision spectroscopy [46]. Sympathetic cooling involves multiple Coulomb interacting ions stored in trap where one ion species is laser-cooled and the other is not laser-cooled. The laser-cooled ions bring all the ions in the trap to thermal equilibrium with the temperature of the laser-cooled ion through their mutual Coulombic interaction [47–49]. The laser-cooled and the sympathetically-cooled ion pair form ordered structures known as Coulomb crystals [50]. Sympathetic cooling does not disturb the internal structure of the molecular ion because the long-range Coulomb interaction energy between the trapped ions is far less than rovibrational energy spacing. Thus, the internal energy of trapped molecular ions is equilibrated to background black body radiation (BBR), which is at room temperature. Because there is no need for direct laser-cooling, sympathetic cooling increases the catalog of ions that can be cooled and trapped. Generally, sympathetically-cooled ions and laser-cooled ions do not have similar transitions such that precision measurements on the sympathetically-cooled ions do not disturb the laser cooling of the atomic ions [51, 52].

Many studies have been conducted with sympathetically-cooled molecular ions including isotope effects in the reaction between Mg^+ and HD [53], charge exchange reactions [54], velocity selected collisions [55, 56], sympathetically-cooled biomolecules [57–60], rovibrational spectroscopy [61–65], and internal cooling of molecules [66–73]. Sympathetically-cooled ions are also applicable to quantum information because

sympathetically-cooled ions are rarely perturbed by the Doppler cooling process of the laser-cooled ions [74–77]. For the vibrational spectroscopy of $^{40}CaH^+$, we use sympathetically-cooled $^{40}CaH^+$ ions with laser-cooled $^{40}Ca^+$ in a Paul trap.

Despite the difficulty in experimenting with molecular ions, several techniques have been employed over the years to measure molecular ion spectra. Some traditional spectroscopy techniques such as crossed beams were implemented but with limited success [16]. Ion fragmentation or photodissociation has received wide spread applicability in molecular ion spectroscopy because of the ease to which the technique can be performed [78]. In ion fragmentation spectroscopy, one or more lasers, tuned to a state of interest, irradiates the ion. If the photons are in resonance with the transition of interest, the molecule will absorb the photons and be excited beyond its dissociation threshold. The fragments can be collected and analyzed for angular distribution, velocity, and types of fragments, to probe dynamics. Alternatively, the number of fragments or speed of fragmentation can be probed as a function of the laser frequency, probing the rovibrational spectra [79]. Several pioneering studies have been conducted using this technique. These include infrared multiphoton dissociation (IRMPD) of polyatomic ions [80, 81], resonant ion-dip infrared spectroscopy (RIDIRS) of water complexes [82, 83], vibrationally and rotationally resolved electronic spectra of metal-ion complexes, vanadium oxide-carbonyl cations [19, 84], and IR dip-ultraviolet photodissociation of protonated tyrosine and phenylalanine [85]. In this thesis, we use ion-fragmentation spectroscopy of single trapped molecular ions to study the vibrational overtones of $^{40}CaH^+$.

1.5 Thesis organization

This thesis will be focused on the vibrational spectroscopy of $^{40}CaH^+$ sympathetically laser-cooled with $^{40}Ca^+$ ions. This is the first such measurement of bound transitions of $^{40}CaH^+$. The rest of the thesis is organized as follows: Chapter 2 discusses the

theory of trapping and laser cooling ion in RF traps. Chapter 3 discusses the molecular orbital theory of $^{40}CaH^+$ found in the literature including the reaction mechanism by which the molecular ion is formed. Chapter 4 shows the kind of instruments used to study the ion. Chapter 5 demonstrates the use of resonance enhanced multiphoton dissociation technique to record for the first time vibrational overtones of $^{40}CaH^+$. Chapter 6 shows a proposal of an experiment where the spectra of $^{40}CaH^+$ is measured by looking at the heating of the sidebands of a ground stated cooled molecular ion. In the same chapter we chronicle the first step towards precision measurements of by cooling the $^{40}CaH^+$ ion motion inside the trap to the ground state and gives indications of future research directions in the Brown lab.

CHAPTER II

THEORY ION TRAPPING AND LASER COOLING

Key to the experiments described in this thesis is the trapping and cooling of charged particles. This is facilitated by a Paul RF quadrupole trap that confines the ions in three dimensions using a combination of RF and DC fields. Doppler cooling is used to reduce the translational energy down to millikelvin temperatures. In this chapter the operation principle of a Paul trap and the interactions of the ions with the lasers is discussed. The reader is referred to the following references for more details [86–94]

2.1 Theory of trapping ions

Trapped ion experiments use an RF Paul trap named after Wolfgang Paul [95]. To achieve trapping a quadrupole field is used to confine the charged particles in space

$$\Phi = \frac{\Phi_0}{2r_0^2}(\alpha x^2 + \beta y^2 + \gamma z^2), \tag{1}$$

where r_0 is the radius of the trap and α, β, γ are trapping coefficients. If the potential is static, the point $r_0 = 0$ is unstable because the Laplace condition $\Delta\Phi$=0 imposes the requirement that $\alpha + \beta + \gamma = 0$. This results in confinement in two of the directions, but anti-confinement in the other because $\gamma = -(\beta + \alpha)$. To overcome this, the voltage is made periodic in time. An oscillating voltage results in focusing and defocussing in the x and z directions. The potential is applied with a DC voltage U_0 and RF voltage V_0 at a frequency Ω

$$\Phi_0 = U_0 + V_0 \cos \Omega t. \tag{2}$$

A schematic of the a typical linear Paul trap is shown in Fig. 1.

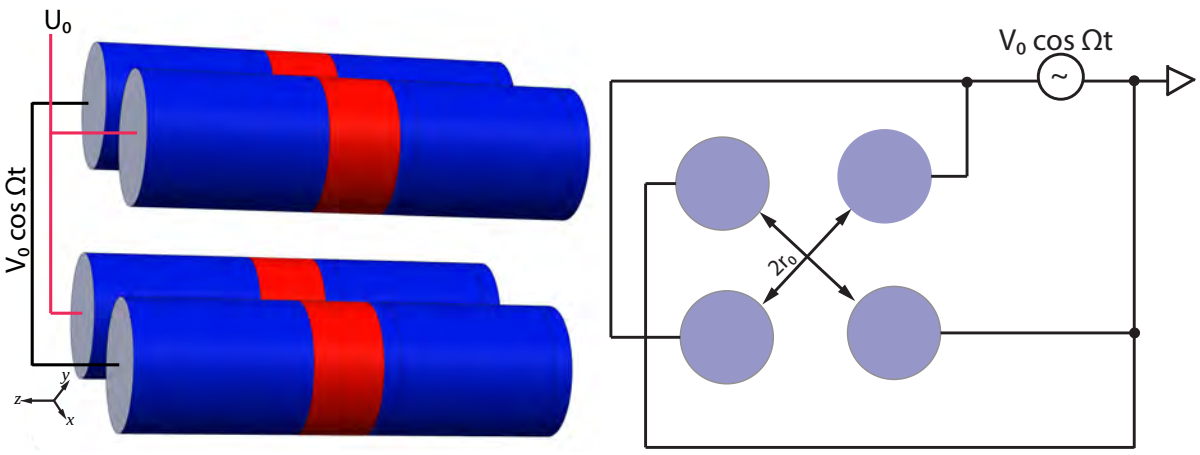

(a) 3D sketch (b) Cross section

Figure 1: A schematic of a linear Paul trap configuration. (a) shows a 3D cartoon of the trap where an RF voltage $V_0 \cos \Omega t$ is applied on two diagonally opposed electrodes while the other two are kept at RF ground. To trap along the z axis, U_0 static voltage is applied along near the end of the segments. The red segments represents RF common segments which can be biased with DC to ensure that the ion sits on the RF null. (b) shows a cross section of trap indicating the radius of the trap.

The applied voltage on the electrodes gives the potential in the trap described by,

$$\Phi = \frac{x^2 - y^2}{2r_0^2} V_0 \cos \Omega t + \frac{\kappa U_0}{r_0^2}(z^2 - \frac{x^2 + y^2}{2}) \tag{3}$$

where κ is the constant geometric factor.

An illustration of the operation of an oscillating field to trap an ion is shown in Fig. 2 which shows the polarity of the field switching and the ion inside the field. As the ion moves in one direction, the field polarity is switched, resulting in repulsion of the ion. When the ion changes direction, the polarity is flipped again causing it to be repulsed again. This makes the ion oscillate back and forth around the center of the trap. The stability of the ion inside the trap requires that ion moves slow relative to the switching.

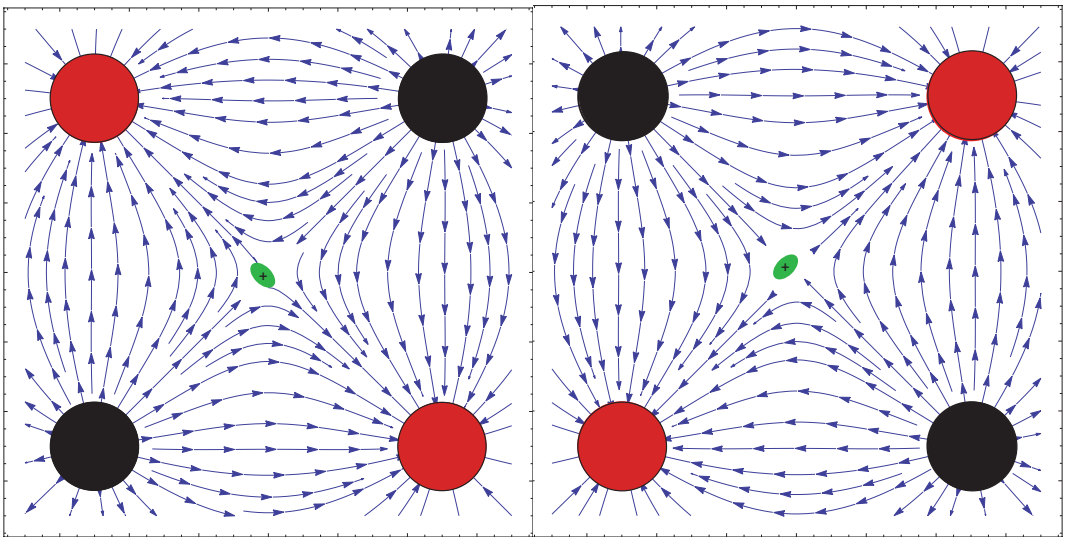

(a) -V (b) V

Figure 2: An illustration of the oscillating field to trap ions showing the two states as the fields oscillates between positive and negative. The polarity of the field is switched continuously to cause the ion to oscillate about the center of the trap. The ion must move slower than the switching in order for trapping to be realized.

2.2 Motion inside a trap

The equations of motion of an ion inside the trap can be a described by a charge in a field governed by,

$$m\ddot{\vec{r}}(x,y,z) = q\vec{E} = -q\vec{\nabla}\Phi. \tag{4}$$

This is done by explicitly expressing each component along the coordinates,

$$\ddot{x} + \frac{e}{m}\Big(-\frac{U_0}{2}\gamma + V_0\alpha\cos\Omega t\Big)x = 0, \tag{5}$$

$$\ddot{z} - \frac{e}{m}(U_0\gamma)z = 0, \tag{6}$$

$$\ddot{y} + \frac{e}{m}\Big(-\frac{U_0}{2}\gamma - V_0\alpha\cos\Omega t\Big)y = 0, \tag{7}$$

where m is the mass of the trapped particle. The ion feels a small averaging force towards the center because the field is inhomogeneous. These equations are the well known Mathieu equations, which in dimensional quantities take the form,

$$\frac{d^2x}{d\tau^2} + (a_x + 2q_x \cos 2\tau)x = 0, \tag{8}$$

$$\frac{d^2z}{d\tau^2} + (a_z - 2q_z \cos 2\tau)z = 0, \tag{9}$$

$$\frac{d^2y}{d\tau^2} + (a_y - 2q_y \cos 2\tau)y = 0, \tag{10}$$

where

$$a_x = a_y = \frac{4\kappa e U_0}{m r_0^2 \Omega^2} = -\frac{a_z}{2}, \tag{11}$$

$$q_x = -q_y = \frac{2eV_0}{m r_0^2 \Omega^2}, \tag{12}$$

$$q_z = 0,\ \tau = \frac{\Omega t}{2}. \tag{13}$$

The equations have stable regions and unstable regions, which are dependent on the values of a and q but not the velocity of the ion. In experiments, the ions are typically confined in a fixed ratio of a/q, depending on the mass of the ion and the applied voltages. It is common to show the stability diagram near $a = 0$ because most traps are designed to operate in this region. The analytical solution of the Mathieu equation can be expressed as,

$$u(\tau) = \alpha' e^{\mu\tau} \sum_{n=-\infty}^{n=\infty} C_{2n} e^{2in\tau} + \alpha'' e^{-\mu\tau} \sum_{n=-\infty}^{n=\infty} C_{2n} e^{-2in\tau}, \tag{14}$$

where $\mu = \alpha \pm i\beta$, α' and α'' are integration constants that depend on the initial conditions, and the coefficients C_{2n} satisfy the recursion relation and depend on the values of a and q. In our experiments, we set the a=0, so that for the $^{40}Ca^{+}$ ion, with mass 40 amu, we trap when $0<q<0.9$ as shown Fig. 3.

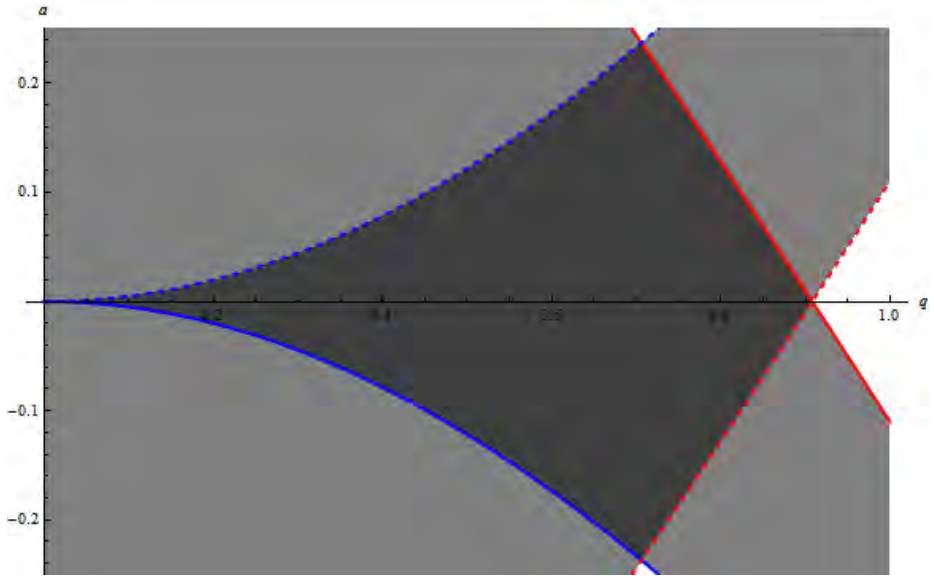

Figure 3: The stability diagram of the quadrupole field showing the lowest stability region. Along the a=0 axis, the ion is stable for $0<q<0.9$. The Mathieu equations have a stable solution inside the darker shaded region. In order to trap ions, U_0 and V_0 parameters are chosen carefully so that they fall inside the stable part of the a-q space.

The stability of the equation is dependent on the value of β. If β is not an integer and μ is purely imaginary, then the solutions of the equation are stable. However, if β is an integer, the solutions are periodic but unstable. To solve the equation, we use the trigonometric relation,

$$e^{i\theta} = \cos\theta + i\sin\theta. \tag{15}$$

If we substitute equation 15 in to equation 14, we obtain

$$u(\tau) = \alpha_1' \sum_{n=-\infty}^{n=\infty} C_{2n}\cos(2n \pm \beta)\tau + \alpha_1'' \sum_{n=-\infty}^{n=\infty} C_{2n}\sin(2n \pm \beta)\tau, \tag{16}$$

where C_{2n} represents the amplitude of the oscillatory motion and $(2n \pm \beta)\tau$ is the

frequency. If we write

$$\omega_n t = (2n \pm \theta)\tau, \tag{17}$$

$$\tau = \Omega t/2, \tag{18}$$

we find the following,

$$\omega_n = \frac{(2n \pm \beta)\Omega}{2}, \tag{19}$$

$$\beta = \sqrt{a + \frac{q}{2}}. \tag{20}$$

The value $n = 0$ describes the fundamental frequency of the ion motion;

$$\omega_0 = \beta\Omega/2, \tag{21}$$

substituting the value of β, we find,

$$\omega_0 = \frac{eV_0}{\sqrt{2}mr_0^2\Omega}, \tag{22}$$

when a=0. The oscillation of the ion inside the trap can be described by the low frequency harmonic oscillation called *secular motion* and the high frequency oscillation called *micromotion*. The potential describing the secular motion is called the pseudopotential to distinguish it from the trapping potential. The depth of this potential, D, is described by,

$$D = \frac{m}{2}\omega r_0^2. \tag{23}$$

For 3D ion traps described above, trap depths between 5 eV to 20 eV are easily achieved.

2.3 Atom interaction with radiation

The interaction of an atomic system with electromagnetic radiation near resonance with an atomic transition can be described by the time dependent Schrödinger equation,

$$i\hbar\frac{\partial\Psi}{\partial t} = H\Psi. \tag{24}$$

The Hamiltonian describing a trapped atom in a harmonic well interacting with a laser can be expressed as,

$$H = H_0 + H_1, \tag{25}$$

where H_0 describes the particle without the laser interaction and the H_1 is the perturbation of the system caused by the atom interaction with the laser. For laser cooling, two levels are typically used and hence will be considered for the treatment of the Doppler cooling process. Suppose the system is described by a simple two-level system with H_0 describing the system with wavefunctions Ψ_0 and Ψ_1 and energies E_0 and E_1 respectively as in Fig. 4. The energy gap is $E_1 - E_0 = h\nu_{10} = \hbar\omega_{10} = -\hbar\omega_{01}$.

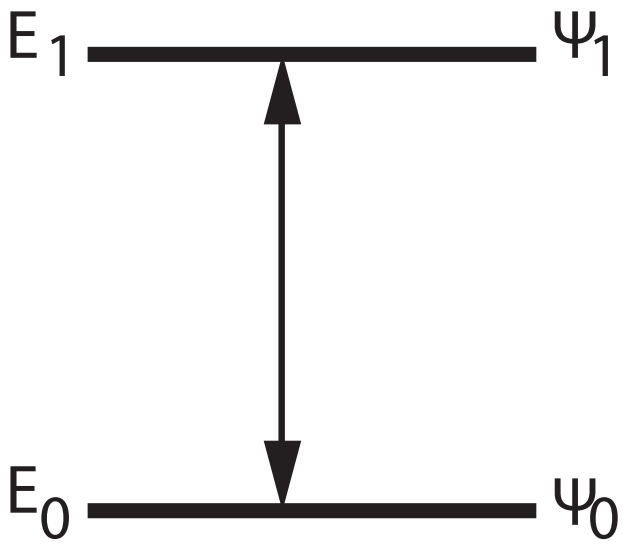

Figure 4: A two level atomic system with the wavefunctions and the energy gap between the levels. E_0 is the energy of the ground state Ψ_0 and E_1 is the energy of the excited state Ψ_1.

The solutions to the unperturbed Hamiltonian take the form,

$$\Psi_0 = \psi_0 e^{-iE_0 t/\hbar} = \psi_0 e^{-i\omega_0 t}, \tag{26}$$

$$\Psi_1 = \psi_1 e^{-iE_1 t/\hbar} = \psi_1 e^{-i\omega_1 t}, \tag{27}$$

where $\omega_i = E_i/\hbar$. The time dependent wavefunction describing the perturbed Hamiltonian becomes a linear combination of the unperturbed wavefunctions as,

$$\Psi(t) = C_0(t)\psi_0 e^{-i\omega_0 t} + C_1(t)\psi_1 e^{-i\omega_1 t}, \tag{28}$$

where the time dependent coefficients $C_0(t)$ and $C_1(t)$ satisfy the normalization condition $\langle\Psi(t)|\Psi(t)\rangle = |C_1(t)|^2 + |C_2(t)|^2 = 1$. The term $|C_i(t)|^2$ describes the probability that the atom will be in the ith state. To determine the evolution of the system, we solve the Schrödinger equation by substituting equation 28 into equation 24 to find

$$i\hbar\big[\dot{C}_0(t)\psi_0 e^{-i\omega_0 t} + \dot{C}_1(t)\psi_1 e^{-i\omega_1 t}\big] = H_1 C_0(t)\psi_0 e^{-i\omega_0 t} + H_1 C_1(t)\psi_1 e^{-iE_1 t/\hbar} \tag{29}$$

where $\dot{C}_i = C_t/\delta t$ is the time derivative of the coefficient. To solve the Schrödinger equation, we multiply by $\psi_0^* e^{i\omega_0 t}$ or $\psi_1^* e^{i\omega_1 t}$ and integrate over all space to obtain,

$$i\hbar\dot{C}_0 = C_0(t)\langle\psi_0|H_1|\psi_0\rangle + C_1\langle\psi_0|H_1|\psi_1\rangle e^{-i\omega_{10}t}, \tag{30}$$

$$i\hbar\dot{C}_1 = C_1(t)\langle\psi_1|H_1|\psi_1\rangle + C_0\langle\psi_1|H_1|\psi_0\rangle e^{i\omega_{10}t}. \tag{31}$$

Since the term H_1 describes the dipole transition μ in the presence of an electric field $\epsilon_0\cos(\omega t)$, making it $-\mu\epsilon_0\cos(\omega t)$, the function is odd, where ϵ_0 is the amplitude of the electric field. However, the products of $|\psi_i|^2$ are even functions. Because atomic states have parity with the respect of the space-fixed coordinates, $\langle\psi_i|H_1|\psi_i\rangle = 0$. Thus the equations 30 and 31 become,

$$i\hbar\dot{C}_0 = -C_1(t)M_{01}\epsilon_0 e^{-i\omega_{10}t}\cos(\omega t), \tag{32}$$

$$i\hbar\dot{C}_1 = -C_0(t)M_{01}\epsilon_0 e^{i\omega_{01}t}\cos(\omega t). \tag{33}$$

The function M_{01} is the transition dipole moment given by $\langle\psi_1|\mu|\psi_0\rangle$. If we define a parameter we call the Rabi frequency as,

$$\Omega_0 = \frac{M_{10}E}{\hbar}, \tag{34}$$

and then we use the trigonometry identity that $\cos(\omega t) = \frac{e^{i\omega t}+e^{-i\omega t}}{\hbar}$, we can rewrite the equations 32 and 33 as,

$$\dot{C}_0 = \frac{iC_1\Omega_0(e^{-i(\omega_{10}-\omega)t} + e^{-i(\omega_{10}+\omega)t})}{2}, \tag{35}$$

$$\dot{C}_1 = \frac{iC_0\Omega_0(e^{i(\omega_{10}-\omega)t} + e^{i(\omega_{10}+\omega)t})}{2}. \tag{36}$$

The terms with $e^{i(\omega_{10}-\omega)t}$ and $e^{-i(\omega_{10}-\omega)t}$ represent the slow oscillations of the function in time while the others, $e^{i(\omega_{10}+\omega)t}$ and $e^{-i(\omega_{10}+\omega)t}$, represent fast oscillations in time. Because the fast oscillations average to zero, they can be ignored, a process called the rotating wave approximation (RWA). If we define the detuning as $\Delta = \omega - \omega_{10}$, then the solution to the coefficients is,

$$\dot{C}_0 = \frac{i\Omega_0 e^{i\Delta}C_1(t)}{2}, \tag{37}$$

$$\dot{C}_1 = \frac{i\Omega_0 e^{i\Delta}C_0(t)}{2}. \tag{38}$$

These equations can be solved analytically using the initial conditions and we find that,

$$C_0(t) = \left[\cos\left(\frac{\Omega t}{2}\right) - i\left(\frac{\Delta}{\Omega}\right)\sin\left(\frac{\Omega t}{2}\right)\right]e^{-i\Delta t/2}, \tag{39}$$

$$C_1(t) = i\left(\frac{\Omega_0}{\Omega}\right)\sin\left(\frac{\Omega t}{2}\right)e^{-i\Delta t/2}, \tag{40}$$

where $\Omega = [(\Omega_0)^2 + \Delta^2]^{1/2}$. The probability that the atom will be found in the excited state is given by,

$$|C_1(t)|^2 = \frac{\Omega_0^2}{\Omega^2}\sin^2\left(\frac{\Omega t}{2}\right). \tag{41}$$

The state of the atoms evolves in time depending on the detuning of the laser from the transition. The on-resonant evolution is shown in Fig. 5.

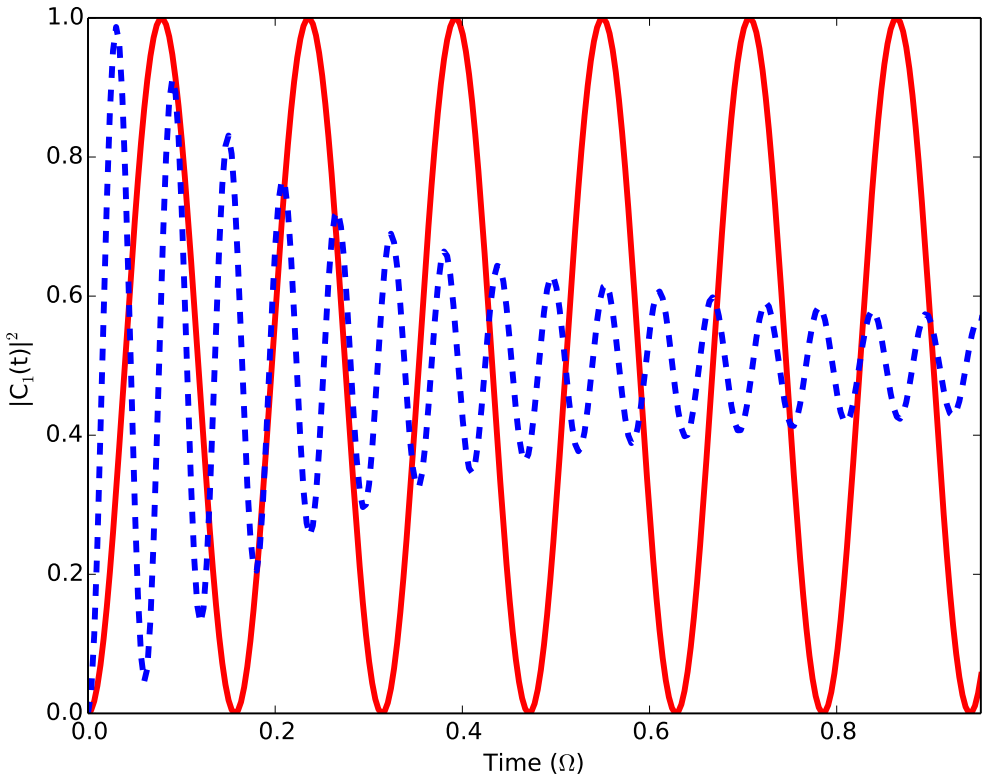

Figure 5: Rabi oscillations. The red solid curve shows the probability of finding the atom in the excited state in a two level system driven by a laser on resonance with the atomic transition if there is no damping of the system. The blue dashed curve shows the decay of coherence between the two states.

2.4 Doppler cooling

The removal of translational temperature of the ion requires optical cycling on an ion transition with a short lifetime, typically <100 ns for practical experimental purposes. This is achieved by using broad, fast decaying transitions that will allow fast cooling times. While laser cooling can be achieved on narrow metastable transitions, these transitions cycle photons slowly to be useful for the first stage of cooling [96, 97]. Laser cooling takes advantage of the Doppler effect. A red-detuned laser traveling in the opposite direction of an ion is absorbed by the ion because the

frequency is Doppler shifted to be on resonance with the atomic transition [98]. The absorbed photon is spontaneously emitted by the ion resulting in a momentum kick, photon recoil. After many photons ($\approx 10^6$) have been scattered, the momentum from the photon recoil is averaged out resulting in a net slowing down of the ion, i.e., translational cooling. This proceeds until the heating from the random momentum kick and the cooling process cancel each other out resulting the Doppler cooling limit.

If the laser is slightly detuned from the atomic transition such that $\omega < \omega_{01}$ with a wave vector $\mathbf{k}$, and it moves with a velocity $\mathbf{v}$ in the direction opposite to the direction of travel of the atom, the Doppler shifted frequency of the photon becomes resonant with the transition through $(\omega - \mathbf{k}.\mathbf{v}) = \omega_{01}$. Since a short lived excited state is chosen for Doppler cooling, the excited state will spontaneously emit photons in a random direction. The radiation field will gain an energy of $\hbar|\mathbf{k}.\mathbf{v}|$ while the atom will lose the same amount in the form of kinetic energy due to the energy conservation. Repeating this cycle many times results in lower kinetic energy and net cooling of the ion due to low kinetic energy.

The velocity capture range Δv of the Doppler cooling process is limited by the natural linewidth, Γ, of the excited state,

$$\mathbf{k}\Delta v \approx \Gamma. \tag{42}$$

Since the radiation emitted by the atom is spontaneous and results in heating and cooling of the atom, the achievable temperature of Doppler cooling is limited by the competition between the cooling and the heating processes [99]. The lowest achievable temperature becomes,

$$T_D = \frac{\hbar\Gamma}{2k_B}, \tag{43}$$

where T_D is the Doppler cooling limit. For Ca^+, the Doppler limit is 0.53 mK.

Key to Doppler cooling is the presence of a fast decaying excited electronic state that will spontaneously decay to the ground state. In addition, it is convenient if

the transitions are accessible with commercially available lasers [96, 100, 101]. To date the atomic ions that have been cooled include Be^+ [102], Mg^+ [103], Ca^+ [104], Ba^+ [105], Sr^+ [106], Yb^+ [107], Hg^+ [108], and Cd^+ [109]. With the exception of Be^+ and Mg^+, the aforementioned atomic ions do not have a simple two-level structure and have other decay channels. These are are plugged with secondary re-pumping lasers to close the cycling transition. Ytterbium possesses several transitions that are suitable for optical-frequency reference standards (clocks) such as the ${}^2S_{1/2} \leftrightarrow {}^2F_{7/2}$ transition at 467 nm.

2.5 Laser cooling of Yb^+

2.5.1 Introduction

The ytterbium ion has several properties that make it an ideal candidate for many applications in physics such as an optical reference standard, quantum computing, and investigations of time variation in fundamental physics [110, 111]. Ytterbium ions have several clock transitions such as the ultra narrow ${}^2S_{1/2} \rightarrow {}^2F_{1/2}$ transition at 467 nm, the ${}^2S_{1/2} \rightarrow {}^2D_{5/2}$, and many others [107, 109, 112–115]. Ytterbium also has an isotope with a nuclear spin $I = 1/2$ (^{171}Yb) with high abundance (14.28%).

2.5.2 Methods

Ytterbium ions are trapped in an UHV chamber with background pressure $\approx 10^{-11}$ torr in a 4.5 inch octagon chamber pumped by a 50 L/sec pump (Daniway pump). The trap is 5-segment with five electrodes and a radius ($r_0 = 0.6mm$). RF voltage (200V) driven at 14.41 MHz is supplied through two diagonalized opposed electrodes while the other two are held to RF ground. DC voltage ($\approx$ 25V) is supplied on the axial side. An optical setup showing the laser-layout is shown in the schematic below in Fig. 6. Four lasers, 369 nm, 399 nm, 935 nm, and 638 nm, are needed to trap ytterbium which will be explained below. About 20 mW of the 399 nm laser is combined with about 1 mW 369 nm laser with a bandpass filter (Semrock 395/20 nm) that reflects the

399 nm laser and transmits the 369 nm laser, which are sent along the trap axis and are focused with a 150 mm achromatic lens to the center of the trap. This reduces the spot size of the laser beams to about 50 μm. Similarly, about 10 mW of the 935 nm laser is combined with about 3 mW of the 638 nm laser via a bandpass filter that reflects the 935 nm laser and transmits the 638 nm laser. The combined lasers are also focused to the center of the trap with a 150 mm achromatic lens to a spot size of about 80 μm.

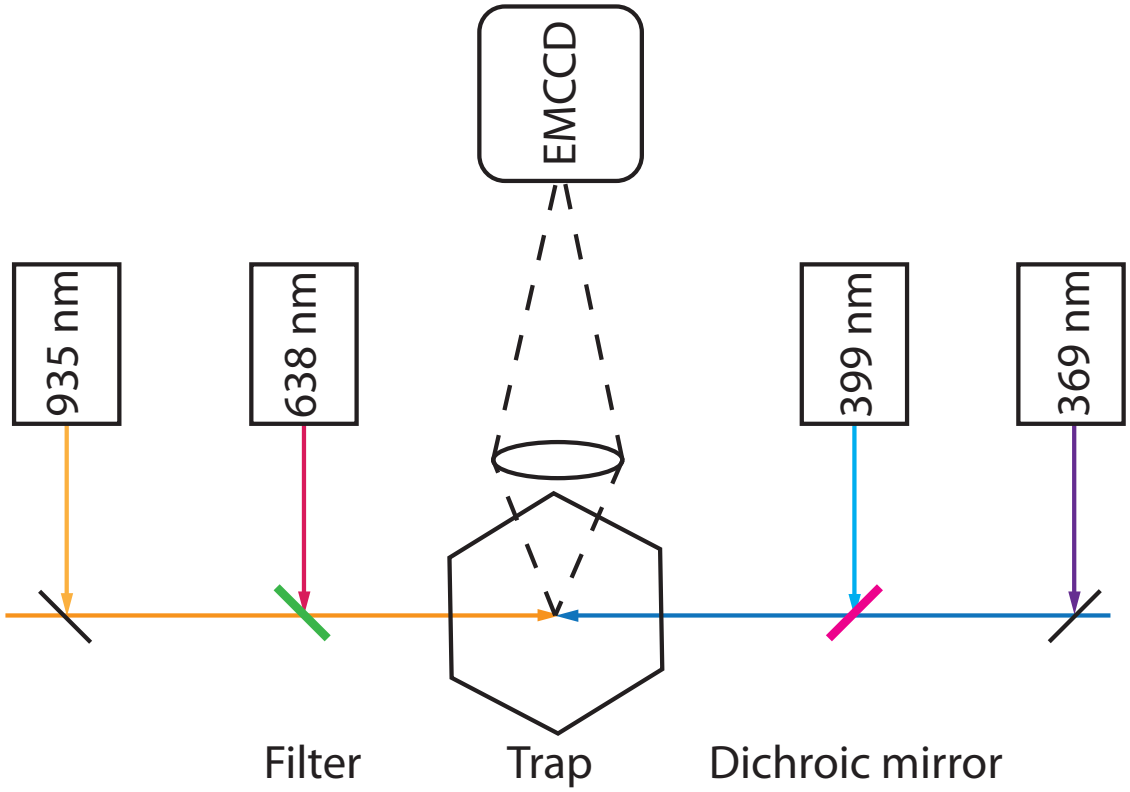

Figure 6: A schematic showing the optical layout of the lasers to trap ytterbium ions. The lasers are coupled into the trap using a combination of filters and dichroic mirrors. The fluorescent light is collected with a setup of optics and focused on the EMCCD camera for imaging as explained in Ref. [116].

Ytterbium ions are produced by two photon ionization of neutral ytterbium. Neutral ytterbium is introduced in the chamber by resistively heating an aluminum oven filled with ytterbium at 1.5 amps. The neutral ytterbium is excited on the ${}^1S_0 \rightarrow {}^1P_1$ transition with a 399 nm laser as shown in Fig. 7a. A fluorescence trace of neutral ytterbium is shown in Fig 7b. A second photon with a wavelength shorter than 394 nm is enough to excite the electron to the continuum. Since a 369 nm laser is required for Doppler cooling, it is also used for the second photon to ionize neutral ytterbium.

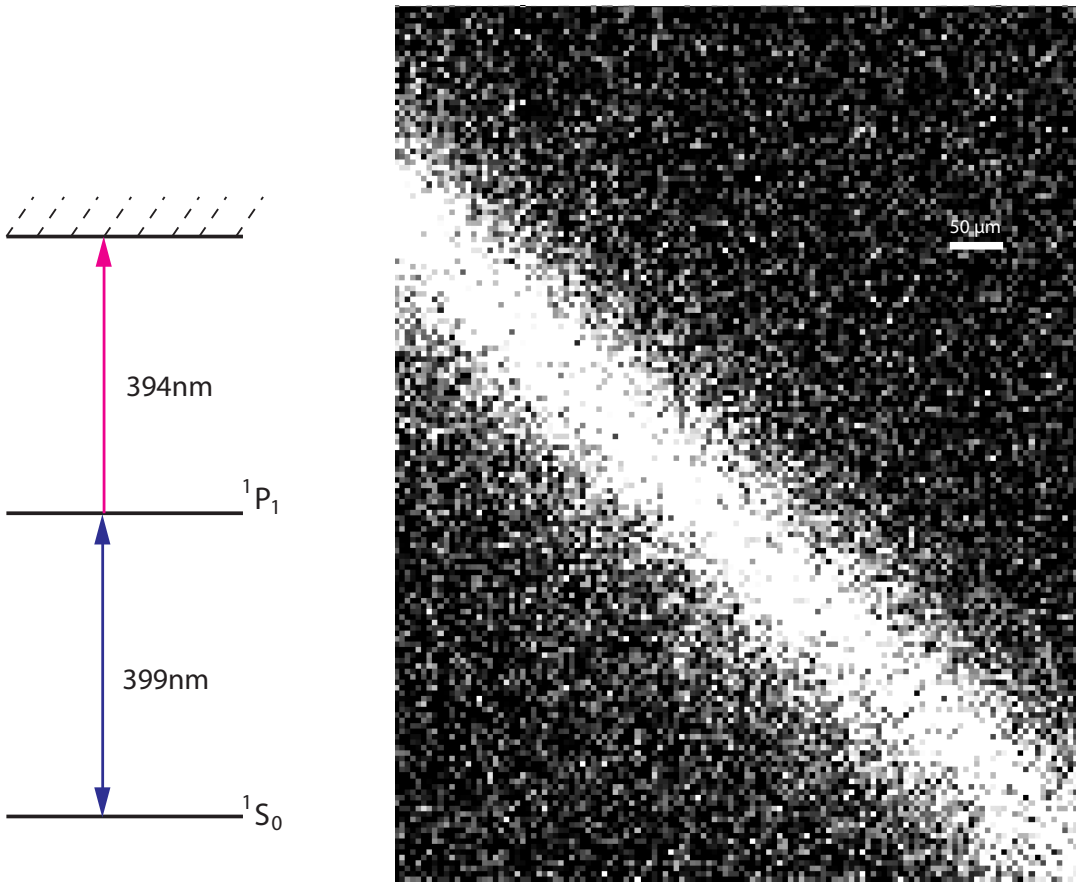

(a) Yb ionization scheme

(b) Yb fluoresce

Figure 7: Ionization of neutral ytterbium. (a) shows the isotopically selective ionization scheme from neutral Yb to the continuum. (b) shows the fluorescence of neutral ytterbium on the ${}^1S_0 \rightarrow {}^1P_1$ transition imaged at 399 nm.

Doppler cooling of Yb^+ relies on the cycling transition at ${}^2S_{1/2} \leftrightarrow {}^2P_{1/2}$ near

369 nm as shown in Fig. 8. Occasionally (≈0.005%), the ion will decay to the $^2D_{3/2}$ meta stable state, which has a lifetime of 52.7 ms [117]. A 935 nm laser is used to pump the ion from the $^2D_{3/2} \rightarrow {}^3[3/2]_{1/2}$, which spontaneously decays back to the $^2S_{1/2} \leftrightarrow {}^2P_{1/2}$ cycling transition. Collisions with background gas causes the ions to fall in to the long lived $^2F_{7/2}$ state which has a lifetime of 5.4 years [118]. Another laser at 638 nm pumps the ion to the $^1[5/2]_{5/2}$ state, which decays to the $^2D_{3/2}$ state and then back to the cycling transition. The odd looking spectroscopic notation of the Yb^+ states are caused by the fact that those states are no longer defined by the normal $L-S$ coupling. One electron from the core f-shell of ytterbium is excited to the s orbital and the spin of the s are coupled with angular momentum L. While the $4f^{13}$ core shell remains $L-S$ coupled with angular momentum, J_c. The sum of the two momenta $K = L + J_c$, gives the resultant coupling which is shown in the square brackets [118].

2.5.3 Results

Trapped ytterbium ions are shown in Fig. 8b. The ions are imaged via an electron multiplied charged couple device(EMCCD) camera(Princeton Instruments PI-532) with a lens system with a numeral aperture (N.A.=0.43) and a magnification of 10× explained in detail in subsection 4.5 [116]. The image shows a Yb^+ crystal of a few hundred ions. In order for the ions to crystallize, the ratio of the potential energy to the kinetic energy must be greater than 173 [119]. That is,

$$\Gamma = \frac{1}{4\pi\epsilon_0}\frac{q^2}{a_w k_B T} > 173, \tag{44}$$

where Γ is the Coulomb coupling parameter, ϵ_0 is the permittivity of the vacuum, q is the charge of the ion, k_B is the Boltzmann constant, T is the temperature, and a_w is the Wigner-Seitz radius defined as $4\pi a_w^3/3 = 1/n_0$ with n_0 being the particle density. The Wigner-Seitz radius describes the effective distance between the ions.

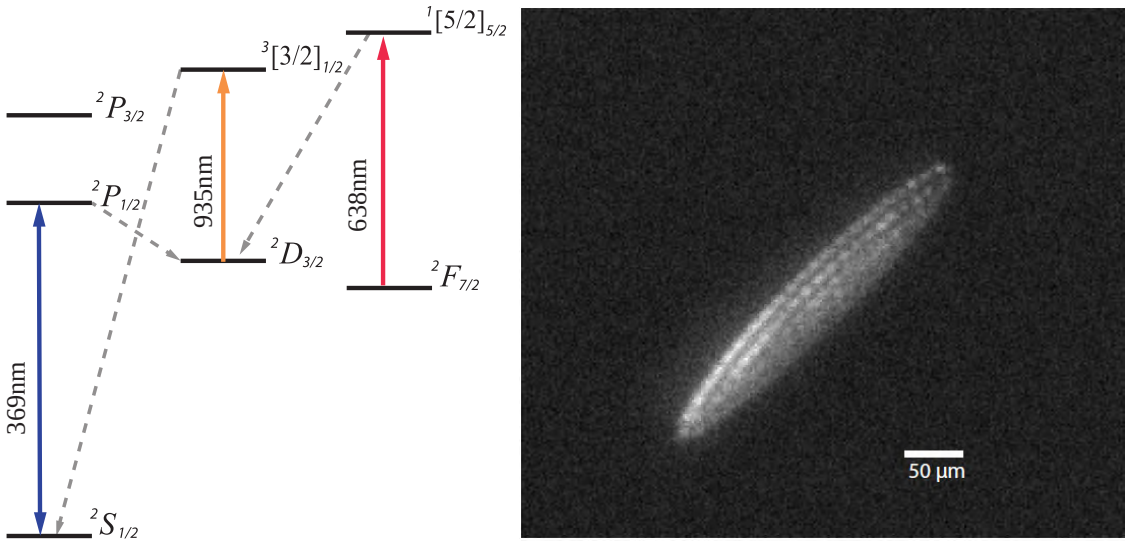

(a) Yb^+ energy levels

(b) A crystal of trapped Yb^+ ions

Figure 8: Energy levels for laser cooling a Yb^+ ion (a). The $^2S_{1/2} \leftrightarrow {}^2P_{1/2}$ transition is used for Doppler cooling. However, Yb^+ has two meta–stable states that the ion decays to and need to be re-pumped; one at 935 nm and another at 638 nm. A crystal of trapped Yb^+ ions is shown in (b).

We were able to trap different isotopes of Yb^+ (Table 1). We identified the different isotopes comparing our frequency with the expected frequency values for those transitions (Ref. [113, 117, 120]). Due to hyperfine splitting, the 171 isotope requires are microwave source of 12.643 GHz to depopulate the ions from the state that is not in the cycling level. To demonstrate that we had trapped $^{171}Yb^+$, we turned on and off the microwave source and the ions appeared and disappeared accordingly.

Table 1: Trapping frequencies for different Yb^+ isotopes. The percentages in brackets reflect the natural abundance of each isotope. The frequencies were measured by the lab wavemeter (HighFinesse WS7). The frequencies are reported in THz. The right most column shows corresponding frequencies for the neutral Yb atoms for the various isotopes. Other isotopes of Yb, were not observed as 168 has very low abundances and 173 has many more decay channels that required additional re-pumping lasers. The $^2F_{7/2} \leftrightarrow {}^2[5/2]_{1/2}$ transition was measured to be 469.43921 THz and no isotopic difference was observed. This was verified by blocking the 638 nm light and waiting for the ion to go dark. The laser would then be unblocked and the ion would appear again.

Yb^+ (amu)	$^2S_{1/2} \leftrightarrow {}^2P_{1/2}$(THz)	$^2D_{3/2} \leftrightarrow {}^2[3/2]_{1/2}$(THz)	Yb $^1S_0 \leftrightarrow {}^1P_1$(THz)
176 (12.76%)	811.2902	320.5746	751.52706
174 (31.83%)	811.2915	320.5720	751.52674
172 (21.83%)	811.2922–30	320.56940	751.52650
170 (3.04%)	811.2939–44	320.5657	751.52612
171 (14.28%)	811.28854	320.568898	751.52610

2.6 Laser cooling Ca^+

The rest of the experiments described in this thesis use $^{40}Ca^+$ for laser cooling. $^{40}Ca^+$ ions are produced from two-photon ionization of neutral calcium atoms. A cloud of calcium atoms is produced by resistively heating an oven filled with calcium. The calcium is the ionized first by exciting the $^1S_0 \leftrightarrow {}^1P_1$ transition with a 423 nm laser. Then a second photon around 388 nm ionizes the neutral calcium as shown in Fig. 9a. Scanning the 423 nm laser shows a fluorescence of the Doppler shifted excitation of the neutral calcium atoms as shown in Fig. 9b.

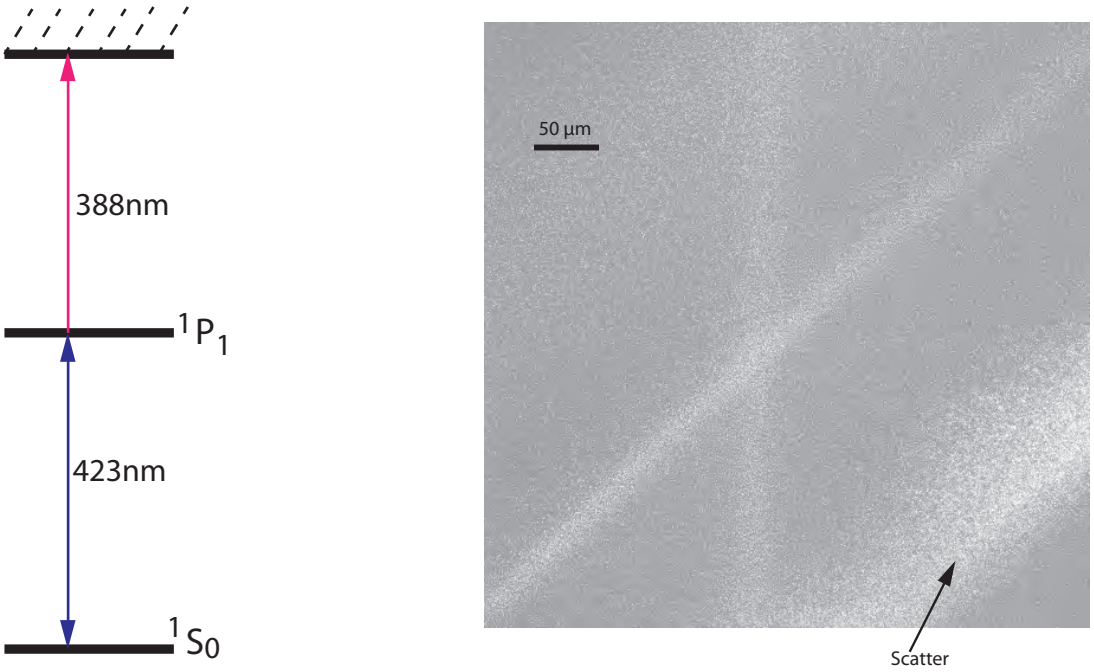

(a) Ca ionization scheme

(b) Ca fluorescence

Figure 9: The ionization scheme for neutral calcium. (a) Isotope selective ionization of calcium is performed by exciting the neutral calcium along the $^1S_0 \rightarrow {}^1P_1$ transition with a tuned 423 nm photon and another photon with wavelength of about 388 nm ionizes it to the continuum. (b) An image of fluorescent neutral calcium atoms imaged on the EMCCD camera.

The Ca^+ ion has a ground state of 4 $^2S_{1/2}$. Two hyperfine levels lie above the ground state, 3 $^2D_{3/2}$ and 3 $^2D_{5/2}$. Above these first excited states are another two hyperfine levels, 4 $^2P_{1/2}$ and the 4 $^2P_{3/2}$ as shown in Fig. 10a. Doppler Cooling is realized by cycling on the 397 nm $^2S_{1/2} \leftrightarrow {}^2P_{1/2}$ transition as shown in Fig. 10a, which has a lifetime 7.1 ns. Occasionally, one in twelve cycles, the ion decays to the $D_{3/2}$ electronic level, which has a lifetime of 1 s, and is re-pumped with a 866 nm laser along the $^2D_{3/2} \leftrightarrow {}^2P_{1/2}$ transition back to the cycling transition. To image the trapped ions, fluorescence from the 397 nm transition is collected with an objective

lens (magnification=10×) as shown below in Fig. 10b.

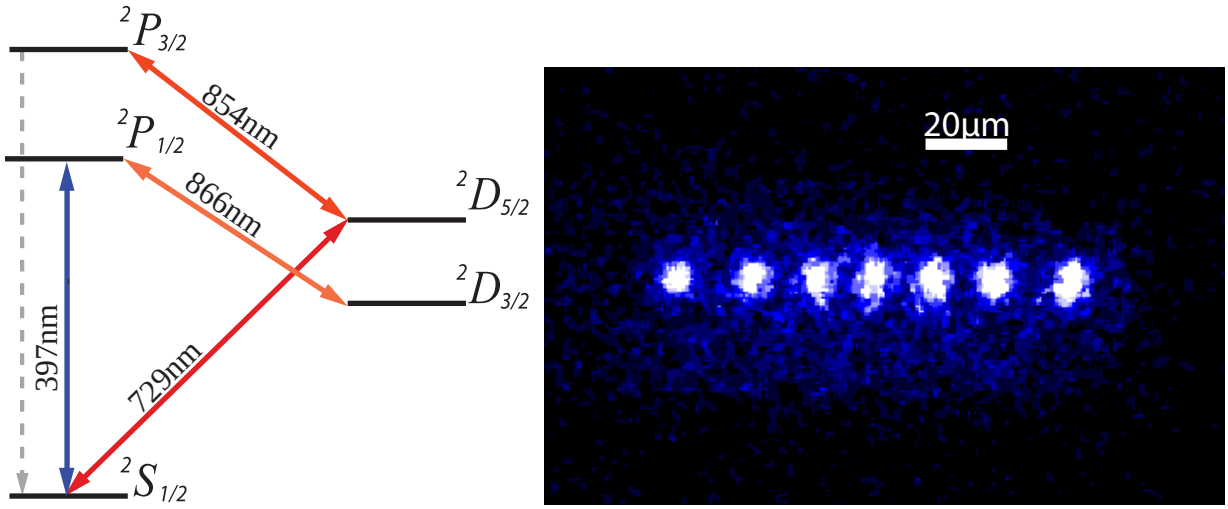

(a) $^{40}Ca^+$ energy levels

(b) A chain of $^{40}Ca^+$ ions

Figure 10: Energy levels for laser cooling the $^{40}Ca^+$ ion (a). The $^2S_{1/2} \leftrightarrow {}^2P_{1/2}$ transition is used for laser cooling near 397 nm. An additional laser at 866 nm laser is used to re-pump the ion from $^2D_{3/2}$ level. The 729 nm and 854 nm lasers are used for sideband cooling, which is explained in detail in section 2.7. A chain of cooled $^{40}Ca^+$ ions (b) imaged on an EMCCD camera is shown.

The frequency of the transitions is measured using a calibrated commercial Fabry-Perot Interferometer called the WS7 (HighFinesse). The accuracy of the measured transition frequencies is limited by the WS7, which has an absolute accuracy of 60 MHz. The measured transitions are shown in the table below (Tab. 2).

Table 2: Frequencies for different transitions of $^{40}Ca^{+}$ measured in the laboratory with the wavemeter (HighFinesse WS7). The frequencies are those observed in air and the right most column is the frequency of the neutral calcium transition.

$^{40}Ca^{+}$ Transition	Frequency (THz)	^{40}Ca $^{1}S_0 \leftrightarrow {}^{1}P_1$(THz)
$^{2}S_{1/2} \leftrightarrow {}^{2}P_{1/2}$	755.2227	709.0783
$^{2}S_{1/2} \leftrightarrow {}^{2}D_{5/2}$	411.0421	
$^{2}D_{3/2} \leftrightarrow {}^{2}P_{1/2}$	346.0003	
$^{2}D_{5/2} \leftrightarrow {}^{2}P_{3/2}$	352.6734	

2.7 Sideband cooling

Narrow transitions on sidebands of trapped atomic ions are ideally suited for precision spectroscopy of molecular ions [121]. Before precision spectroscopy can be achieved, the ion–molecular-ion pair need to be sideband cooled to remove the motional energy of the ion in the trap. For sideband cooling, the trap frequency must be larger than the laser linewidth and the decay rate of the excited state. This makes it possible to address each individual sideband, which is critical for sideband cooling. When the laser is detuned to the red sideband, the sideband with lower motional energy, an excitation to the upper level results in a reduction of motional energy.

Since the sideband cooling state is long-lived, it is coupled to a short-lived state with another laser for faster cooling rate. Spontaneous decay does not change the vibrational quantum number of the ions. For Ca^{+} the $^{2}S_{1/2} \leftrightarrow {}^{2}D_{5/2}$ transition is used for sideband cooling with a 729 nm laser. The long lived $^{2}D_{5/2}$ state is coupled to the short-lived $^{2}P_{3/2}$ state with an 854 nm laser to increase the cooling rate. A magnetic field splits the degenerate level in the sideband transition to about ten states. For sideband cooling, the $^{2}S_{1/2}(m = -1/2) \rightarrow {}^{2}D_{5/2}(m = -5/2)$ since there is no Zeeman level lower that the $^{2}D_{5/2}(m = -5/2)$ state. Hence, there will not be

a sideband closer to energy with any of the red sidebands of the ${}^2D_{5/2}(m = -5/2)$ state. It is convenient to start the theoretical description of sideband cooling from the Lamb-Dicke regime since that is where sideband cooling experiments begin; that is, sideband cooling is proceeded by Doppler cooling. The Lamb-Dicke regime is when the ions are confined in a space much smaller than the wavelength of the transition. The Lamb-Dicke regime is characterized by the Lamb-Dicke parameter η which is defined as,

$$\eta = kx_0 << 1, \tag{45}$$

where k is the wavevector and $x_0 = \sqrt{\hbar/2m\omega}$ and ω describes the harmonic oscillation frequency. Furthermore,

$$\eta^2 = \frac{(\hbar k \cos\theta)^2}{2m}/\hbar\omega, \tag{46}$$

where θ is the angle between the wave vector and the trap axis. Thus, the square of the Lamb-Dicke describes the ratio between photon recoil energy and the energy level spacing the in the harmonic oscillator. In the Lamb-Dicke regime, the interaction Hamiltonian can be written as,

$$\langle \psi_1, n'|H_1|\psi_0, n\rangle = \frac{1}{2}\hbar e^{-i\Delta t}\Omega\langle n'|e^{i\eta(a^\dagger + a)}|n\rangle, \tag{47}$$

where $n = 0, 1, 2....$ are the levels of the harmonic oscillator and Ω is the Rabi frequency. Because η is very small, the exponential term in the Hamiltonian can be expanded using the Taylor series as,

$$e^{i\eta(a^\dagger + a)} = 1 + i\eta(a^\dagger + a) + O(\eta^2). \tag{48}$$

This results in processes that change the vibrational quantum number by more than one to be suppressed and favor changes by ± 1. The interaction Hamiltonian defines the allowed transitions which broadly fall into three categories:

- *Red sideband transition*-These are transitions where the change in vibrational quantum number is $\Delta n = -1$. That is the transition results in an overall

decrease in the motional energy.

$$\Omega_{n-1,n} = \eta\sqrt{n}\Omega_0. \tag{49}$$

- *Carrier transition*-There are transitions where excitation to a higher electronic state results in no change in the vibrational quantum number i.e. $\Delta n = 0$ and,

$$\Omega_{n,n} = \Omega_0(1 - \eta^2 n). \tag{50}$$

- *Blue sideband transition*- These are transitions where an electronic change increases the vibrational quantum number by $\Delta n = +1$ and,

$$\Omega_{n+1,n} = \eta\sqrt{n+1}\Omega_0. \tag{51}$$

The Rabi frequencies of the sidebands are proportional to η^x. The transitions are shown schematically in Fig. 11.

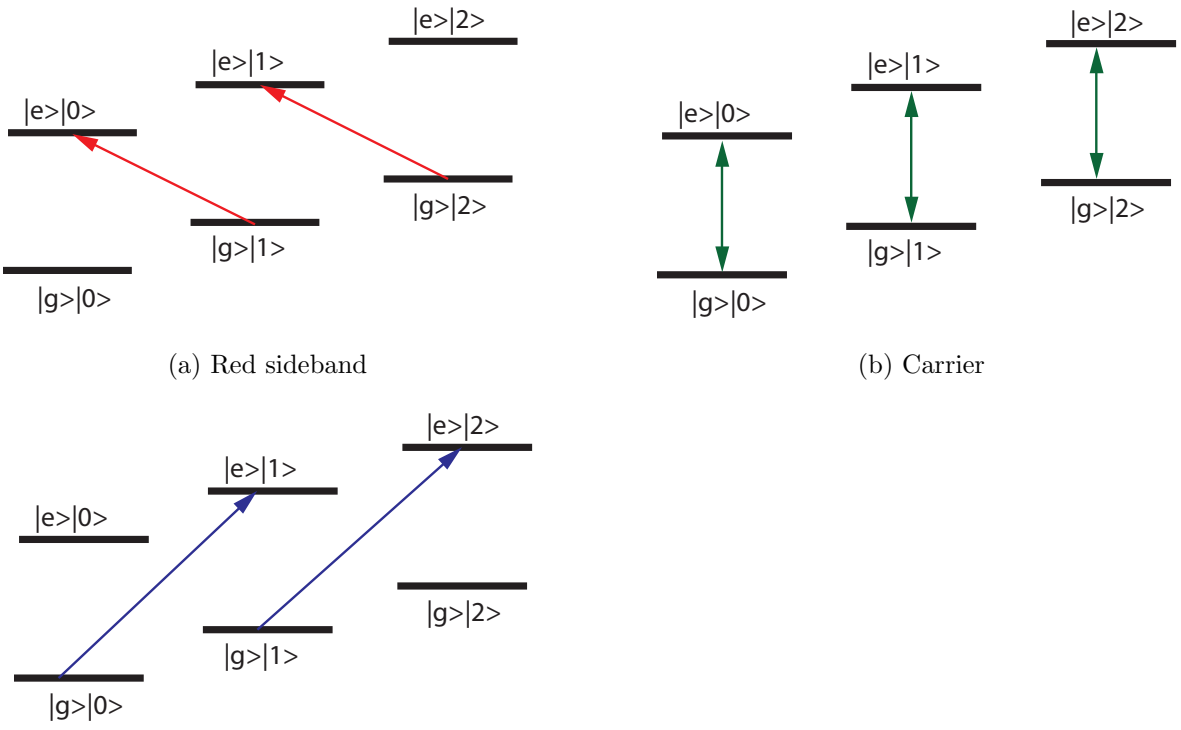

(a) Red sideband

(b) Carrier

(c) Blue sideband

Figure 11: An illustration of the driven transition. (a) shows the red sideband transition, (b) shows the carrier transition, and (11c) shows the blue sideband transition. g and e represent the electronic state, while 0, 1 and 2 represent the lowest vibrational states.

Repeated transitions on the red sideband removes the vibrational quanta to the motional ground state. This process is called sideband cooling and is used to cool ions beyond the Doppler cooling limit [122–130].

2.8 Non-destructive identification of molecular ions

To do chemistry in ion traps, the identity of the reactant must be ascertained accurately. Because of the controlled nature of chemical reactions in ion traps, only mass spectrometry is sufficient to accurately identify ions inside the trap. Traditionally, mass spectrometry was carried out with time of flight (TOF) and quadrupole mass

filter (QMF) techniques. These methods destroy the ions on measurement. An alternative technique would be to measure the mass of the ion *in situ* without destroying it so that experiments can be carried out on that ion after identification. We used a non-destructive technique that relates the oscillation frequency of the ions in the trap with their mass [131, 132]. Since the ions are coupled by their Coulombic interaction, any perturbation on one ion affects the other ion. Thus for this technique to work the identity and frequency of one ion must be known prior the addition of the second unknown ion. For two ions, the axial frequencies are governed by the equation

$$\nu_{+/-}^2 = [(1+\mu) \pm \sqrt{1-\mu+\mu^2}]\nu_1^2, \tag{52}$$

where ν_+ is the breathing mode (out-of-phase oscillation) and ν_- is the center of mass mode (in-phase oscillation) of the oscillation of the ions, μ is the ratio of the two ions M_1/M_2. To identify the resonance frequency of the ions, a sinusoidal varying voltage is applied on one of the electrodes. When the frequency of the applied voltage is on resonance with the secular frequency of the ion crystals, the crystal mode motion is excited and the fluorescence signal of the lase-cooled atomic ions is perturbed. This will show up as either a dip or a spike in the fluorescence spectrum depending on the detuning of laser.[1] Monitoring the fluorescence signal as a function of the frequency of the drive voltage, the identity of the unknown ion can be deduced from the above equation. This technique was pioneered by the Baba and Waki group in Japan and the Drewsen group in Denmark [61, 131–133]. An example using this technique is shown below in Fig. 12. This method is commonly referred to as a tickle scan because the voltage tickles the secular motion of the ions in the trap.

[1] If the laser is red-detuned from the atomic transition, an excitation of the oscillation mode by the applied voltage causes a heating of the crystal, which brings the red-detuned laser on resonance with the laser-cooled ion, resulting in an increase in fluorescence counts, a peak. However, if the laser is on resonance with the laser-cooled atomic ion prior to the excitation, the heating caused by the excitation of the oscillation mode will result in overall heating of the trapped crystal, leading to poor cooling and low fluoresce counts. This shows up as a dip in the spectrum.

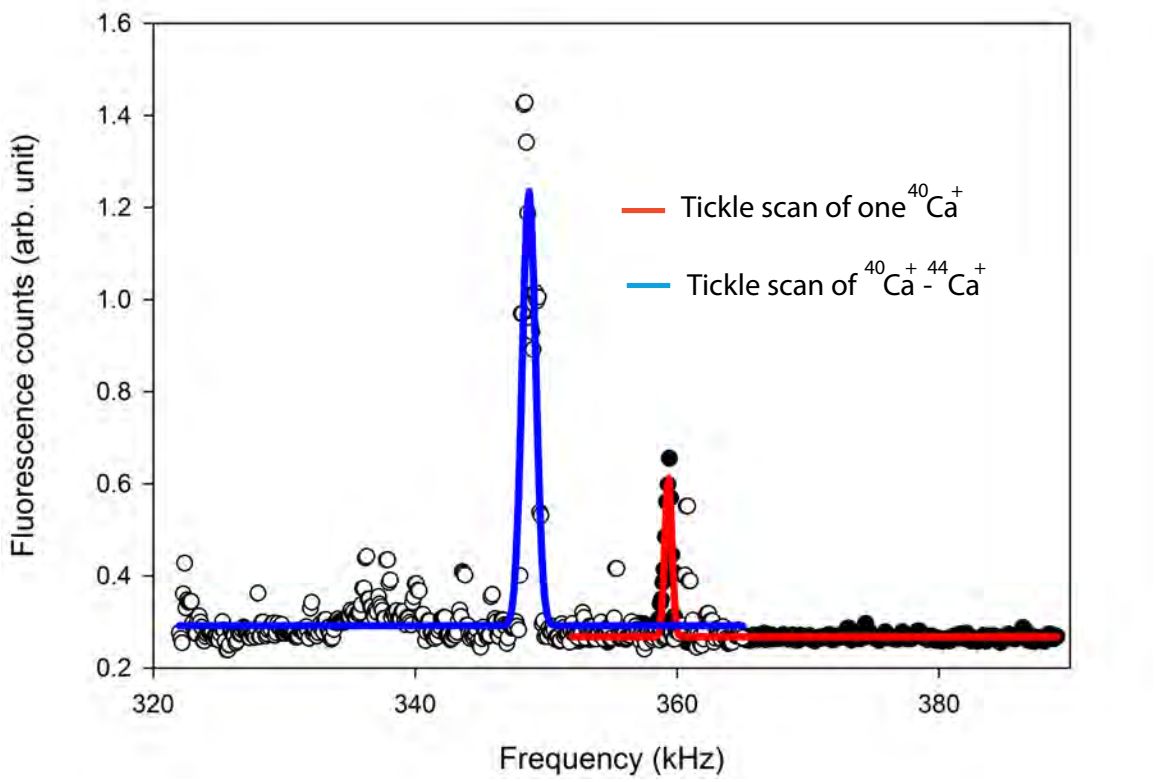

Figure 12: The secular frequency scan on the center of mass mode showing two peaks. The circles are the data, while the lines are Gaussian fits to the data. The peak at 359 kHz (red curve) shows a tickle scan of one $^{40}Ca^{+}$ ion where else the peak at 348 kHz (blue curve) shows a tickle scan of one $^{40}Ca^{+}$ and another unknown ion. The identity of the unknown ion was determined to be $^{44}Ca^{+}$ based on equation 52.

In this example, two species of Ca^{+} isotopes were trapped. One was the known $^{40}Ca^{+}$, while the other was unknown. Prior to trapping two species, only one $^{40}Ca^{+}$ was trapped. The secular frequency of the known $^{40}Ca^{+}$ was determined by applying an oscillating frequency on the electrodes while the laser was slightly red detuned from the cooling transition. An excitation of the secular frequency of the trapped ion results in heating of the ion which causes the Doppler shifted laser to be closer to resonance of the atomic transition increasing the cooling. This shows up in the spectra

as an increase in the fluorescence counts. The red trace in Fig. 12 is a Gaussian fit to the data that determined the frequency. Another isotope of Ca^+ was trapped along with the $^{40}Ca^+$ ion. However, this isotope was not fluorescent, hence its identity was unknown. A tickle voltage was applied on the crystal and the resultant scan is shown as the solid circles. The data was fit with the blue Gaussian line. Using equation 52, the identity of the unknown isotope was found to be $^{44}Ca^+$. The determined mass was within 0.5 amu difference with the predicted mass.

CHAPTER III

MOLECULAR SPECTROSCOPY AND $^{40}CaH^{+}$ MOLECULAR ION

To assign the spectra of a molecule, several properties of the molecule have to be known first. These properties, called spectroscopic constants, come from the Schrödinger equation describing the molecular system. In this chapter, the basics of spectroscopic transitions will be reviewed as well as a summary of the $^{40}CaH^{+}$ molecular ion.

3.1 Spectroscopy and selection rules

The molecular Hamiltonian has many degrees of freedom and can be written as [134, 135],

$$H = -\frac{\hbar^2}{2}\sum_{k=1}^{2}\frac{1}{M_k}\nabla_k^2 - \frac{\hbar^2}{2m_e}\sum_{i=1}^{N}\nabla_i^2 + \frac{e^2}{4\pi\varepsilon_0}\left[\frac{Z_1Z_2}{R} + \sum_{i,j}\frac{1}{r_{i,j}} - \sum_{i}\left(\frac{1}{r_{i,1}} + \frac{1}{r_{i,2}}\right)\right] \quad (53)$$

where M_k is the mass of the nucleus, m_e is the electron mass, ε_0 is the permittivity of free space constant, Z_i is the charge of the nucleus, e is the charge of the electrons, R is the distance between the two nuclei and r_i is the coordinate of the electrons. The first term describes the kinetic energy of the nuclei, the second term the kinetic energy of the electrons. The terms in the square brackets describe the potential energy generated by the repulsion of the nuclei, electron-electron repulsion and electron-nuclear attraction respectively. Because the motion of the nuclei is much slower than that of the electrons, the nuclei appear static compared to the electronic motion. The Born-Oppenheimer approximation [136] allows for the separation of nuclear motion and electronic motion. Thus the wavefunction can be separated as,

$$\left|\Psi_{molecule}\right\rangle = \left|\Psi_{nuclear}\right\rangle \otimes \left|\Psi_{electronic}\right\rangle. \quad (54)$$

Thus the Hamiltonian can be separated into the electronic contribution, the vibration and rotation of the nuclei as follows:

$$H_{molecule} = H_{electronic} + H_{vibrational} + H_{rotational}. \tag{55}$$

The Hamiltonian of the vibrational and rotational contributions for a diatomic molecule can be approximated to first order as,

$$H_{vibrational} = \omega_e(\nu + \frac{1}{2}), \tag{56}$$

$$H_{rotational} = BJ(J+1), \tag{57}$$

where the constants expressed in (cm^{-1}) are,

$$\omega_e = \frac{1}{hc}.\hbar\sqrt{\frac{k}{\mu}}, \tag{58}$$

$$B = \frac{1}{hc}.\frac{\hbar^2}{2I}, \tag{59}$$

where, ω_e is the angular frequency of the transition, c is the speed of light, k is the force constant, h is Planck's constant, $\hbar$ is the reduced plank constant, I is the molecule's inertia in terms of the reduced mass,

$$I = \mu r_0^2, \tag{60}$$

$$\mu = \frac{m_1 m_2}{m_1 + m_2}, \tag{61}$$

with r_0 being the equilibrium bond length. Since vibrational and rotational motions are coupled, the energy of the molecule is expressed as the sum of the rovibrational energy,

$$E_{rovib} = \omega_e(\nu + \frac{1}{2}) + B_v J(J+1). \tag{62}$$

The above equations describe ideal situations of a perfect harmonic oscillator and rigid rotor. In reality, the energy of a molecule becomes perturbed at high energies.

Thus corrections are added to account for the anharmonicity of a molecule. An approximation to this anharmonicity is the Morse potential and it takes the form,

$$V(r) = D_e((1 - e^{-a(r-r_e)})^2 - 1), \tag{63}$$

where D_e is the depth of the potential i.e. the dissociation energy for the molecule and $a = \sqrt{k_e/2D_e}$. The energies of the rovibrational oscillator become second order in ν and fourth order in J as,

$$E_{rovib} = \omega_e(\nu + \frac{1}{2}) - \omega_e x_e(\nu + \frac{1}{2})^2 + B_v J(J+1) - D_v J^2(J+1)^2. \tag{64}$$

The new terms $\omega_e x_e$ and D are the anharmonicity constant and the centrifugal distortion constant respectively. In order to have a rovibrationl spectrum, there has to be a change in the dipole moment accompanying that vibration or rotation. The change in vibrational motion for a harmonic oscillator is governed by the selection rule that $\Delta\nu = \pm 1$. However, due to the anharmonicity of molecular vibrations other transitions such as $\Delta\nu = \pm 2, \pm 3, \pm 4...$ are possible albeit at decreasing intensities. On the other hand, for molecular rotations, the selection rule $\Delta J = 0, \pm 1$ holds true even when rotor is distorted. This is because D $\ll$ B hence the distortion is very small. Transitions with $\Delta J = 0$ are observed when there is a change in electronic energy. Transitions with $\Delta J = +1$ are labeled the R branch, transitions with $\Delta J = 0$ are called the Q branch, and transitions with $\Delta J = -1$ are called the P branch. Thus from an observed rovibrational spectrum, we can calculate the vibrational and rotational constants, $\omega_e, \omega_e x_e, B_v$, and D_v. Conversely, if we can calculate from first principles the rovibrational constants, we can approximately predict where the lines for that spectrum will be.

When spectra is accompanied with changes in electronic energy, electronic transition selection rules apply together with the rovibrational selection rules. These rules are governed by the angular momentum of the electrons about the internuclear axis. The motion of the electrons about the axis gives rise to orbital angular momentum

L which precesses about the nuclear axis and its projection about the axis is called $\mathbf{M}_L$. At faster precession speeds, **L** ceases to be a good quantum number, while its projection remains a good quantum number. Hence electronic states are classified based on $\mathbf{M}_L$, which is labeled $\Lambda = |M_L|$. The values that Λ can take are $\Lambda = 0, 1, 2, 3.....L$. The molecular states are labeled accordingly to each value of Λ as $\Sigma, \Pi, \Delta, \Phi$ and so on. The molecules with Σ state has symmetry properties about the plane through the internuclear axis and can take the form Σ^+ or Σ^-. The electrons in the molecules have spin **S** , which can also be projected on to the internuclear axis where it is called $\mathbf{M}_S$. Similar to the case orbital angular momentum, **S** no longer becomes a good quantum number while its projection remains defined. For bookkeeping, we call the projection $\mathbf{M}_S$ to be Σ in molecules. There are 2S + 1 possible values of Σ. The total angular momentum of electronic motion becomes the sum of the orbital angular momentum and the spin angular momentum;

$$\Omega = |\Lambda + \Sigma|, \tag{65}$$

Where Ω can be $|\Lambda - \Sigma|, |\Lambda - \Sigma| + 1, ...|\Lambda + \Sigma|$.

When electronic change is coupled with rotational change, the two motions become coupled which give rise to changes in the spectra. There are different ways in which the momenta can couple and the different schemes are grouped into Hund's couple cases. While the coupling cases range from (a) to (e), the most common cases are Hund's coupling cases (a) and (b), which will be reviewed here. For the rest the reader can refer to [1].

3.2 Hund's case (a)

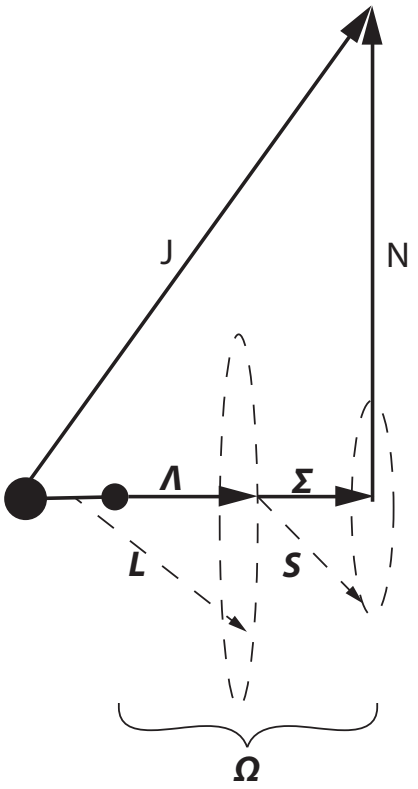

Figure 13: A vector diagram showing Hund's case (a). It is defined by strong spin-orbit coupling to the internuclear axis to give the resultant angular momentum

In Hund's case (a), the motion of electrons couples strongly to the internuclear axis to give a large spin-orbit coupling. **N** represents the rotation of the nucleus. **N** and Ω precess around **J**, which is the resultant angular momentum. The rotational energy of the molecule becomes,

$$E(J) = B[J(J+1) - \Omega^2] \tag{66}$$

3.3 Hund's case (b)

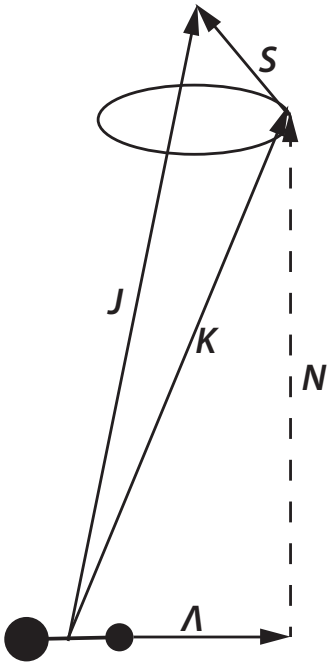

Figure 14: A vector diagram showing Hund's case (b). The spin angular momentum is weakly coupled to the internuclear axis, instead it couples to the sum of the nuclear rotation and electronic angular momenta

When $\Lambda = 0$ and $\mathbf{S} \neq 0$, the spin is not strongly coupled to the internuclear axis. Under this condition, Ω is no longer a good quantum number. Instead Λ and $\mathbf{N}$ form the resultant angular momentum $\mathbf{K}$ without the spin. The spin, $\mathbf{S}$ couples with $\mathbf{K}$ to form the resultant angular momentum $\mathbf{J}$. For CaH^+ the ground state is described by rigid rotor since $\Lambda = 0$ and $\mathbf{S}= 0$, some of the excited electronic states by Hund's case (b).

3.4 Electronic selection rules

For molecules where λ is well defined, the selection rule is that transitions must have $\Lambda = 0, \pm 1$. Thus the possible electronic transitions are $\Sigma - \Sigma, \Sigma - \Pi$ and so on. In

addition, Σ states cannot change symmetry during a transition. So the transitions $\Sigma^+ \leftrightarrow \Sigma^+$ and $\Sigma^- \leftrightarrow \Sigma^-$ are possible but not $\Sigma^+ \leftrightarrow \Sigma^-$.

3.5 $^{40}CaH^+$

Similar to other alkaline earth hydrides ions, $^{40}CaH^+$ molecular ions are of particular scientific interest because of potential applications to astrophysics and fundamental physics. Although not detected, these hydrides are thought to be present in ISM and comets [14, 15, 20, 137–140]. Kajita and Moriwaki have identified halides of alkali metals as ideal candidates for the testing of μ, proton-to-electron mass ratio. $^{40}CaH^+$ has been proposed as a good candidate for these measurements [141]. Kajita and coworkers have also performed high precision *ab initio* calculations on $^{40}CaH^+$ vibrational overtones [25]. In particular, we are interested in using our laboratory techniques to perform the first measurements of $^{40}CaH^+$ vibrational spectra. We will focus on the transitions from $\nu' = 9 \leftarrow \nu = 0$ and $\nu' = 10 \leftarrow \nu = 0$. These occur at 883.9 nm and 813.8 nm, respectively.

Despite the lack of experimental evidence, there has been a significant amount of theoretical investigations into the $^{40}CaH^+$ molecule. To measure the spectra of an unknown molecule, we consulted the theory calculations as a guide. Table 3 shows a summary of the spectroscopic constants found in the literature.

Table 3: A summary of published theoretical spectroscopic constants of $^{40}CaH^+$ found in literature. For the experiments described in this thesis, we use the values from [24, 25]. The other calculations used a lower level of theory, while the others did not evaluate the vibrational wavefunctions.

Reference	$D_0(cm^{-1})$	$\alpha_e(cm^{-1})$	R($\AA$)	Be(cm^{-1})	$\omega_e(cm^{-1})$	$\omega_e x_e(cm^{-1})$
Ref [17]	14809	0.13	1.936	4.609	1511.0	23.5
Ref [14]			2.085		1416.8	
Ref [20]	17000		1.864	4.85	1504	21.01
Ref [139]	16719.9	0.0985	1.881	4.85	1482	21.01
Ref [142]	15500		1.926		1482	
Ref [21]	17972		1.873		1453	
Ref [22]	17876		1.86			
Ref [143]	17876.80		1.936	4.609	1468	
Ref [24]	14804		1.936	4.609	1511	
Ref [25]	16267.39	0.09	1.926	4.611	1457.7	

The energetics of the $^{40}Ca^+ + H_2$ reaction are similar to those of neutral Ca and H_2 [55, 139, 144–147].[1] The bond energy of H_2 is 4.478 eV, while the bond energy of $^{40}CaH^+$ is 1.788 eV. This makes the reaction endogernic with an energy difference of 2.77 eV [144]. To get over the barrier, the $^{40}Ca^+$ is excited with the 397 nm laser (3.12 eV) to the $^2P_{1/2}$ state in order for the reaction $^{40}Ca^+ + H_2 \rightarrow {}^{40}CaH^+ + H$ reaction to occur. Once reacted, the molecule forms a stable compound with an equilibrium bond length of about 1.92 $\AA$. The molecule forms an ionic, closed shell bond of Ca^{2+}–H^- with a 1/R curve. The ground state of the molecule has an asymptote $^{40}Ca^+(4s)$

[1] This is because the energy barrier for the neutral Ca reaction with H_2 is close in energy to that of ionized calcium with hydrogen. Furthermore, studied reactions between Mg^+ and H_2 had similar reaction dynamics with those of the neutral magnesium and hydrogen [148–151].

+ H(1s) with a $(4s\ \sigma)^2\ ^1\Sigma^+$ symmetry. The potential energy surfaces of $^{40}CaH^+$ are shown in Fig. 15. The first excited state has an asymptote of $^{40}Ca^+(3d)$ + H(1s) with the electronic configuration of $4s\sigma 3d\sigma$, which produces the molecular states $^{1,3}\Sigma$, $^{1,3}\Pi$, and $^{1,3}\Delta$. The are other higher electronic state which are below the ionic limit, however, for this thesis only the first excited asymptote will be considered.

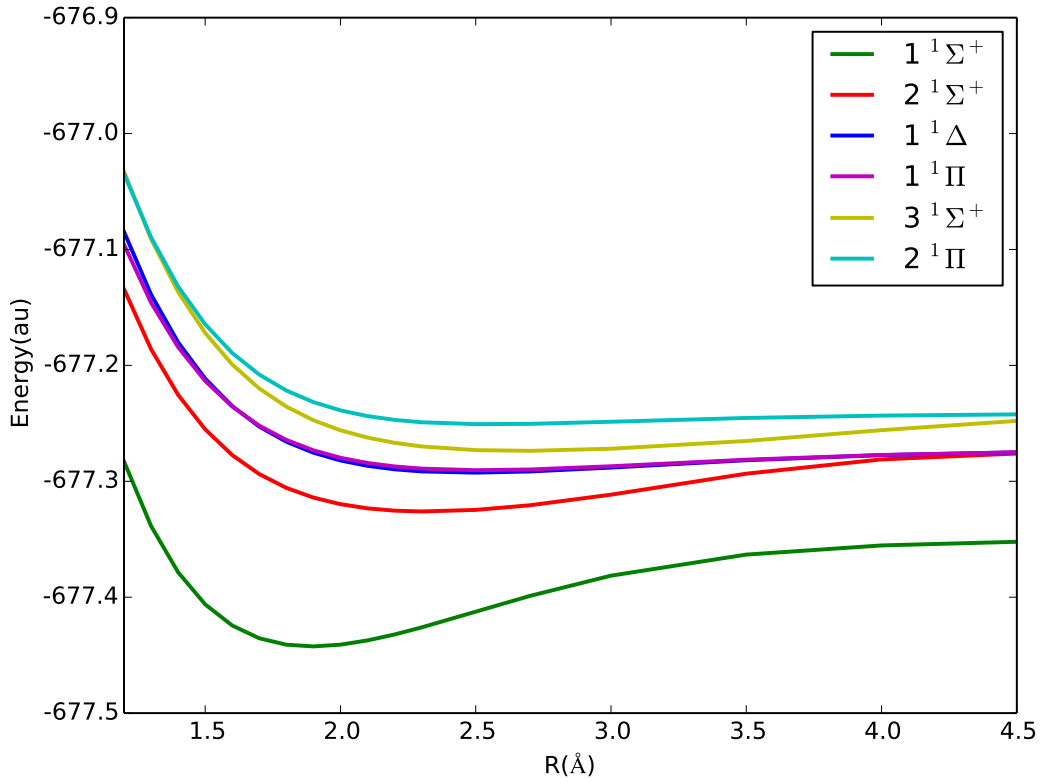

Figure 15: Potential energy curves of the ground state and the lowest excited states of $^{40}CaH^+$ computed at the EOM-CCSD/cc-pCVQZ level of theory provided by [152].

The $^{40}CaH^+$ molecule possesses a permanent dipole moment, which makes it possible have a pure rotational spectrum for future precision measurements. The computed dipole moment is shown in Fig. 16.

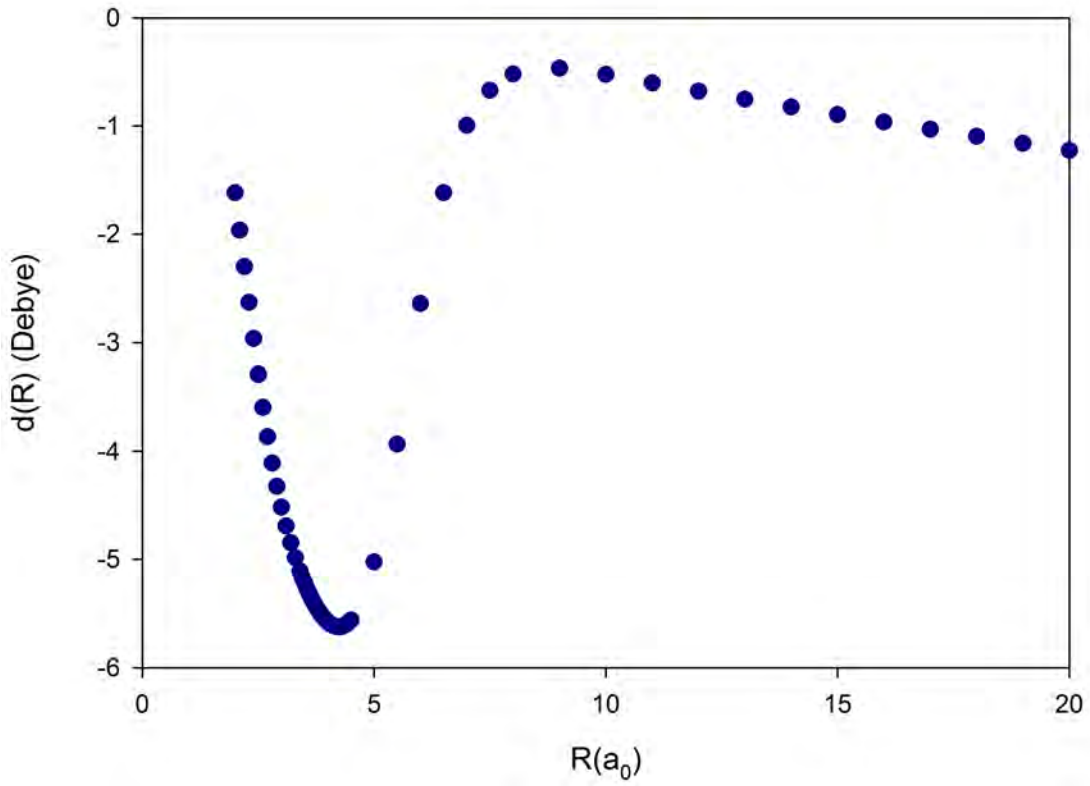

Figure 16: The dipole moment of the ground state of $^{40}CaH^{+}$ provided by [141].

For experimental convenience, we chose to investigate the $\nu' = 9 \leftarrow \nu = 0$ and the $\nu' = 10 \leftarrow \nu = 0$ expected around 883 nm and 813 nm respectively. This is because those transitions are in the range of a commercially available titanium-sapphire laser without any modification as explained in detail in subsection 4.2. Because these are higher-order overtones the coupling strength becomes very weak and the intensity becomes very weak. The expected transition strength were calculated with the LEVEL program to compute the expected matrix elements of the transitions as shown in table 4 [153].

Table 4: Matrix elements of the $X\nu \leftarrow X\nu' R(0)$ transitions calculated with the LEVEL program provided by Ref. [154]. Here the ν indicates the lower level while ν' indicates the upper level. E(2)-E(1) is the difference in energy between the two states. The calculations were based on the $^{40}CaH^{+}$ potential given by [25].

dJ(J")	ν–ν'	E(lower)	E(2)-E(1)	A(Einstein)	F–C Factor	$\langle \nu J \vert M \vert \nu' J' \rangle$
R(0)	9–0	-16714.06	11320.89	2.14694E-4	1.21794E-16	-3.7622E-5
R(0)	10–0	-16714.06	12295.00	5.54952E-5	2.28182E-17	1.69003E-5

3.6 Multiphoton techniques in spectroscopy

Because many spectroscopic transitions of interest generally do not exactly fall in the range of commercially available lasers, it is a common tool in spectroscopy to use a combination of laser to access the transition(s) of interest. Multiphoton techniques employ the absorption of two or more photons of different or same frequency to study transitions that may not be easily accessible with one laser or the detection of that state is is not accessible with other detection methods such as fluoresce quenching. Typically, one photon excites the molecule to an intermediate state and then a second photon excites it to the final state. From these techniques several properties of the molecule can be studied. If the first photon is resonant with a fluorescent low excited state, the second transition can be probed by scanning the second laser light and observing the change in signal. In principle many lasers can be employed covering a big energy gap.

For neutral molecules, typical methods of detection include observing the change in fluorescence when stimulated emission occurs from the intermediate state once second laser is turned on, ionizing the molecule and counting the number of ions produced at a given wavelength, (e.g. resonance enhance multiphoton ionization(REMPI)). This method is advantageous because the observed transitions are those that are

are in the intermediate state. Therefore, even in molecules with many electronic states with overlapping vibrational states can be discriminated with multiphoton spectroscopy. Multiphoton spectroscopy has been applied in the study of Doppler free spectroscopy in sodium [155], hydrogen bonding in aromatic-X clusters [156], rotational spectroscopy in CaH and CaD [157], spectroscopy of biomolecules such as tryptophan [158], torsional barriers in nonrigid molecules [159], studies of Rydberg states [160], the development of laser photoelectron spectroscopy [161] and many other experiments.

3.6.1 Multiple photon dissociation

Molecular ions, on the other hand, present a challenge to some multiphoton techniques since electrostatic repulsions between ions limits densities. In addition the methods of detection for neutrals become difficult for ions. In REMPI, ionization is used to probe the intermediate state [162–164]. Molecular ions have very high ionization potentials that would be impractical for the most part. Most molecular ions do not fluoresce and makes it difficult to detect them. For these reasons, resonance enhanced multiphoton dissociation (REMPD) is employed in the study of molecular ions [81, 165–169]. A schematic of REMPD is shown in figure 17.

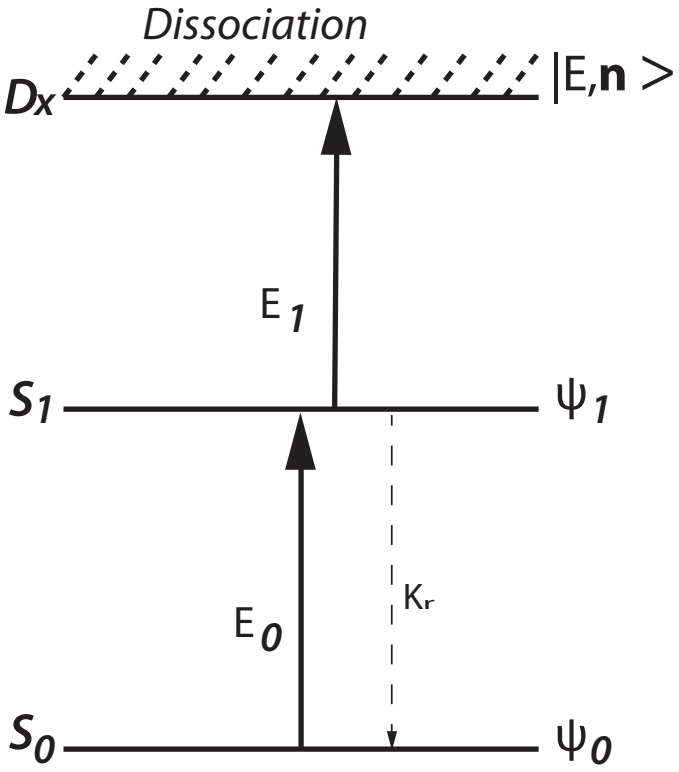

Figure 17: A schematic showing (1+1′) REMPD spectroscopy. The ion dissociate in the dissociative state D_x via an intermediate state S_1 from the ground state S_0 by absorbing two photons with energy E_0 and E_1. The spontaneous emission rate K_r, competes with the REMPD process but because the REMPD process is significantly faster than spontaneous emission, it is neglected in the theoretical treatment.

In REMPD, a molecular ion in the ground state is excited to an immediate state (rovibrational, electronic) by one laser ν_1. A second laser, ν_2, couples that excited state with dissociative state. This technique was introduced by the Syage and Wessel in 1987 when they studied the dissociation spectroscopy of napthalene ions [163]. The Ito group in Japan demonstrated the technique subsequently in the spectroscopy of benzene, $p-$difluorobenzene and 1,3,5-trifluobenzene [170]. Schlag's group demonstrated ion dissociation spectroscopy in CH_3I^+, CD_3I^+, benzene, fluorobenzene, [164, 165, 171, 172]. Since then a number of different groups have applied

this technique with great resolution on the spectroscopy [58, 61, 63, 64, 81, 166–168, 173–178].

3.7 Theory of two-photon dissociation

This formalism is based on [179–182]. The dynamics of two-photon dissociation can be described by the evolution of the molecular system upon interaction with laser radiation. We begin with the time-dependent Schrödinger equation,

$$i\hbar\frac{\partial\Psi}{\partial t} = H\Psi. \tag{67}$$

Where $H = H_0 + H_1$ and H_0 is the radiation free Hamiltonian of the molecule, while H_1 represents the interaction with the radiation. Following the treatment of the earlier section, now we have two lasers coupling three states. We have a pulse laser described by the electric field, $\vec{\epsilon}_1 = \hat{\epsilon}\cdot\epsilon(t)\cos(\omega_0 t)$ and a CW laser described by $\vec{\epsilon}_2 = \epsilon_0\cos(\omega_1 t)$, where $\hat{\epsilon}$ is the polarization of the pulse laser, $\epsilon(t)$ is the slow varying amplitude of the electric field of the pulse laser, ϵ_0 is the amplitude of the electric field CW laser. The interaction Hamiltonian follows as,

$$H_1 = -\mu_0\cdot\vec{\epsilon}_0(t) - \mu_1\cdot\vec{\epsilon}_1(t). \tag{68}$$

The wavefunction describing the process becomes a linear combination of the radiation free wavefunctions, which is given by,

$$|\Psi(t)\rangle = c_0|\psi_0\rangle e^{-iE_0\hbar} + c_1|\psi_1\rangle e^{-iE_1\hbar} + \sum_n\int dE\ c_{E,\mathbf{n}}|E,\mathbf{n}^-\rangle e^{-iEt/\hbar}, \tag{69}$$

where the coefficients, c_0, c_1, and $c_{E,\mathbf{n}}$ are time dependent and satisfy the condition that $\langle\Psi(t)|\Psi(t)\rangle = 1$. We insert the wavefunction into the time-dependent Schrödinger

equation 67 to get a set of first order differential equations for the coefficients as,

$$\frac{d}{dt}c_0 = i\Omega_0^* e^{-i\Delta_0 t}c_1(t), \tag{70}$$

$$\frac{d}{dt}c_1 = i\Omega_0 e^{-i\Delta_0 t}c_0(t) + i\int dE \sum_n \Omega_{1,E,\mathbf{n}} e^{-i\Delta_E t}c_{E,\mathbf{n}}(t), \tag{71}$$

$$\frac{d}{dt}c_{E,\mathbf{n}} = i\Omega_{1,E,\mathbf{n}}^* e^{-i\Delta_E t}c_1(t), \tag{72}$$

where,

$$\Omega_0(t) = \frac{\langle\psi_1|\mu_0|\psi_0\rangle\epsilon_0(t)}{\hbar}, \qquad \Omega_{1,E,\mathbf{n}}(t) = \frac{\langle\psi_1|\mu_1|E,\mathbf{n}^-\rangle\epsilon_1(t)}{\hbar}, \tag{73}$$

$$\Delta_0 = \frac{E_1 - E_0}{\hbar} - \omega_0, \qquad \Delta_1 = \frac{E - E_1}{\hbar} - \omega_1. \tag{74}$$

We can solve for the continuum coefficient by imposing the boundary condition that prior to the lasers being turned on, there is no population in the excited state and the continuum. We obtain,

$$c_{E,\mathbf{n}}(t) = i\int_0^t dt'\ \Omega_{1,E,\mathbf{n}}^*(t')e^{i\Delta_E t'}c_1(t'). \tag{75}$$

We can eliminate the continuum coefficient from equation 71 by substituting the solution from equation 75 to obtain,

$$\frac{d}{dt}c_1 = i\Omega(t)e^{i\Delta_0} - \int dE \sum_n \Omega_{1,E,\mathbf{n}} e^{-i\Delta_E t} \times \int_0^t dt'\Omega_{1,E,\mathbf{n}}^*(t')e^{i\Delta_E t'}c_1(t'). \tag{76}$$

To solve the above equation, we make the assumption that all the matrix elements of the continuum states vary slowly with energy i.e. the states are "flat". This means that energy of each continuum state can be replaced by some average energy such that $E_L = E_1 + \hbar\omega_1$,

$$\sum_n |\langle E,\mathbf{n}^-|\mu_1|\psi_1\rangle|^2 \approx \sum_n |\langle E_L,\mathbf{n}^-|\mu_1|\psi_1\rangle|^2 \tag{77}$$

This is assumption is called the slowly varying continuum approximation (SVCA). At this point it becomes intuitive to express the equation in terms of the spectral

autocorrelation function, $F_1(t-t')$, which is defined as the Fourier transform of the absorption spectrum,

$$F_1(t-t') = \int dE\ A_1(E) e^{-i\omega_{E,1}(t-t')}, \tag{78}$$

where $A_1(E)$ is the absorption coefficient from the ith state expressed as,

$$A_i(E) = \sum_n |\langle E_L, \mathbf{n}^- | \mu_i | \psi_i \rangle|^2. \tag{79}$$

The SVCA localizes the autocorrelation function such that defining it in terms of equations 77 and 78, we find,

$$F_1(t-t') = 2\pi\hbar A_1(E_L)\delta(t-t'). \tag{80}$$

If we rewrite the differential equation for c_1 in terms of the autocorrelation function, and then integrate the function over E and t', we obtain,

$$\frac{d}{dt}c_1 = i\Omega_0(t)e^{i\Delta_0 t}c_0(t) - \Omega_1(t)c_1(t), \tag{81}$$

where $\Omega_1(t)$ is the Rabi frequency given by,

$$\Omega_1(t) = \pi \sum_n \frac{\langle E_L, \mathbf{n}^- | \mu_1 | \psi_1 \rangle \epsilon_1(t)}{\hbar}. \tag{82}$$

The probability of observing the dissociation into state $|\mathbf{n}\rangle$ over some fixed energy E, becomes the square of the photodissociation coefficient,

$$P_{\mathbf{n}}(E) = |c_{\mathbf{n},E}(t \to \infty)|^2 = \left| \frac{\langle \psi_1 | \mu_1 | E, \mathbf{n}^- \rangle}{\hbar} \int_0^t dt'(t') \epsilon_1^*(t) e^{i\Delta_E t'} c_1(t') \right|^2. \tag{83}$$

In our REMPD experiments, we observe the change in the probability of dissociating the molecule as a function of the detuning from the vibrational transition.

CHAPTER IV

EXPERIMENTAL SETUP

In this section the instruments used for the experiments will be discussed in detail including the lasers systems used and the control of the laser frequencies.

4.1 Calcium ion diode laser system

Diode lasers are an important tool in atomic physics. Due to their low costs compared to dye lasers and good stability, diode lasers are lasers of choice for most atomic physicists. Briefly, a diode laser operates by emitting photons when current is run through the active region of between a n-type and p-type cladding layers. This creates electron-hole pairs that recombine to emit photons. The energy of the emitted photon is determined by the band-gap of the semiconductor [183]. Typical semiconductors used are AlGaAs for the 750-890 nm region, InGaAsP for the 1300–1500 nm region and GaN for violet light with a range 365-405 nm.

For Doppler cooling and sideband cooling $^{40}Ca^{+}$, continuous wave (CW) lasers are used. The lasers used are diode lasers (Toptica DL100), which are advantageous for research because of their ease of use, stability, and relatively low cost. While the design of the lasers is the same, the use of different semi-conductors gives a range of available wavelengths. For Toptica, lasers operating wavelengths with a range 370–1770 nm are available. For the main cooling laser for $^{40}Ca^{+}$ at 397 nm a second harmonic generated frequency multiplied laser is used with the fundamental lasing at 794 nm. A typical Toptica laser is shown in the picture below in Fig. 18.

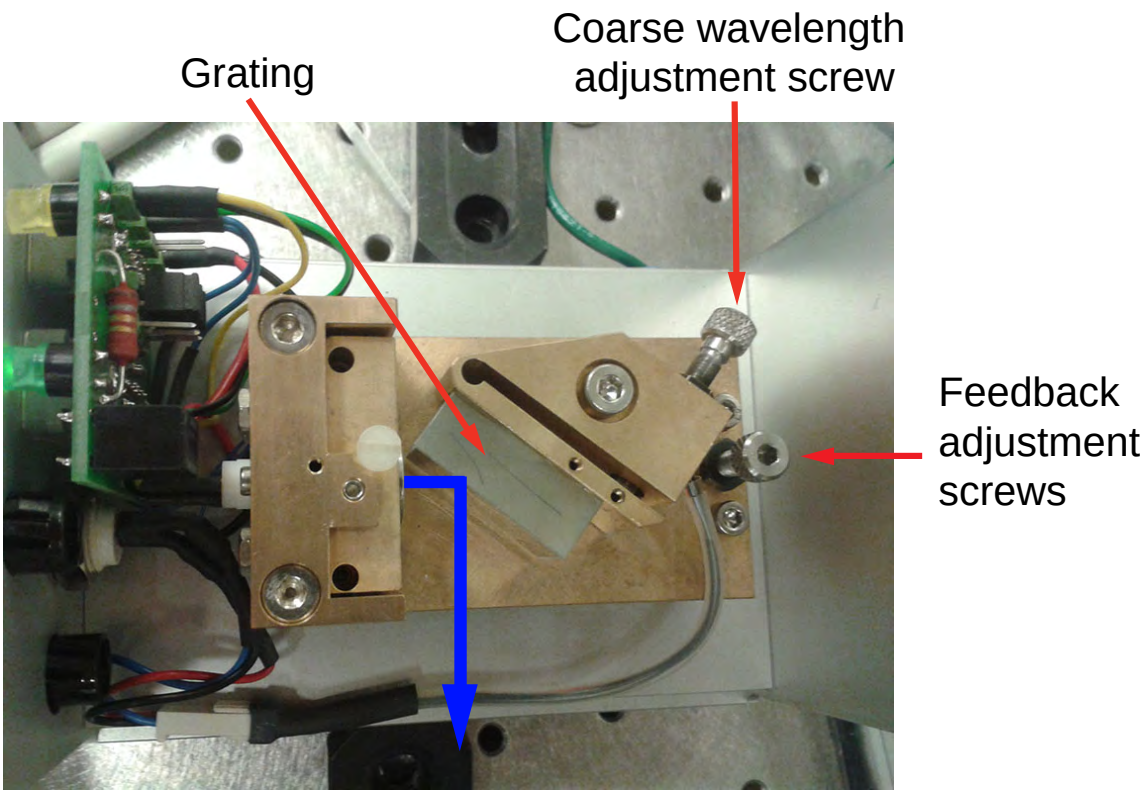

Figure 18: A picture of the inside of a Toptica laser (DL 100). The blue arrow shows the direction of the laser beam coming out of the laser. The wavelength is coarsely adjusted with the screw and the grating position. The feedback screws are used to optimize lasing.

The lasers are typically coupled to the traps with optical fibers from another optical table since the lasers are shared between experiments. Because the main Doppler cooling transition requires greater precision for the experiments, an additional instrument is used to control the frequency of the 397 nm laser, which also has the ability to turn on and off the laser. For our experiments we used an acousto-optic-modulator (AOM, Brimrose 7998). An AOM can control the frequency, intensity, and the direction of the laser beam. The device works by Bragg diffracting incoming light with acoustic wavepackets that are propagating through the crystal. The amplitude and frequency of the acoustic wavefronts can be changed to modulate the diffracted

light. For more information on the operation of AOMs, the reader is directed to Ref. [184].

For our experiments we used a double pass configuration to set up the AOM. Since the beams are fiber coupled to the traps, any change in the angle of the beam entrance to the fiber coupler results in loss of intensity on the trap side. However, scanning the frequency of the AOM results in changes of the angle. To overcome this, a double pass configuration is utilized. In experimental setups, the first order positive diffracted light which is retro-reflected through the AOM for a double pass is used. This removes the angle shift in the output beam such that the input beam is co-aligned with the output beam. To separate the beams we use polarization optics as shown in Fig. 19. Light is first passed through a half-wave plate which rotates the beam by 45 degrees. It then passes a polarizing beam splitter cube before a lens focuses it into the AOM. The diffracted beam on the other side of the AOM is then re-collimated with a second lens. The wanted diffraction order is selected with an iris while the rest are blocked. That light passes through a quarter-wave plate twice, which makes the output beam orthogonally polarized to the incoming beam.

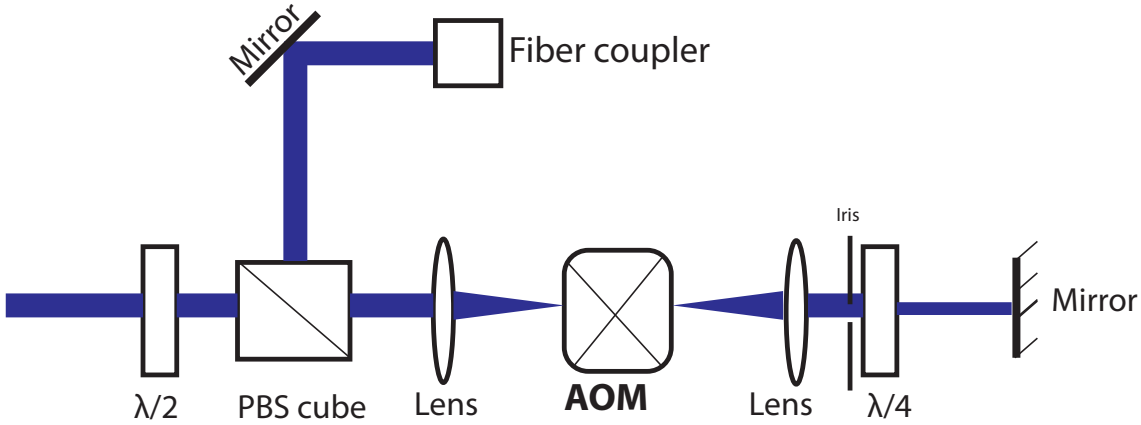

Figure 19: A schematic showing the optical setup for the double pass aucosto-optic modulator (AOM). The setup uses polarization to separate input and output beams which are co-aligned. $\lambda/2$ is a half-wave plate, PBS is a polarizing beam splitter cube,and $\lambda/4$ is a quarter-wave plate. The iris is used to block unwanted beams from being retro-reflected

4.1.1 Wavemeter

The frequency of the CW lasers is monitored with a HighFinesse WS/7 wavelength meter, which is housed in a thermally isolated casing. The instrument has an absolute frequency accuracy of 60 MHz and a frequency range of 350–1120 nm and acquisition speed of 150 Hz. However, since we have to monitor many lasers at once during the experiments, an external fast operating switch is coupled via a multi-mode fiber to the wavemeter. This reduces the the absolute accuracy of the wavemeter to a relative accuracy of 200 MHz. Once a month or so the wavemeter would drift due to thermal fluctuations of the room and the wavemeter was re-calibrated with a HeNe laser while an ion was trapped. Typical measured frequency changes after recalibrations were on the order of 100s of MHz.

4.2 Femtosecond laser system

For the resonance enhanced multiphoton dissociation experiments, we required a broadband laser that could address all the rotational levels. We use a mode-locked femtosecond Titanium-Sapphire (Ti:Sapph) laser. For our experiments, we used a Coherent Mira Optima 900-F femtosecond laser. The laser is pumped by a Verdi-V10 with 15 W of power and outputs about 2 W of mode-locked power that can be scanned from 700 nm to 980 nm. Pulses from the lasers come out at a repetition rate of 76 MHz and have a length below 200 fs with peak power of 176 kW.

To check that the pulse is not distorted when it passes through optics, we measured the characteristics of the laser pulses using frequency-resolved optical grating (FROG) method provided to us by Rick Trebino's group [185, 186]. The beam was measured at different locations before and after the trap. Briefly, a pulsed laser has an intensity and phase vs time (space), which can be described with an electric field written in the time domain as,

$$E(t) = Re\big[\sqrt{I(t)}e^{i\omega_0 t - \phi t}\big], \tag{84}$$

where $I(t)$ is the intensity and $\phi(t)$ is the phase. In the frequency domain, the field can be written as,

$$\tilde{E}(\omega) = \sqrt{S(\omega)}e^{-i\varphi(\omega)}, \tag{85}$$

where $S(\omega)$ is the spectrum and $\varphi(\omega)$ is the spectral phase. The FROG apparatus measures both shaped and unshaped pulses by measuring the intensity and phase of a femtosecond pulses. The FROG trace can be characterized as,

$$I_{FROG}(\omega,\tau) = \left[\int_{-\infty}^{\infty} E(t)E_g(t-\tau)e^{-i\omega t}dt\right]^2, \tag{86}$$

where $E(t)$ is the electric field of the unknown pulse, ω is the frequency, and τ is the delay. Thus a FROG measurement shows spectral resolved autocorrelations of

intensity versus the frequency and the delay to characterize the pulse. A typical FROG trace is shown Fig. 20.

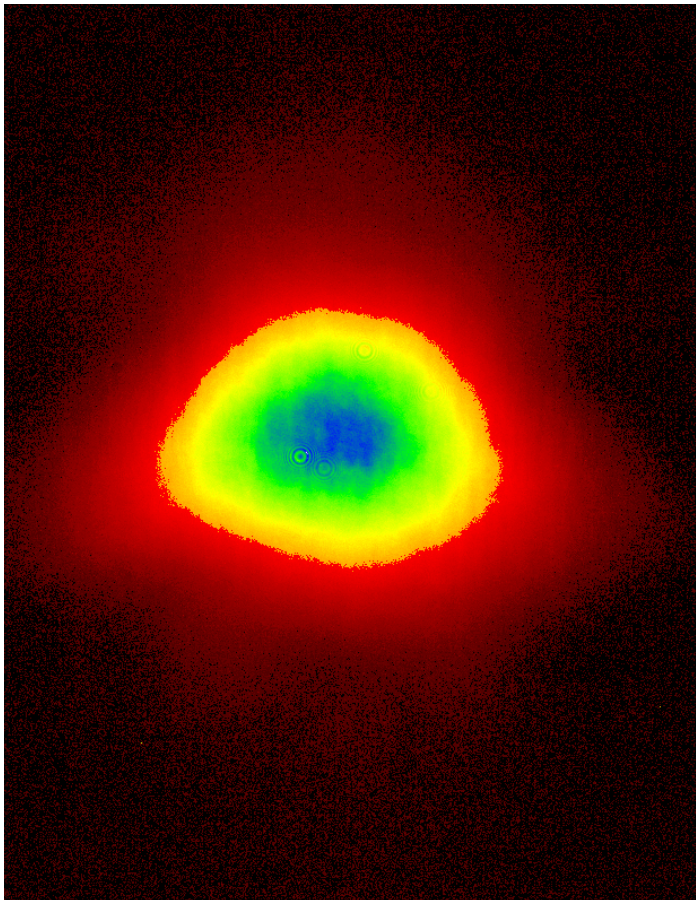

Figure 20: A FROG trace of the laser

The data from the FROG measurements is shown in the two plots below in Fig. 21. The temporal spectrum in Fig. 21a shows the intensity as a function of the delay, which gives information about the pulse length. According to the plot the pulse length is 163.2 fs, which is in agreement with the manufacture specifications. The frequency spectrum in Fig. 21b shows the width of the peak of the laser as a function of wavelength. At this central frequency, the width was 8.51 nm.

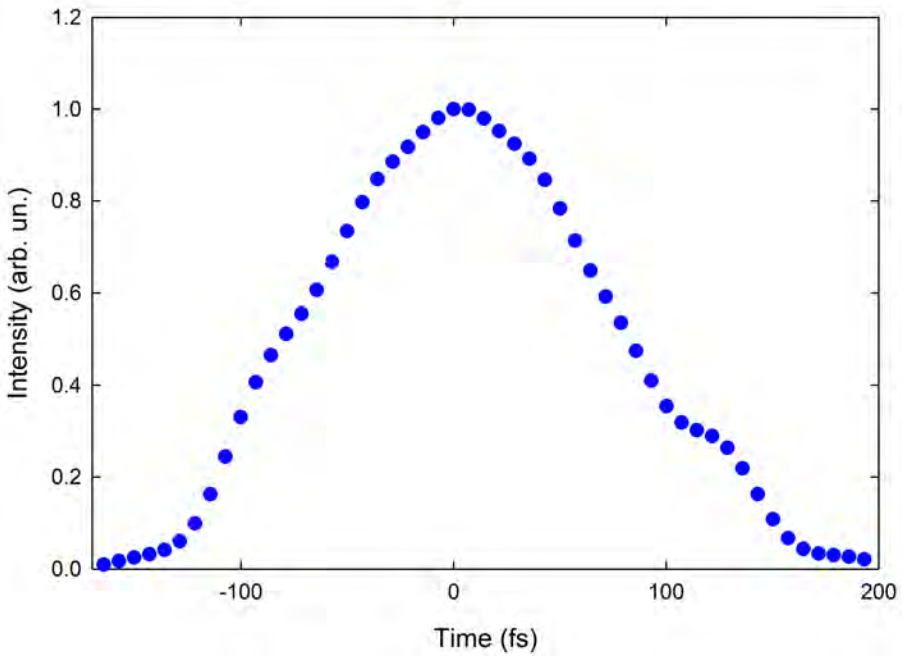

(a) Temporal spectrum

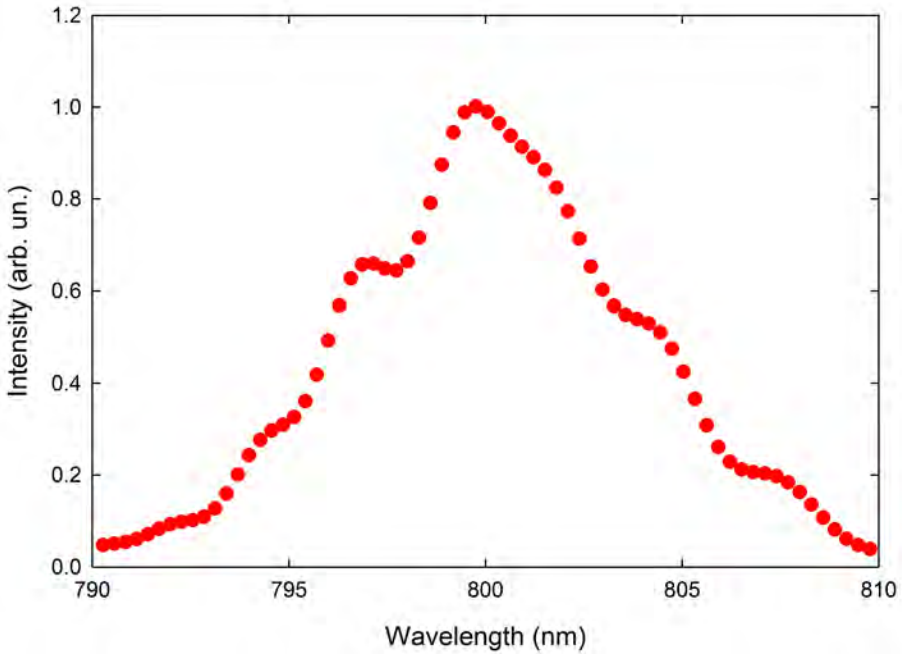

(b) Frequency spectrum

Figure 21: Spectrum from the FROG profile. (a) shows the autocorrelation between the intensity and the delay while (b) shows the autocorrelation between the intensity and the frequency.

To measure the frequency of the laser during the experiment, we used Ocean-Optics HR2000+CG spectrometer, which shows only the intensity as a function of the frequency.

4.3 Vacuum chambers

In order to trap and laser-cool ions, we need to put them in an isolated environment where collisions are minimized. For this reason, ultra-high vacuum(UHV) chambers are used in tandem with RF Paul traps. Typically, the stainless steel parts connected together with CF sealing are used to build the chamber. To maintain low pressures, an ion pump is used (Duniway Stockroom/Gamma Vacuum) with pump speeds of 50 L/s or more. An additional titanium sublimation pump is also used to remove any excess particles inside the chamber, which helps maintain low pressures inside the chamber. In the Brown lab, two UHV chambers with two different traps were used for molecular experiments. For historical reasons, we called them the molecular chamber and the atomic chamber. A drawing of the chamber housing each trap is shown in Fig. 22.

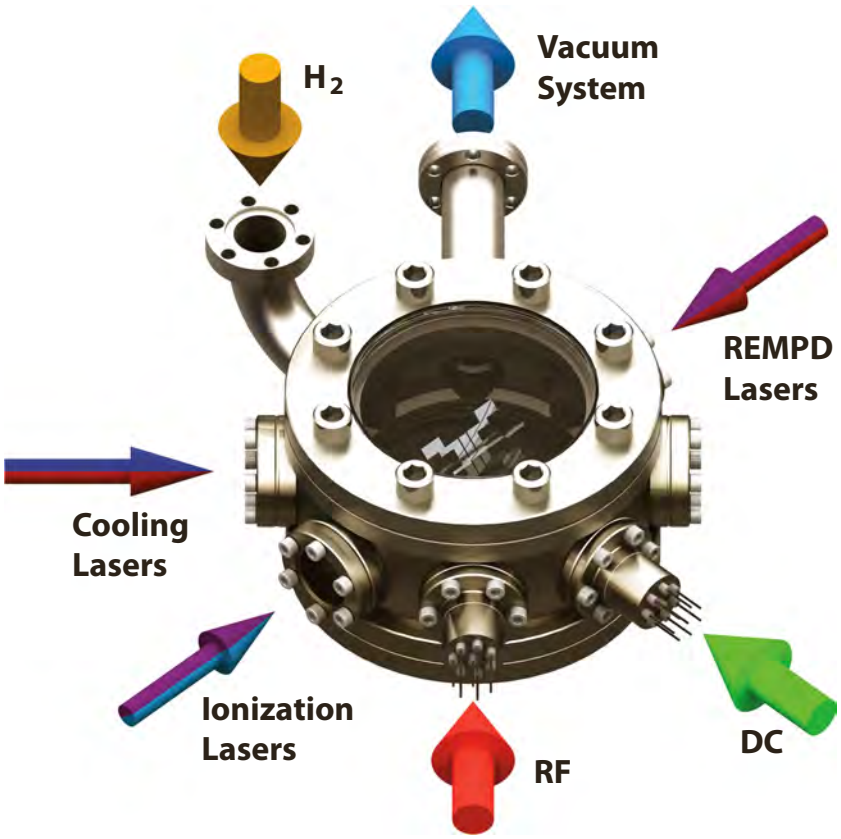

Figure 22: A schematic showing an assembled chamber. The arrows represents the components used to trap ions such as the RF and DC feedthroughs, the lasers, the vacuum system, and the H_2 leak valve.

4.3.1 Molecular Chamber

Laser-cooled atomic ions as probes for molecular ions

Kenneth Brown, C. Ricardo Viteri, Craig R. Clark, James E. Goeders,**Ncamiso B. Khanyile**, and Grahame D. Vittorini, *AIP Conf. Proc.* **1642**, 392 (2015)

We setup and initially trapped in the Molecular Trap which had an eleven segment trap designed by one of the former graduate student, James Goeders [187]. The trap is a 11-segmented trap which makes it possible to trap in five different regions. The electrodes are Nitronic 50 stainless steel with curvatures of about 0.5 mm. The trap has a radius (r_0=1.0 mm) where ions are trapped. Trapping RF voltage is applied to

diagonally opposed electrodes while the other electrodes are kept to RF ground. To confine the ions axially, DC voltage is applied to nine 3-mm-long electrodes diagonally opposite from each other while there are additional two 10-mm-long endcaps. To trap ions, the trap was driven at $\Omega/2$=10.41 MHz with 400V of RF voltage.

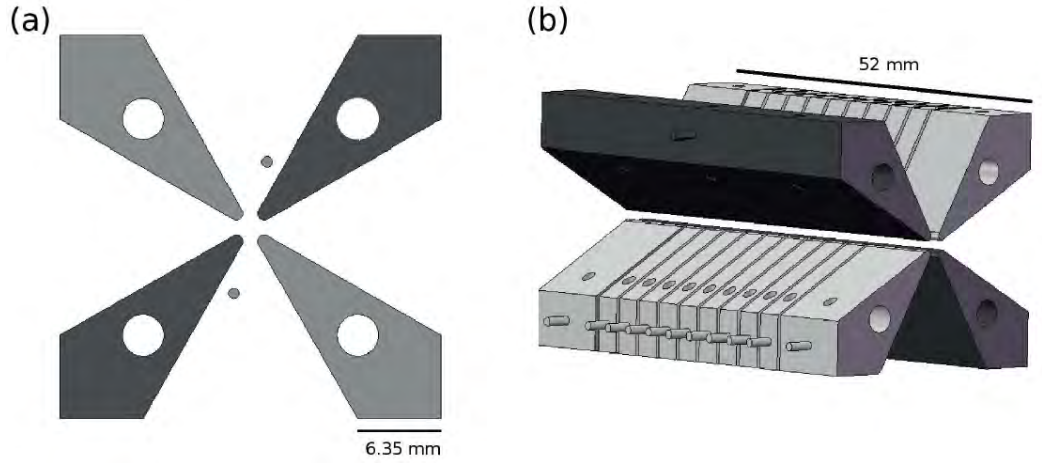

Figure 23: A schematic showing the 11 segmented Paul trap, we call the Molecular Trap. (a) Shows the cross section of the electrodes while (b) shows a 3D representation of trap.

4.3.2 Atomic Chamber

All the other experiments described in this thesis were done in the other chamber, which we historically called the Atomic Chamber. The experiments include trapping Yb^+ ions with the different isotopes (Chapter 2), sympathetic heating spectroscopy [188], sideband cooling of $^{40}Ca^+$ and $^{40}CaH^+$ [189], and measuring the vibrational overtones of $^{40}CaH^+$ (Chapter 5). The trap was designed by the Urabe group in Japan [190]. The trap is a 5-segmented trap with a radius (r_0=0.6 mm). Two diagonally opposed non-segmented stainless steel 1-mm thick, 3-mm long electrodes mounted on insulation spacers are used to apply RF voltage. The plates have a cross-section curvature of 0.5 mm. The DC voltage is applied to two of 3-mm-long segmented electrodes that are arranged at intervals of 0.5 mm to confine the ions

radially. To compensate for stray electric fields, additional voltage is applied to non-segmented electrodes and the electrodes at the center of the trap. To trap $^{40}Ca^{+}$, we drove the trap with 200V of RF voltage at $\Omega/2$=14.34 MHz.

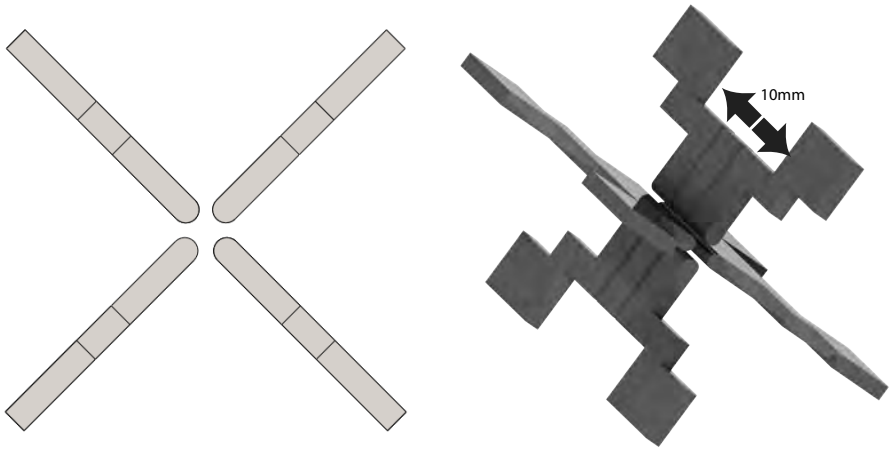

(a) RF electrodes (b) Full trap

Figure 24: A schematic of the 5-segmented Urabe trap. (a) shows a cross-section of the RF electrodes while (b) shows a 3D view of the trap.

4.4 Radio frequency drive

To trap ions, about 200 V of RF is applied to the electrodes. To generate the needed voltage, a functional generator is used to produce a sinusoidal wave at the desired frequency. The produced RF is the amplified with a commercial amplifier before being introduced into the trap. To introduce the voltage in the trap, a helical resonator is used, which matches the impedance between the trap and the function generator; enabling high voltages to be introduced in the trap. In addition, the resonator also acts as a filter that limits any noise injected into the trap [191]. The performance of a helical resonator is determined by the resonant frequency, $\omega_0 = \frac{1}{\sqrt{LC}}$ and the quality factor, $Q = \frac{1}{R}\sqrt{\frac{L}{C}}$, where L is the inductance and C is the capacitance. When designing the helical resonator, the various parameters shown in Fig. 25 are

taken into account.

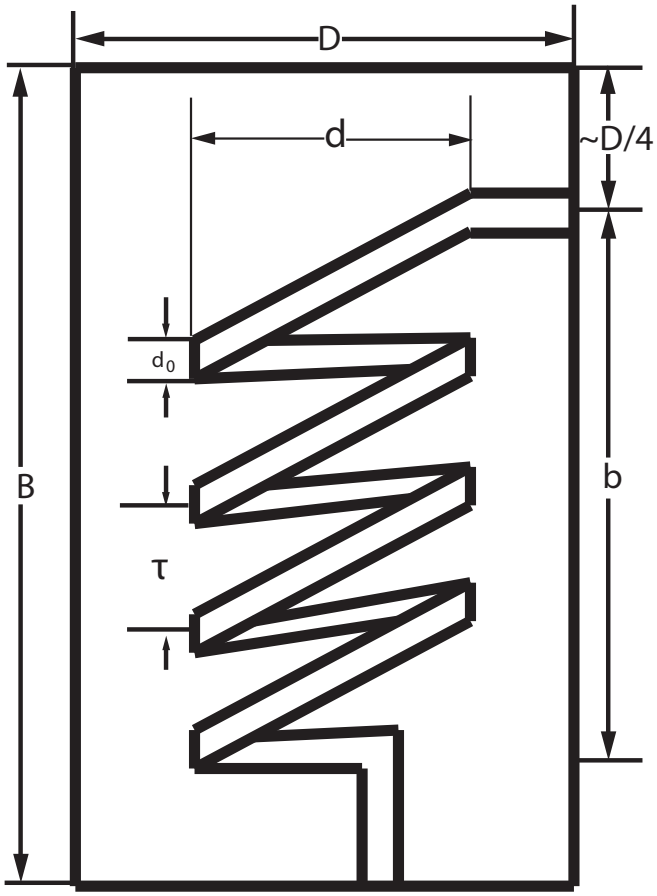

Figure 25: A schematic showing the design of a helical resonator. Here the case diameter is shown as D, the case height as B, the coil diameter d, coil height b, the winding pitch τ, the coil wire diameter d_0.

To design the helical resonator the following equations are used with the parameters above. In terms of the parameters, the quality factor can be express as,

$$Q = 35.9d\sqrt{f}, \tag{87}$$

where f is the resonant frequency of the resonator. Other characteristics can be calculated with the following equations,

$$N = \frac{2674}{d \cdot f}, \qquad Z_0 = \frac{136190}{d \cdot f}, \tag{88}$$

$$\tau = \frac{1759}{d^2 \cdot f}, \qquad d_0 = \frac{1}{2\tau}, \tag{89}$$

$$\tag{90}$$

where N is the number of turns and Z_0 is the characteristic impedance of an air-filled helical transmission. The characteristic capacitance resonator is given by

$$C_s \approx bK_{C_s}(d, D), \tag{91}$$

where

$$K_{C_s} = 39.37 \frac{0.75}{log(\frac{D}{d})} \times 10^{-12} F/m. \tag{92}$$

Generally, these parameters act as a guide for the design. The resonator is normally optimized empirically to suit the needs of the experiment. For the resonator used in the atomic trap, the resonant frequency was 14.14 MHz while the quality factor Q was 120. The Q factor is relatively high for a resonator at this low frequency.

4.5 Ion detection

Trapped ions are detected via fluorescence from the spontaneously emitted photons on the cooling transition. Since the scattered photons from the ions are scattered in random directions, efficient imaging optics with high numeral apertures (N.A.) are needed to collect the photons and image them [116]. In addition, the imaging optics need to work close to the diffraction limit. The collected photons are then imaged with an EMCCD camera and counted with a photon multiplier tube (PMT). For our experiments the lens system was designed and optimized with Zeemax commercial software. A schematic of the lens system used to collect photons is shown in Fig. 26.

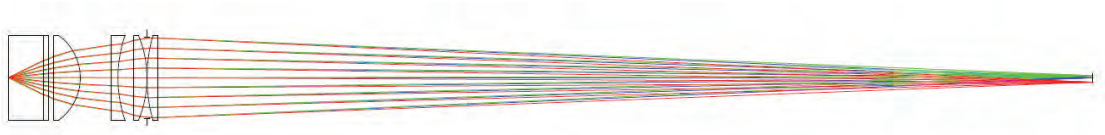

Figure 26: A design of the lens system to image fluorescence from a 4.5 inch octagon. The lenses used are NBK-7 coated to minimize back reflection from the lens windows

The lens system had an N.A.=0.43, a magnification of 10× and had a total length of 660 mm. The lenses used were bought from Thorlabs inc, and they were LA1401(d=2 inches, f=60.0 mm), LC1611 (d=2 inches, f=-150.0 mm), LA1384 (d=2 inches, f=125.0 mm), LA1399 (d=2 inches, f=175.0 mm), where d is the diameter of the lens and f is its focal length. The lenses are listed in their order of appearance from the trap.

4.6 Frequency stabilization of laser systems

For laser cooling experiments, the frequency of the laser must not drift by more than the linewidth of the transition (≈20 MHz). However, the laser frequency is affected by environmental factors such as the fluctuations in temperature and pressure. To counter this, an external cavity is used to lock the frequency of the laser.

Lasers are often locked to one of the modes of a Fabry-Perot interferometer (FPI) [192]. However, because an FPI cavity needs to be actively temperature controlled and under vacuum to minimize pressure fluctuations, it makes the setup expensive. A cheaper alternative is to use a cavity in ambient pressure, which is referenced to a stable laser [193, 194]. In our lab, we use a stabilized HeNe laser with a drift of about 2 MHz/8 hrs, which is ideal for laser cooling experiments.

The transfer cavity works by aligning a stable laser, in our case a HeNe, and unstable laser(s) to a cavity. Light transmitted from the cavity is monitored while the cavity length is scanned with a piezo actuator, which produces peaks as a function

of the distance traveled by the piezo [195]. The cavity is locked to the position of the HeNe peak while the lasers are locked to their position through feedback to the laser.

Light enters the cavity by leaking through a backside-polished mirror. The light is reflected between the two cavity mirrors. As the piezo is scanned, light in the cavity is amplified when the mirror spacing is in resonance with an integer number of the half-wavelengths like,

$$2L/\lambda = n, \tag{93}$$

where L is the length of the cavity, λ is the wavelength, and n is an integer. This causes constructive interference when $\delta n = \pm 1$. The intensity of the light inside the cavity increases and leaks through the back mirror where it is detected with a photodetector.

4.6.1 Realization of a transfer cavity

We locked three lasers,397 nm, 866 nm, and 854 nm with a transfer cavity to the HeNe. Since the 397 nm laser is generated by frequency, we used the fundamental to lock it because the IR wavelengths have better finesse with the mirrors we used. The setup and the cavity are shown below in Fig. 27.

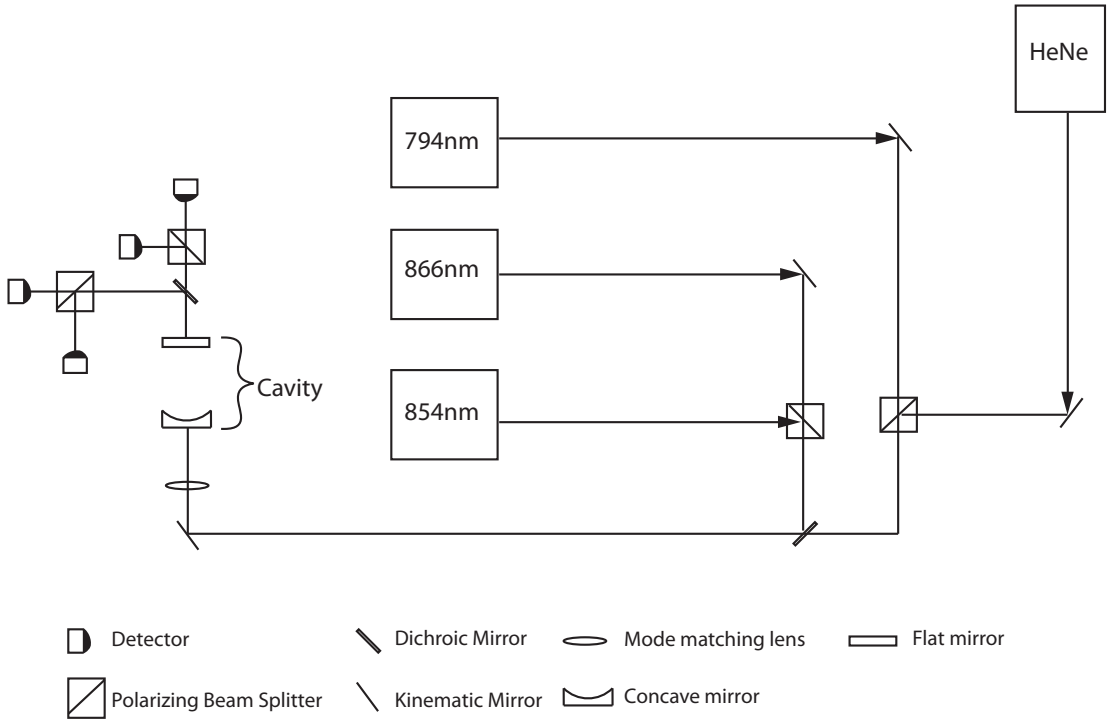

Figure 27: A schematic showing the optical layout for the transfer cavity. Lasers are coupled into the cavity using a combination of polarization and band-pass filters. An achromatic lens in front of the cavity mode-matches the lasers to the cavity. The light transmitted from the cavity is sent to detectors for signal processing and feedback to the lasers.

An important feature of coupling light into the cavity is the use of polarization and band pass filters to combine and separate the different wavelengths. Since the 794 nm and the 633 nm of the laser are relatively close in wavelength, we use a polarization beam splitter (PBS) cube to combine them and we do the same for the 854 nm and the 866 nm. To combine the 854/866 nm and the 794/633 nm lasers, we use a dichroic mirror (Thorlabs DMSP-805). The lasers are then mode-matched to the cavity using an achromatic lens where the lasers are focused to the back mirror. The cavity is a half-concentric etalon with the first mirror being a backside polished concave mirror (Thorlabs CM254-075-E02P) and the back mirror is a flat broadband

(Semrock MaxMirror) mirror that has over 99% reflectivity over a wide range as shown in Fig. 28. The lasers are separated in the same manner they were combined to individual detectors. To ensure no leakage of other light to the detectors, narrow band filters are placed in front of each detector.

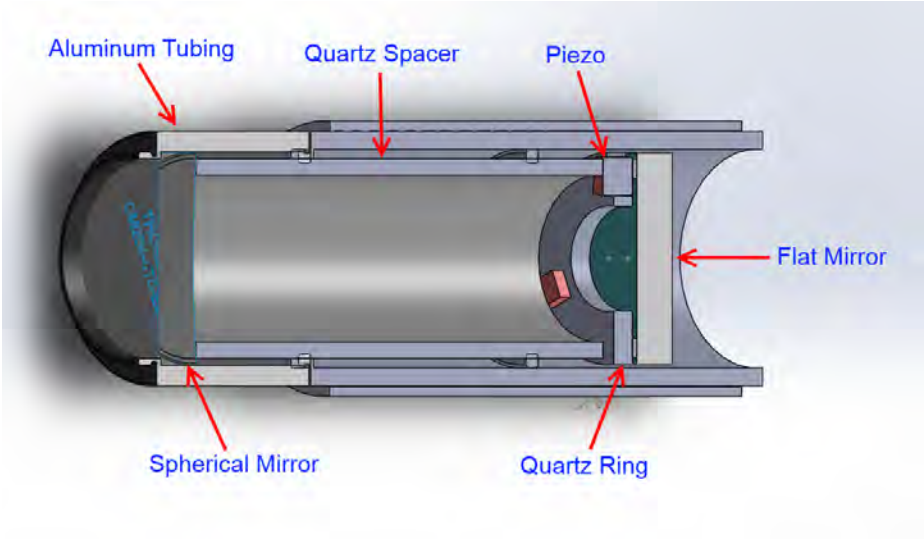

Figure 28: A schematic showing a cross section of the cavity. The cavity is made of a concave mirror and a flat mirror inside a 1-inch tube. The mirrors are separated by a low-thermal-expansion quartz spacer. The flat mirror is scanned with a piezo to cover the free spectral range of the lasers.

The cavity is housed in a one inch tube and the two mirrors are separated with a low-expansion quartz spacer ($\delta L/L \approx 0.54 \times 10^{-6}$ K^{-1}), three piezos are mounted on the back, flat mirror and a sinusoidal voltage of 50 V is applied at 30 Hz. This gives the cavity a scanning range of about 2.1 μm, which is enough to cover the free spectral range of all the lasers. A scan showing the transmission of the 397 nm laser as the piezo is scanned is shown in Fig. 29.

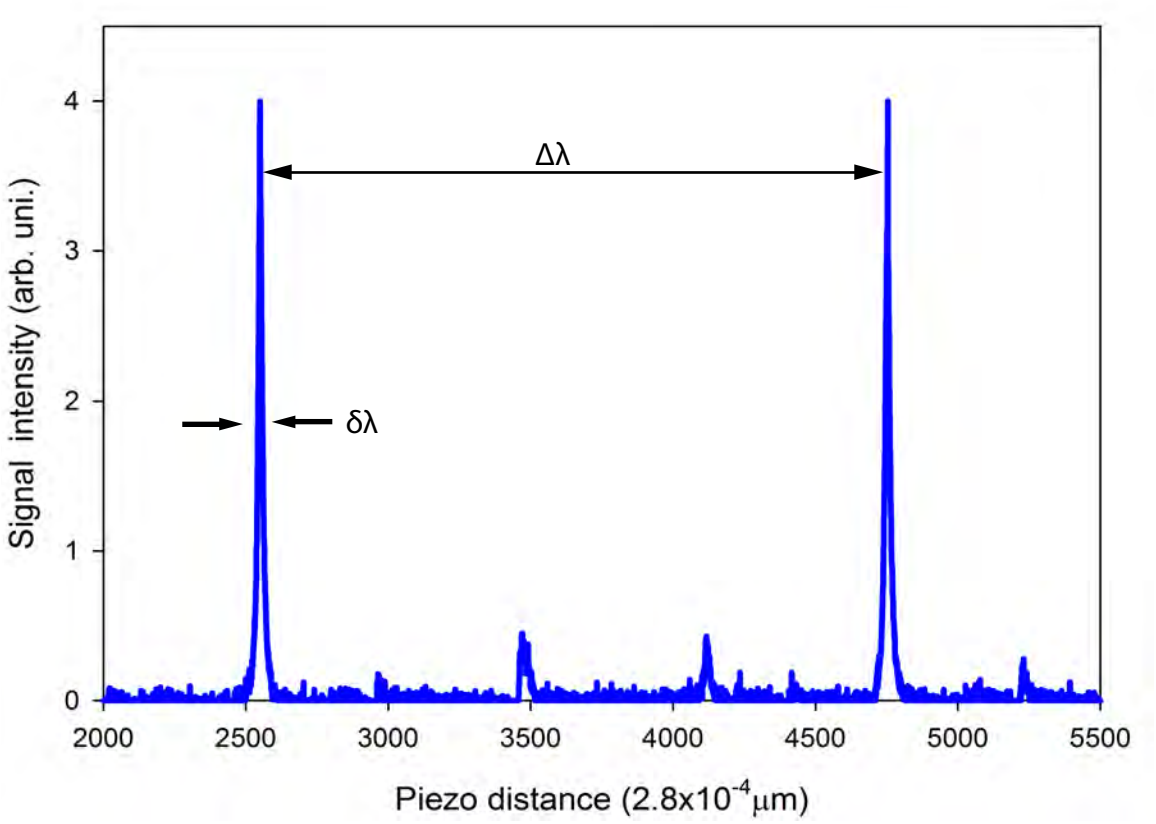

Figure 29: Transmission of the 397 nm laser through the cavity. The peaks occur when the piezo is in a position where it is on resonance with half-integer wavelengths of the laser. The distance between two peaks, $\Delta\lambda$, is called the free spectral range. The full width half maximum, $\delta\lambda$, is the linewidth of the cavity. Together these two parameters describe the finesse of the cavity by $f = \frac{\Delta\lambda}{\delta\lambda} = \frac{\pi R^{1/2}}{(1-R)}$, where R is the reflectivity of the mirrors. For our transfer cavity, the finesse is ≈120.

4.6.2 Locking performance

To lock the lasers we used home-made photodiode detectors, along with National Instruments cards to collect the data, process the error signal and send feedback to the laser. To evaluate the performance of the cavity, we looked at the frequency the 397 nm laser as a function of time is shown below in Fig. 30.

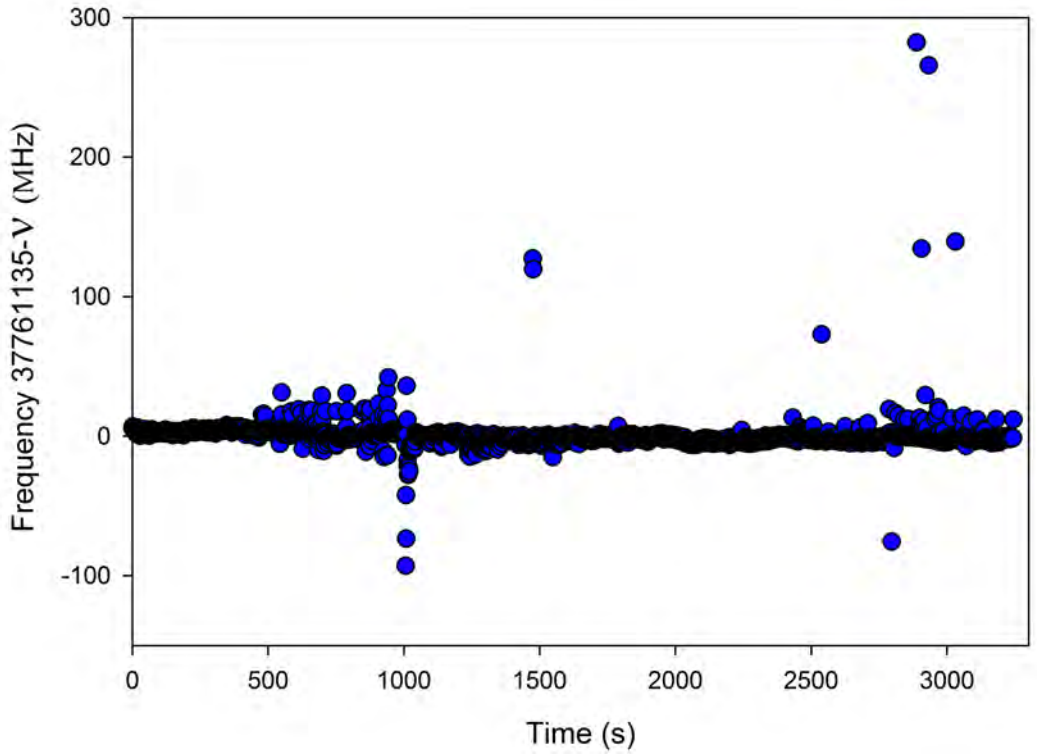

Figure 30: A plot showing the frequency of a locked 397 nm laser over time. The spikes in the frequency are from sudden pressure changes in the room such as someone opening and closing the door. The black trace is a running average of the individual blue data points. The measurement in the case is also limited by the accuracy of the multi-channel switch of the wavemeter, which has a relative accuracy of ±200 MHz.

To test the stability of the locked laser we plot the Allan variance of the frequency of the laser over time. The Allan variance is an averaging statistic used to measure the stability of an oscillator [196, 197]. The Allan variance is described by the equation,

$$\sigma_y(\tau) = \sqrt{\frac{1}{2(M-1)} \sum_{i=1}^{M-1} (y_{i+1} - y_i)^2}, \tag{94}$$

where y_i describes frequency offset[1] measurements of the $y_1, y_2, ...y_n$ values, M is the

[1]This is the deviation of the measured frequency from the ideal frequency.

number of values in the series, and τ is the segment between the data points measured in seconds. A plot of the Allan variance shows the improvement of the measurement as the averaging period (τ) is increased. To test the stability transfer lock we input the measurements of the 397 nm laser frequency from the WS7 in to the Allan equation and we get the plot shown in Fig. 31.

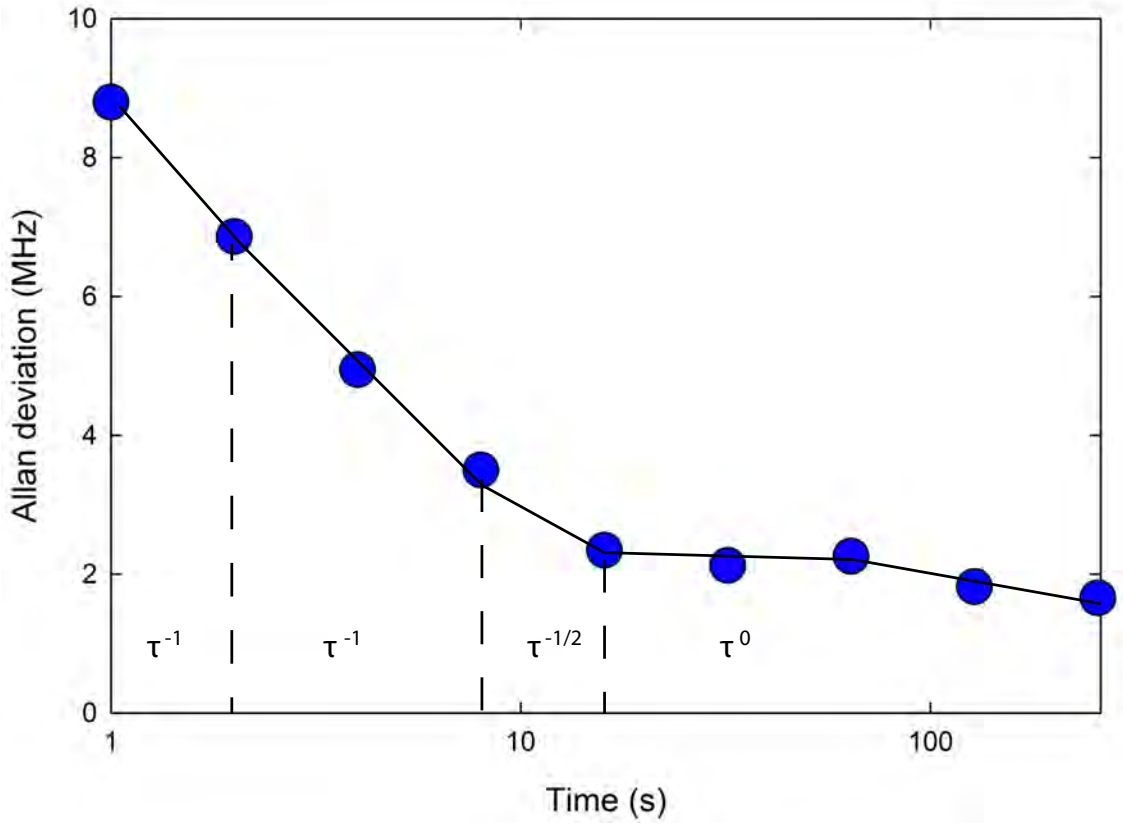

Figure 31: An Allan variance of the locked 397 nm laser, which was locked to the transfer cavity. The plot shows that the deviation in the laser reaches about 2 MHz over the course of a day. The slope of the Allan variance identifies the type of noise in the system. τ^{-1} is flicker noise and white noise, $\tau^{-1/2}$ is the white frequency noise and τ^0 is the flicker frequency. The Allan variance shows the removal of flicker noise and white noise as we increase the averaging. Longer averaging though can increase the noise in the form of random walk noise. In this graph, if we continued to average, we would expect the slope to be positive. Normally, we would expect that increasing the averaging time further than tau^0 would result in poor performance, hence the graph would start going up. In our example, it looked like we had stopped the experiment prematurely.

We can see from these plots that the transfer cavity effectively stabilizes the laser

over a long time. The spikes in the frequency data represent short term perturbations such as an opening and closing of the door, which the cavity does not respond fast enough to. However, during the course of a day we see stabilities of ± 4 MHz, which is sufficient for laser cooling experiments.

CHAPTER V

OBSERVATION OF VIBRATIONAL OVERTONES BY SINGLE MOLECULE RESONANT PHOTODISSOCIATION

This chapter is currently in review.

Ncamiso Khanyile, Gang Shu and Kenneth Brown, *in review* (2015)

5.1 Introduction

Precision spectroscopy of molecules and molecular ions can yield insight into the fundamental physical constants and astrochemical processes [198, 199]. Coulombic crystals of molecular ions and laser-cooled atomic ions are ideal systems for these measurements [98]. Cold molecular ions have been used to study cold chemistry [57, 103, 200], to control rovibrational states [66, 67, 70, 73, 201, 202], and to precisely measure molecular transitions [63, 203]. However, expanding these techniques to a wider array of molecular ion species remains a challenge due to the lack of experimental data on molecular ions transitions. This requires new methods for obtaining spectral information. The spatial localization of molecular ions in a Coulomb crystal results in the required ion density for spectroscopy with low ion numbers relative to traditional techniques. This enhanced sensitivity has recently been used to directly observe dipole-forbidden transitions, whose transition frequencies were previously inferred from measurements of allowed transitions [203].

Coulombic crystals composed of laser-cooled atomic ions and molecular ions provide a pristine environment for studying the properties of molecules. The laser-cooled

atomic ions serve as both a coolant that reduces the temperature and a sensitive detector that allows for single molecule measurements. The system has been used to study fundamental reaction dynamics ranging from kinetic isotope effects [103] to observing the relative reaction rates of molecules whose shape differs by the orientation of a single bond [57]. It is also a natural system for precision measurements of molecular ion transitions. Molecular transitions allow for the precise study of fundamental constants using physics that is inaccessible in atomic systems [204, 205]. Spectroscopy with Coulomb crystals has been used to directly measure dipole-forbidden transitions in N_2^+ [203] and accurately determine the rovibrational spectrum of HD^+ [63]. Future experiments to test the stability of fundamental constants in time have been proposed [28] using the two-ion-species techniques already exploited in the most precise atomic ion clocks [31, 121].

Systems built for high-precision measurement are often incompatible with the survey spectroscopy required to find unknown transitions. However, this is not the case for Coulomb crystals, where the long ion storage time provides multiple opportunities to probe the molecule and the fluorescence of the laser-cooled atomic ion serves as a fast, low-noise detector. $^{40}CaH^+$ is a candidate molecule for testing the possible variation in the proton-to-electron mass ratio [141]. It is also expected to be relatively abundant in space due to observation of CaH, but has not yet been directly observed [17]. In both cases, laboratory measurements of bound transitions in $^{40}CaH^+$ are required for scientific progress

Here we measure two previously unobserved vibrational overtones of $^{40}CaH^+$ without any prior experimental data to guide our search. We use small crystals of $^{40}Ca^+$ and $^{40}CaH^+$ to observe vibrational transitions via resonance enhanced multiphoton dissociation detected by $^{40}Ca^+$ fluorescence. Based on theoretical calculations [25], we assign the observed peaks to the transition from the ground vibrational state, $\nu = 0$, to $\nu = 9$ and $\nu = 10$. Our method allows us to track single molecular events, and it

can be extended to work with any molecule by using normal mode frequency shifts to detect the dissociation. This survey spectroscopy serves as a bridge to the precision spectroscopy required for molecular ion control. Our results are an important step towards using molecular vibrations to test possible time variation in the proton-to-electron mass ratio [28, 29, 141] and to control cold molecular reactions one molecule at a time.

5.2 Methods

We use laser-cooled $^{40}Ca^+$ ions to sympathetically cool $^{40}CaH^+$ molecules. The $^{40}Ca^+$ ions are trapped in a RF Paul trap ($r_0 = 0.6$ mm) driven at $\Omega = 2\pi \times 14$ MHz to confine the ions radially, while static DC voltage applied at the endcaps confines the ions axially. The trap is kept at a base pressure of about 4×10^{-9} Pa. The ions are detected by laser induced fluorescence at 397 nm onto a photon multiplier tube (PMT) and electron multiplying charge coupled device (EMCCD) camera. A narrow bandpass filter is used to ensure that only 397 nm light is detected.

A $^{40}CaH^+$ molecule is produced by leaking about 5×10^{-7} Pa of molecular H_2 into the chamber via a leak valve. A chain consisting of three $^{40}Ca^+$ ions is trapped before leaking in the H_2. The $^{40}CaH^+$ is produced via inelastic collisions in the gas phase between $^{40}Ca^+(4P_{1/2})$ and the H_2 as $^{40}Ca^+ + H_2 \rightarrow {}^{40}CaH^+ + H$. The occurrence of a reaction is determined when one of the ions goes dark and there is a drop in fluorescence counts. Once a reaction occurs, the leak valve is closed and the experiment is delayed until the base pressure is reached. After this pump down time, the internal degrees of freedom of the molecule are expected to be at room temperature due to weak coupling with the cold translational degrees of freedom. The identity of the molecule can be determined by resolved sideband spectroscopy [206] and under these experimental conditions we have only observed the formation of $^{40}CaH^+$.

To measure the vibrational overtones of $^{40}CaH^+$, we use $(1 + 1')$ REMPD. A

broadband mode-locked Ti:Sapph (IR) laser excites a specific vibrational transition of $^{40}CaH^+$, a second photon, a fixed ultraviolet (UV) cw laser (380 nm) dissociates the ion from the upper vibrational state by coupling it to a repulsive electronic state. Upon dissociation, the previously dark $^{40}CaH^+$ ion, will be broken into $^{40}Ca^+$ + H, the $^{40}Ca^+$ will fluoresce again and there will be an increase in fluorescence counts as shown below in Fig. 33. Other possible dissociation channels, including two UV photon absorption and UV induced electron bombardment, are measured to be low compared to the REMPD dissociation rates by performing control experiments with the IR blocked. A pinhole before the PMT allows partial light collection from all three ions and reduces background due to scattered light. Misalignment from the crystal center results in three distinct collection efficiencies for each ion position. This allows us to detect the position of the dark ion from the fluorescence as shown below in Fig. 33.

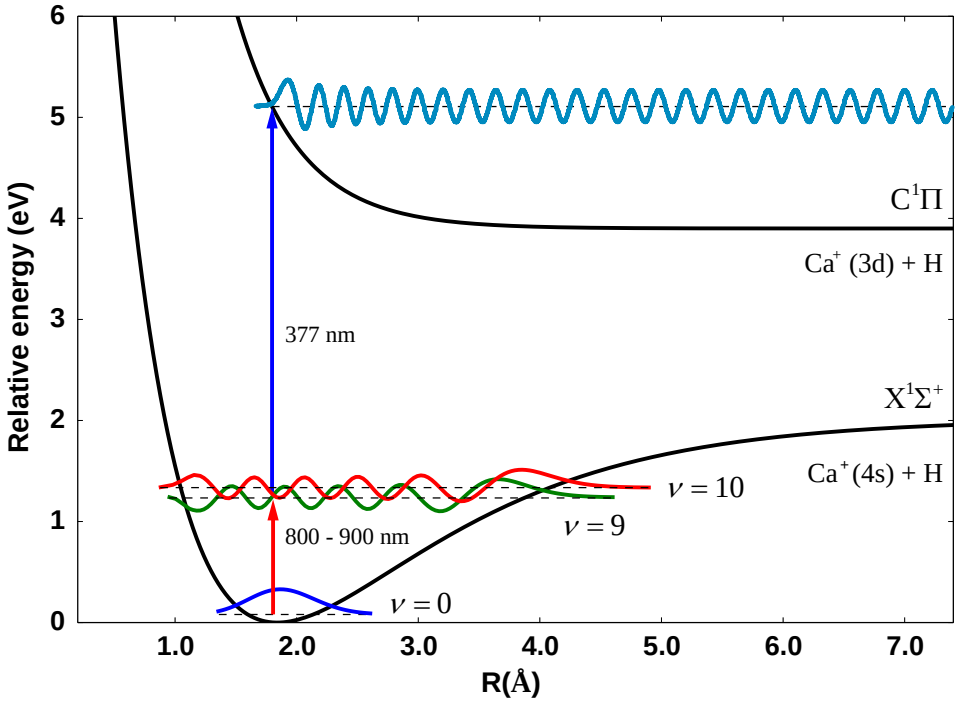

Figure 32: Energy level diagram of $^{40}CaH^+$. Simplified $^{40}CaH^+$ energy level diagram showing the overtones excited by a pulsed, tunable infrared laser (800-900 nm). A second ultraviolet laser (377 nm) excites the overtones to the unbound state to dissociate the molecule.

The calculated values for $^{40}CaH^+$ properties are from Abe *et al.* [25] and based on the method NRel/cc-pCV5Z/CASPT2.

Resonance Enhanced Multi-Photon Dissociation (REMPD) is a common tool in physical chemistry where conditional on a resonant transition a final photon dissociates the molecule. It can be applied to study the vibrations of molecules from diatomics with a single electron [64] to peptides [207]. Ion fragments are typically detected by an electron multiplier after mass selection [207, 208]. Embedding the molecular ions in laser-cooled atomic ions opens up other approaches of detection based on changes in the Coulomb crystal shape [209] and modulation of the atomic

ion fluorescence by driving the resonant motion of the molecular ions [64]. Resolved sideband spectroscopy on a narrow transition of the atomic ions can also be used to identify the fragments [206]. For the case of $^{40}CaH^+$, the measurement is simplified by the trapped fragment $^{40}Ca^+$ fluorescing brightly. This allows us to use the ion recycling approach that was previously used to measure the reaction kinetics of $^{40}Ca^+$ + HD by direct dissociation [210].

Although the molecular ion is at a translational temperature of a few millikelvin, the internal degrees of freedom are in equilibrium with the room temperature vacuum chamber via black body radiation. The calculated vibrational frequency of the molecule is 1478.4 cm^{-1} and we expect that the molecule will be in the ground vibrational state $X^1\Sigma^+$ greater than 99.9% of the time [25]. On the other hand, the calculated ground state rotational constant, 4.711 cm^{-1}, is small relative to room temperature. The rotational states will be populated with an expected value of $J = 5.36$ and the lowest ten J states are expected to have more than 94% of the population. Our experiment uses a single molecule at a time, but the blackbody radiation will randomize the J state on the order of minutes. To cover this rotational broadening we use a 150 fs mode-locked laser to drive the overtones. Alternative approaches include reducing the rotational state space by sympathetic cooling with a buffer gas [70] or a cloud of laser-cooled neutral atoms [73] or prepare the molecular ions at a specific state by threshold ionization [209]. Rotational cooling by optical pumping [66, 67, 211] is currently impossible for $^{40}CaH^+$ due to the lack of data on bound transitions.

The experiment takes place in a chamber described previously [188]. We start with loading three $^{40}Ca^+$ ions by isotope selective photoionization and then laser cooling the ions to form a three ion chain. Hydrogen gas is leaked into the chamber at 5×10^{-7} Pa until a single ion reacts as detected by a loss of fluorescence. Occasional collisions with background gas will rearrange the ion chain as observed by the relative position of the dark ion. A pinhole in front of the photomultiplier tube allows us to

detect these collisions by modulation in the photon signal as shown in Fig. 33.

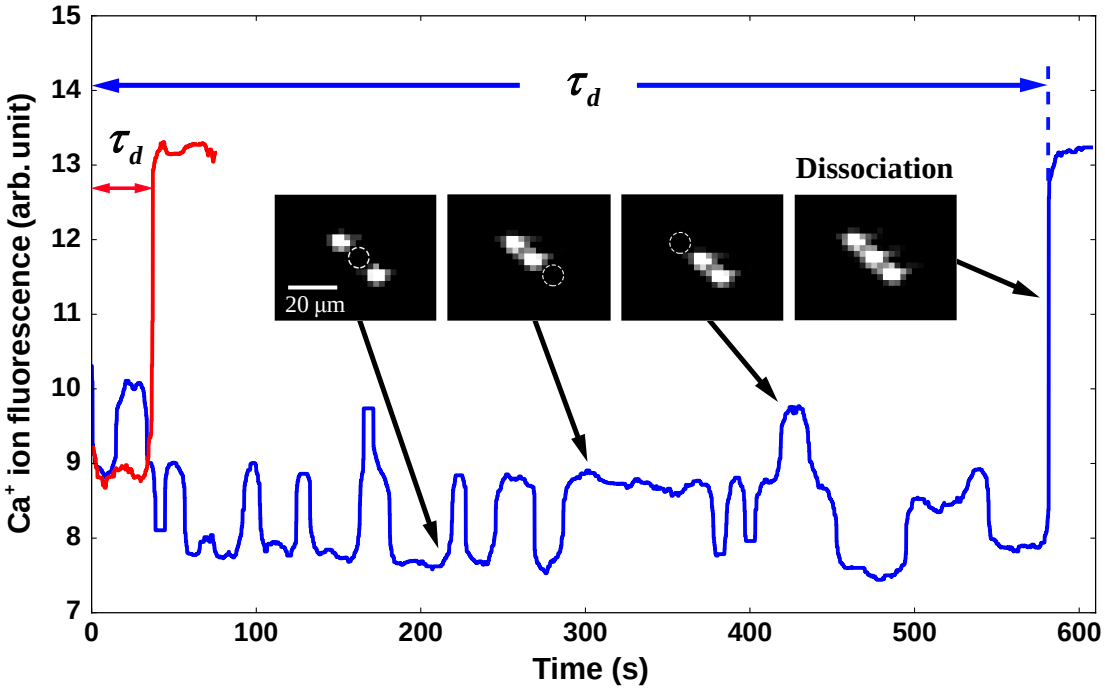

Figure 33: Dissociation measurement. After reaction with hydrogen, a mixed Coulomb crystal of two $^{40}Ca^+$ ions and one $^{40}CaH^+$ ion. The dissociating lasers are applied and the time to dissociation, τ_d, is measured by observing the change in fluorescence. The red trace shows an example dissociation event when the infrared laser is resonant with an overtone. The blue trace is an event when the infrared laser is blocked. A pinhole in the optical system allows us to correlate fluorescence with not only the number of $^{40}Ca^+$ ions but also the relative position of the molecular ion.

The two photon photodissociation occurs by first exciting a vibrational overtone of $X^1\Sigma^+$ and then photodissociating to the state $C^1\Sigma$ as shown in Fig. 32. We drive the overtone using a femtosecond mode-locked spectroscopy laser with 5 nm bandwidth, allowing us to ignore the line broadening due to rotational transitions. The second photon comes from a continuous-wave laser at 377 nm. For each central wavelength of the spectroscopy laser, we expose the molecular ion to the dissociation lasers and record the time for the molecule to dissociate, τ_d as shown in Fig. 33. The transition

strength is proportional to $1/ < \tau_d >$.

5.3 Results and discussion

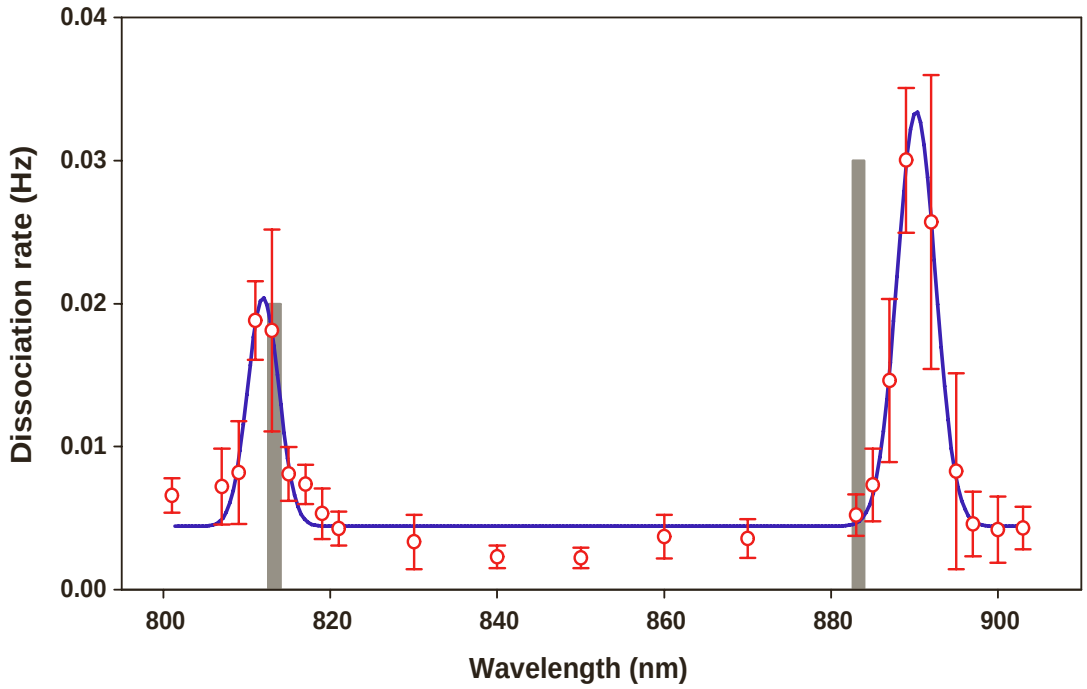

Figure 34: $^{40}CaH^+$ vibrational overtone spectra. The measured τ_d are averaged over eight experiments and the inverse is plotted as a function of the IR wavelength. Error bars are propagated from the standard deviation of $\langle \tau_d \rangle$. The data reveal two peaks which are fit assuming a Gaussian line shape. Gray bars are centered at the calculated theoretical values[25] for the $\nu' = 10 \leftarrow \nu = 0$ and $\nu' = 9 \leftarrow \nu = 0$ overtones.

The spectrum clearly shows two peaks which we identify as the $\nu' = 10 \leftarrow \nu = 0$ and $\nu' = 9 \leftarrow \nu = 0$ overtones of $^{40}CaH^+$ based on theoretical calculations [25] as shown in Fig. 34. We measure the $\nu' = 10 \leftarrow \nu = 0$ transition to be at 812(3) nm compared to the theoretical value of 813.3 nm and $\nu' = 9 \leftarrow \nu = 0$ transition to be at 890(3) nm compared to the theoretical value of 883.3 nm. This disagreement is in line with observed differences between calculated and measured vibrational transition frequencies in other metal hydrides [25].

Our experimental setup was intended for high-precision quantum logic spectroscopy [212] experiments on molecular ions. We have shown that the same setup can be used for the preliminary large range spectroscopy necessary to observe even weak lines despite trapping only a few ions at a time. The next step for precision spectroscopy of $^{40}CaH^+$ is to reduce the rotational temperature by sympathetic cooling with neutral atoms and then rotationally resolve these transitions and the fundamental transition [70, 73]. Then quantum logic spectroscopy can be performed on ground state cooled $^{40}Ca^+$-$^{40}CaH^+$ crystals [189] in order to reach the precision necessary for observing relative changes in fundamental constants [31].

Our current experiment takes advantage of the fluorescence of the dissociated product and can be easily applied to other fluorescent product ions. The method can be modified for dark product ions by periodically blocking the dissociation laser and measuring the mass of the product ion. This can be achieved by monitoring the sidebands of the atomic ions and calculating the mass of the unknown ion from the observed normal modes [206]. We expect that few ion Coulomb crystals will provide a method for discovering the spectra of astrochemically relevant ions that are difficult to make in the high numbers required for traditional spectroscopic methods.

The two photon photodissociation occurs by first exciting a vibrational overtone of $X^1\Sigma^+$ and then photodissociating to the state $C^1\Sigma$ as in Fig. 32. We drive the overtone using a femtosecond mode-locked [pulsed] spectroscopy laser with 5 nm bandwidth, allowing us to ignore the line broadening due to rotational transitions. The second photon comes from a continuous-wave laser at 380 nm For each central wavelength of the spectroscopy laser, we expose the molecular and record the time for the molecule to dissociate, τ_d. The transition strength is proportional to $1/ < \tau_d >$ Fig. 33.

5.4 Experimental tests and controls

There are different mechanisms that can lead to the dissociation of the molecule inside the trap. To ensure that the signal we obtained from the measurement was due to resonant dissociation only, we conducted some experimental controls. The molecule can be dissociated by background collisions, successive excitation caused by absorbing many IR photons, electron impact dissociation from electrons scattered of the electrodes of the trap. These can compete with REMPD and were investigated.

5.4.1 Infrared multiple photon dissociation

Prior to conducting the experiment, we worried about the competition between REMPD and infrared multiple photon dissociation (IRMPD). This is a process where absorption of multiple infrared photons can induce dissociation of strongly bound molecules [81, 156, 166, 176, 213]. IRMPD requires the absorption of a few hundred photons; hence, very strong gas discharge lasers are used such as CO_2 lasers. The MIRA laser has very high peak power (176 Kilowatts) and delivers about 1.13×10^{11} photons per pulse, which could supply the necessary number of photons needed for dissociation. The energy needed to couple the ground state of $^{40}CaH^+$ ($X\ ^1\Sigma^+$) with the repulsive excited electronic state ($C\ ^1\Pi$) at 272 nm could be achieved by three photon excitation close to the $\nu' = 10 \leftarrow \nu = 0$ transition at 816 nm as shown below in Fig. 35a. We investigated the possibility of such an event occurring by irradiating the crystals with the IR laser only around where we expect the peak. The data was found to be consistent with no peak as shown in Fig. 35b.

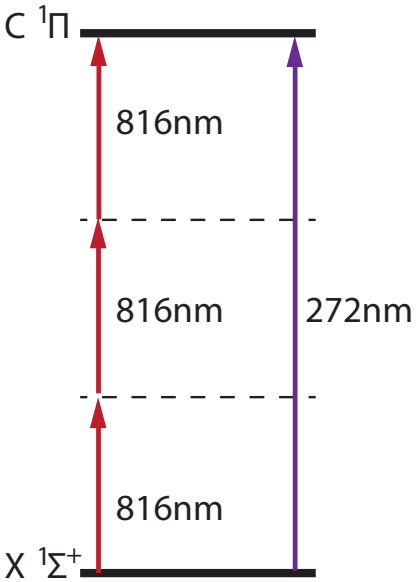

(a) Principle of IRMPD

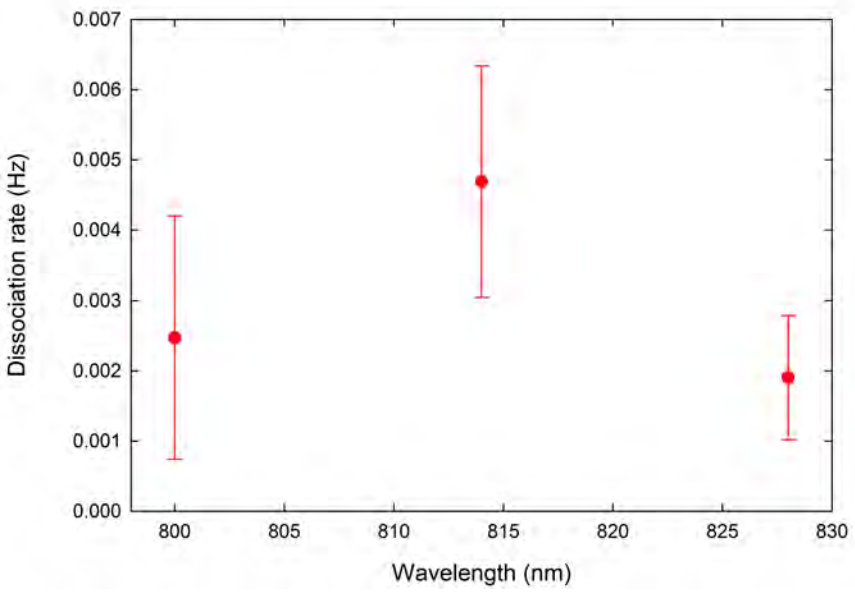

(b) IRMPD data

Figure 35: A plot of IRMPD data and principle. (a) shows the principle of infrared multiphoton dissociation while (b) shows the data from IRMPD experiment. The data indicates the three-photon process is indistinguishable from the background rate.

Each experiment data point was repeated six times and averaged. The resulting

spectra show an essentially flat line indicating no significant triple photon dissociation of the the molecular ion. In addition, the dissociation time was very slow, $\approx 5 \text{x} 10^2$ s. Thus, we can conclude that the peak was not caused by IRMPD but rather by REMPD. This could be because the excited states have very low absorption cross sections and there might not be virtual states present for multiple photon dissociation.

5.4.2 Dissociative recombination

Initial investigations into the dissociation spectra were conducted with two pulsed lasers. One was the MIRA while the other one was the Paladin tripled Nd:YAG laser at 355 nm. The laser combination was enough to couple the bound state to the dissociative state. Initially, only the $\nu' = 10 \leftarrow \nu = 0$ vibrational overtone was investigated. The data from those experiments is shown below in Fig. 36. The data are shown in the red circles with the corresponding error bars. The blue curve is a simulated spectrum given the width of the laser. The data and the simulated spectra agree very well. The point around 800 nm differs a little bit from the spectra, which is similar to the point around 870 nm. This could be due to the fact that the simulation uses an average width for the laser while the width changes as the wavelength changes.

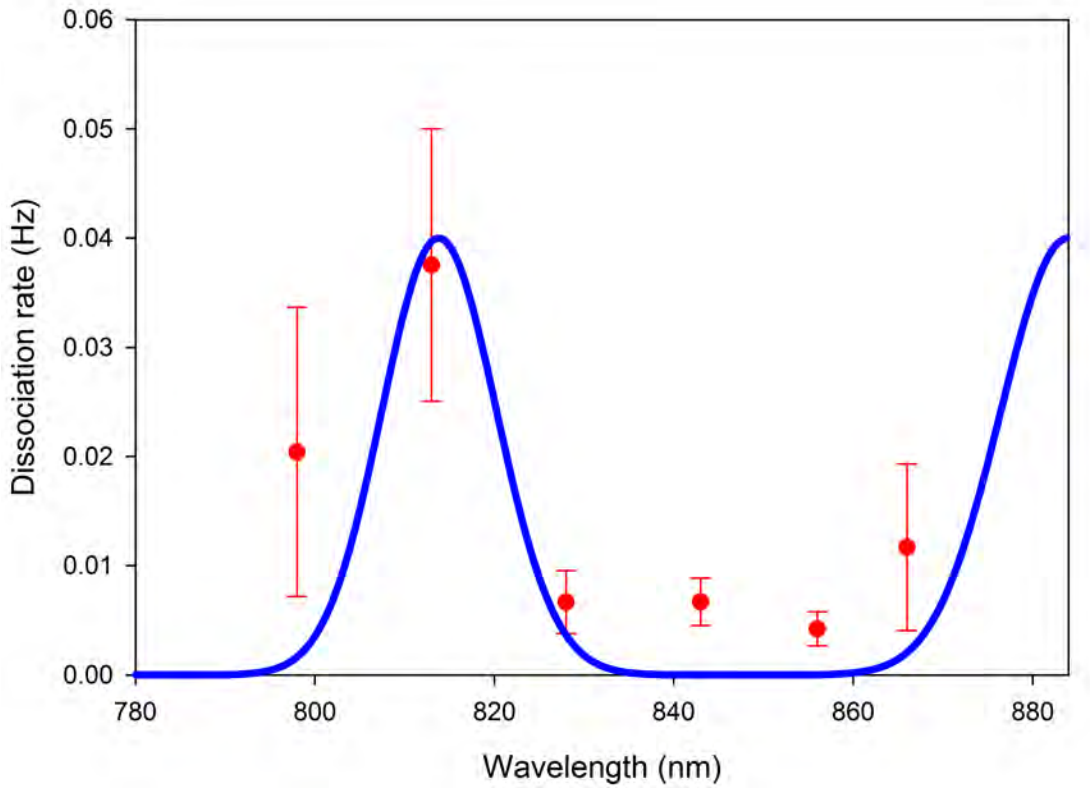

Figure 36: Spectrum of the $\nu' = 10 \leftarrow \nu = 0$ vibrational overtone obtained by using two pulsed lasers. One being the MIRA and for dissociation, a tripled Nd:YAG at 355 nm.

We switched the pulsed laser to a CW laser at 377 nm, which would also couple the bound state with the dissociative state. The Paladin had a clean Gaussian profile, while the CW laser had the typical elliptical shape of diode lasers [183]. We noticed that at some point the UV would detach electrons from the surface of the electrodes, which would in turn dissociate molecule. We observed in the spectra very fast dissociation rates as shown in Fig. 37. The dissociation rate with the UV only were faster than the expected dissociation rate, which were observed with the paladin. We attributed to electrons stripped from calcium that coated the surface of the electrodes in the trap. The work function of calcium is 2.9 eV, while the energy of the UV laser

is 3.2 eV, which means the laser had the energy required to strip the electrons. The molecular ion could then be dissociated by the combination with the electron in one of the two ways. Either through dissociative excitation ($^{40}CaH^+ + e^- \rightarrow CaH^* \rightarrow Ca^+ + H + e^-$) or ion pair formation ($^{40}CaH^+ + e^- \rightarrow CaH^* \rightarrow Ca^+ + H^-$) [214]. These two processes are normally endothermic, however, since the electrons become accelerated by the trapping electric field, these processes can be observed. We did not conduct a study to determine the actual dissociative mechanism in our trap.

To get around this problem, we opened and cleaned the trap to get rid of the calcium with warm sulfuric acid. Furthermore, we cleaned up the mode 377 nm laser to minimize scattering of the laser from the trap electrodes. This reduced the number of electron bombardment events on the dissociation rates. An electron bombardment event was when the dissociation time was less ten seconds, which was faster than the expected dissociation time. During each experiment, we checked for electron bombardment by running the dissociation experiments with the UV only and observing the dissociation times. After about six experiments that are consistent with the background dissociation rate, we would begin REMPD experiments as shown in Fig. 37.

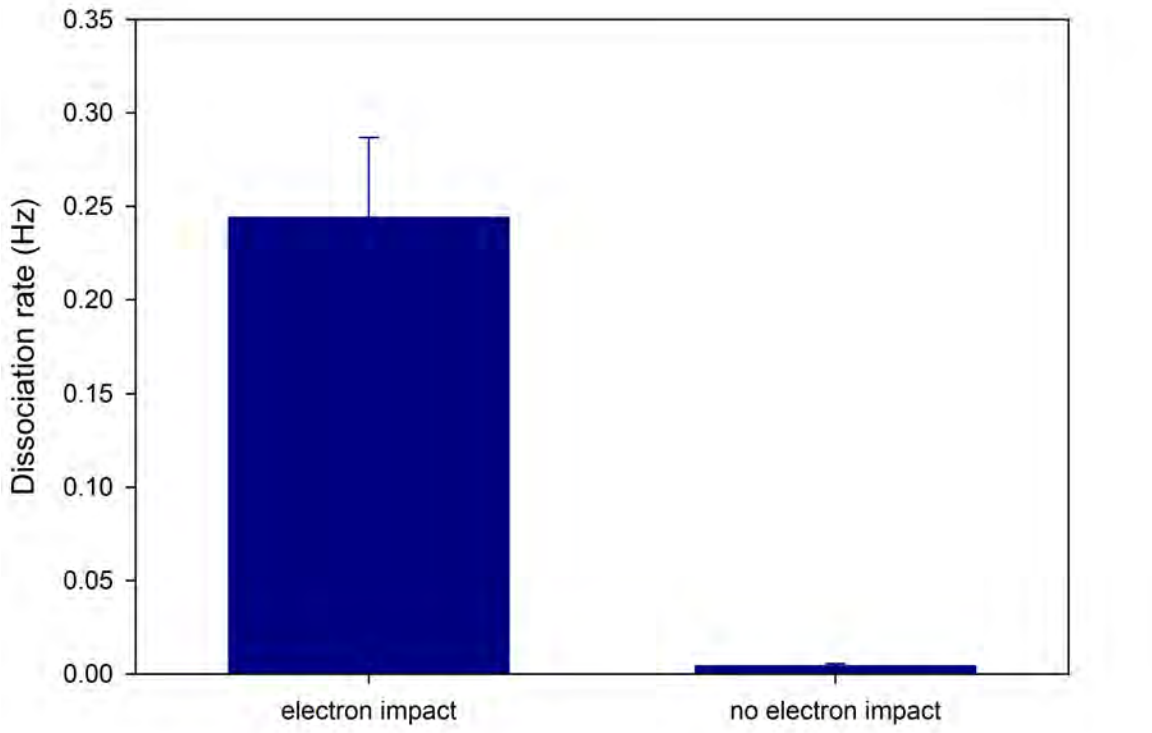

Figure 37: Figure showing the effects of electron recombination on the dissociation rate. Electron recombination resulted in dissociation rates that were significantly faster than the observed background rates and significantly higher than two-photon dissociation rates (Fig. 34). The processes to get around electron recombination resulted in significant lower dissociation rate as shown in the figure.

CHAPTER VI

FUTURE DIRECTIONS AND GROUND STATE COOLING OF A MOLECULAR ION

6.1 Introduction

Resonance enhanced multiphoton dissociation is a great tool for initial survey of molecular ion spectra because of the relative ease of implementation. However, the limit of REMPD is the linewidth of the laser. To get the kind of precision needed for probing fundamental physics ($\approx 10^{-15}$), higher precision measurements are needed. Such a technique was demonstrated by the Wineland group at the National Institute of Standards and Technology (NIST) when they measured the clock transition of an Al^+ ion co-trapped with Be^+ [31]. The method called quantum logic spectroscopy (QLS) coupled the motion of the ions in trap with the internal excitation of the ions [31, 51, 212, 215, 216]. Thus, the clock transition of Al^+ was measured to a high accuracy (10^{-17}) without the need to directly laser-cool the ion. Such a technique is congenial for spectroscopy of molecular ions because most molecular ions cannot be directly laser-cooled.

However, the implementation of QLS is rather difficult as it requires sophisticated experimental control. An alternative to QLS is to observe the heating of a trapped crystal caused by internal excitation and spontaneous emission of a sympathetically-cooled ion. In our lab, we implemented such a technique, which we called sympathetic heating spectroscopy (SHS) [188]. Briefly, two ions are trapped; one is directly laser-cooled (logic ion) while the other is sympathetically-cooled (spectroscopy ion). A transition on the spectroscopy ion is probed by observing the heating of the crystals as a function of the detuning from that transition. While the probed ion scatters a few

photons, they are enough to cause observable heating that can be detected. While SHS works well for electronic transitions, molecular transition scatter even fewer photons because of the availability of many decay channels. Thus a more sensitive technique is required. For this purpose we proposed observing the heating of sidebands of ground cooled crystals to detect molecular transitions. We called this technique quantum sympathetic heating spectroscopy (QSHS). Another group demonstrated this technique albeit on an atomic ion, which they termed photon recoil spectroscopy (PRS) [217]. A schematic of the technique is shown in Fig. 38.

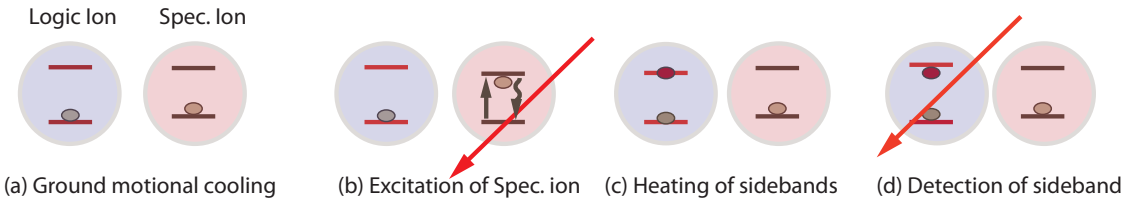

Figure 38: A schematic of QSHS. The red energy spacing lines represent the motional state, while the black lines represent the internal state of the molecule. (a) An ion (logic ion)-molecule (spectroscopic ion) crystal is ground state laser-cooled. (b) A transition in the spectroscopy ion is probed through multiple pulses, which causes emission of photons. (c) The photons cause heating of the sidebands of the crystal, which can be detected (d) as a function of the detuning of the wavelength.

QSHS works by cooling the crystal to the ground motional state, typically the axial mode. A transition on the molecular ion is probed with a series of pulses. Changes in angular momentum of the spectroscopy ion is transferred to the logic ion through the strong Coulomb attraction in the ion-molecular ion pair. Photon scattering at the molecule causes heating of the motional modes which can be detected. For $^{40}CaH^+$, we propose to frequency double the Ti:Sapph laser to excite the electronic transition of $^{40}CaH^+$ of the $2^1\Sigma^+ \leftarrow 1^1\Sigma^+$ electronic transition. The ν'=2 (393 nm), ν'=3 (382

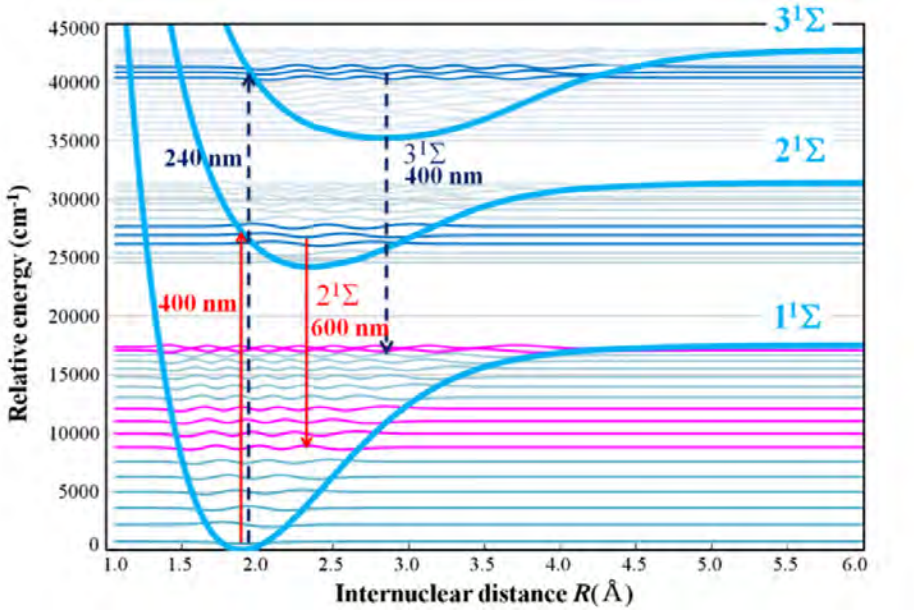

Figure 39: The proposed experiment to measure the electronic transition $2^1\Sigma^+ \leftarrow 1^1\Sigma^+$ of $^{40}CaH^+$ taken from Ref. [24].

nm) and ν'=4 (371 nm) have strong Frank-Condon overlap with the ground state. The excited molecule should fluoresce around 616–686 nm. This photon is enough to cause significant heating in the sidebands, which can be monitored as a function of frequency of the Ti:Sapph laser.

A prelude to QSHS is ground state cooling of the ion-molecular ion pair, which we achieved as shown in the next section.

6.2 Ground state cooling of a molecular ion

Part of this section is from, *Sympathetic cooling of molecular ion motion to the ground state*

R, Rugango, J.E Goeders, T.H. Dixon, J.M. Gray, **N. Khanyile**, G. Shu, R. J. Clark, K. R. Brown, *New J. Physics*, **17**, 035009 (2015).

6.2.1 Methods

To cool the motional state of a crystal, narrow transitions on a metastable state are utilized as described in the preceding chapters. Sideband cooling is prefaced by

Doppler cooling upon which the ion is confined in a space much smaller than the wavelength of the transition. A laser with a narrow linewidth can be tuned to the lower motional state. After each excitation to the excited state, the vibrational energy is removed as shown in Fig. 40a. Since the states are typically long-lived, to ensure cooling proceeds faster than heating processes, the long lived state is coupled to a fast decaying state as shown in Fig. 40b.

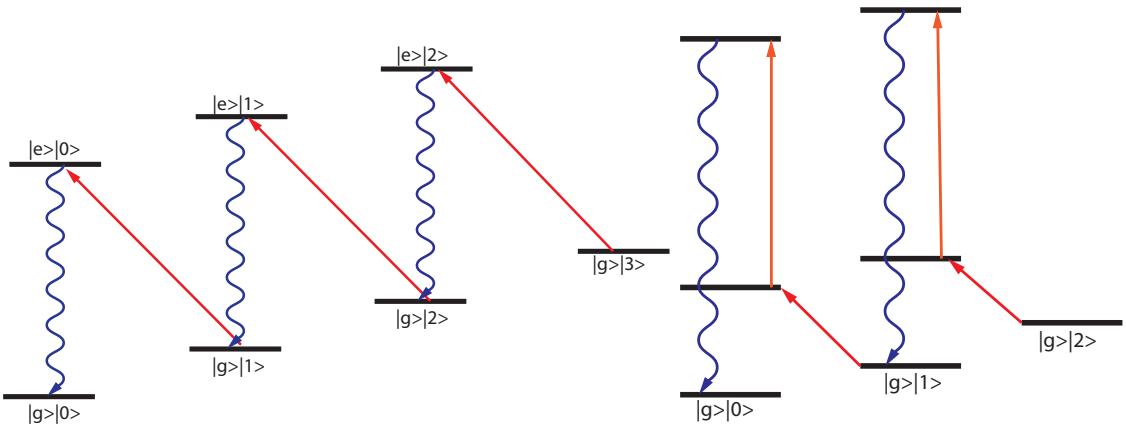

(a) Lowering the motional state (b) Coupling to a fast decay channel

Figure 40: A schematic of sideband cooling. (a) An excitation to an upper electronic state removes one quanta of motional energy while spontaneous decay results in no change of the motional state. (b) the lifetime of the $D_{5/2}$ state is shortened by coupling it to the $P_{3/2}$ state, which spontaneously decays to the $S_{1/2}$ state.

For calcium ions, the $S_{1/2} \leftrightarrow D_{5/2}$ (729 nm) transition is used for sideband cooling experiments. The $D_{5/2}$ state has a relative long lifetime(1 sec), the cooling process is sped up by coupling to the $P_{3/2}$ (854 nm) state for fast cooling. Typically, a magnetic field ($\approx$1 Gauss) splits the degenerate Zeeman states to distinct sublevels. The transitions for sideband cooling are then chosen as the $S_{1/2}(m = -1/2) \leftrightarrow D_{5/2}(m = -5/2)$ driven at 729 nm and the metastable state is the coupled to the $P_{3/2}(m = -3/2)$ with an 854 nm laser. The $P_{3/2}(m = -3/2)$ decays primarily back to

the $S_{1/2}(m = -1/2)$. To ensure that all the population is in the $S_{1/2}(m = -1/2)$ state, spin polarization is used to transfer the population from $S_{1/2}(m = +1/2)$ state. This is achieved by driving the $S_{1/2}(m = +1/2) \leftrightarrow D_{5/2}(m = -3/2)$ then again depopulating it with an 854 nm laser to the to the $P_{3/2}(m = -1/2)$ state (Fig. 41). This process is repeated until over 95% of the population is transferred to the $S_{1/2}(m = -1/2)$. Any leakage to the $D_{3/2}$ state is depopulated with an 866 nm that is always kept on during the entire procedure.

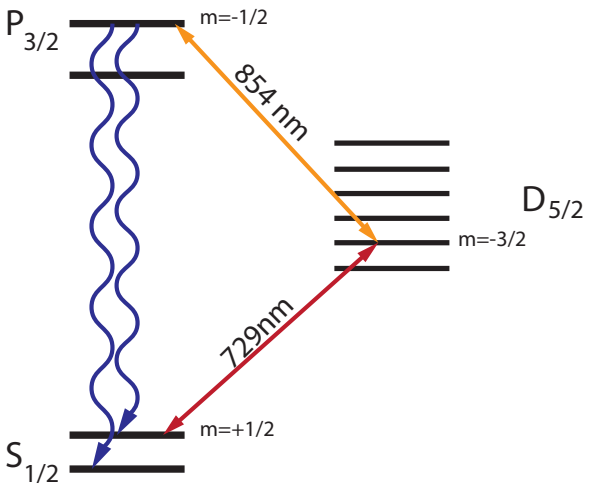

(a) Spin polarization

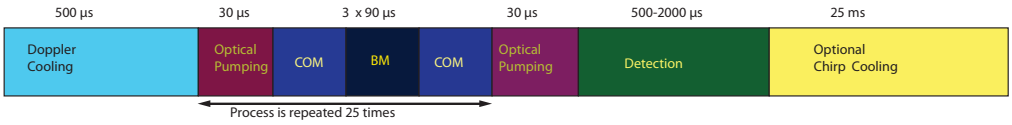

(b) Sideband cooling scheme

Figure 41: Spin polarization and sideband cooling. (a) shows a schematic of spin polarization to prepare the population in the $S_{1/2}(m = -1/2)$ state, which precedes sideband cooling. The typical sideband cooling scheme is shown in (b).

Sideband cooling is then commenced on the transition stated above. The electron shelving technique is used to detect the state of the ion. Since the metastable D state is non-fluorescent, turning on the Doppler cooling laser can reveal whether the ion is

the D state or the S state by the observation of no fluorescence versus fluorescence. A typical sequence for sideband cooling is shown in Fig. 41b.

6.2.2 Cooling of single ion

Prior to cooling a molecular ion, we demonstrated sideband cooling of a single molecular ion. Briefly, the ion was trapped in a trap driven at 14.426 MHz resulting in radial secular frequencies of 1.419 MHz (x-direction) and 1.475 MHz (y-direction). DC voltage confines the ion in the axial direction with a secular frequency of 568 KHz. Upon trapping, the ion is Doppler cooled and sideband cooled. The results are shown in Fig. 42.

To determine the temperature of the ion after sideband cooling, we compare the population in the red and blue sidebands. Briefly, after sideband cooling the average motional state $\langle n \rangle$ is in a Maxwell-Boltzmann distribution [129],

$$P_n = \frac{\langle n \rangle^n}{(\langle n \rangle + 1)^{n+1}}. \tag{95}$$

We can determine the population in the red sideband by applying a pulse of length t. The probability that the ion is in the red sideband is,

$$\rho_{rsb} = \sum_{n=1}^{\infty} \frac{\langle n \rangle^n}{(\langle n \rangle + 1)^{n+1}} \sin^2(\Omega_{n,n-1} t/2). \tag{96}$$

For the blue sideband, the population is given by,

$$\rho_{bsb} = \sum_{n=0}^{\infty} \frac{\langle n \rangle^n}{(\langle n \rangle + 1)^{n+1}} \sin^2(\Omega_{n,n+1} t/2). \tag{97}$$

If we expand the $\sin^2(\Omega t/2)$ terms around 0 and then use the Mclaurin series and compare the two probabilities, we obtain the average motional quanta. That is,

$$\frac{\rho_{rsb}}{\rho_{bsb}} = \frac{\langle n \rangle}{\langle n \rangle + 1}. \tag{98}$$

Rearranging the above equation and solving for $\langle n \rangle$, we find,

$$\langle n \rangle = \frac{\rho_{rsb}}{\rho_{bsb} - \rho_{rsb}}. \tag{99}$$

Once we measure the population distribution of sidebands we can calculate the temperature of the ion by the simple energy relation,

$$k_B T = \hbar\omega_0\big(\langle n\rangle + \frac{1}{2}\big), \tag{100}$$

where ω_0 is the secular frequency of the trapped ions.

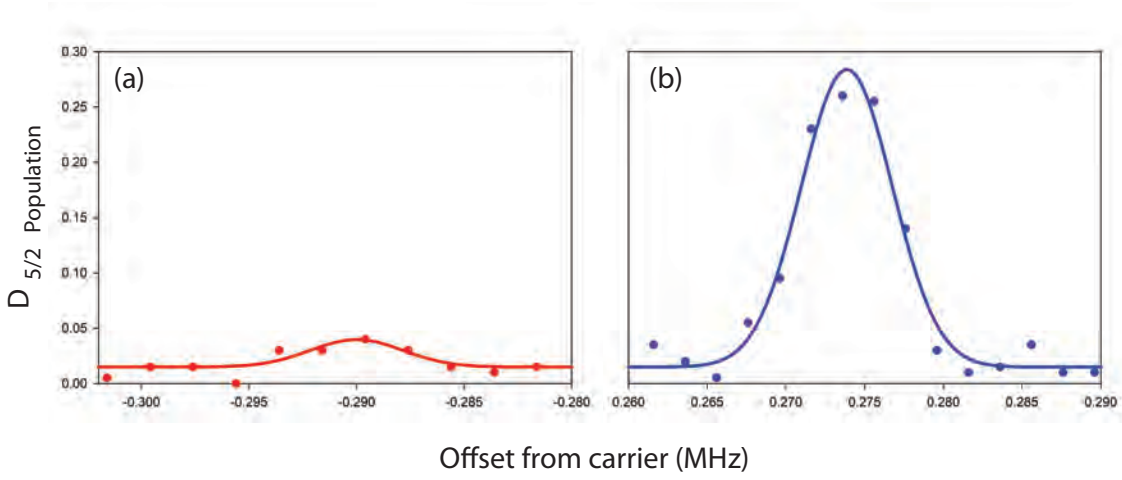

Figure 42: Sideband cooling of one ion. (a) shows population in the red sidebands after sideband cooling while (b) shows the population in the blue sideband. The overall energy of the system is found by comparing the two peaks.

After Doppler cooling, the sidebands are approximately the same height. The temperature is measured to be $T = 0.75$ mK using the carrier Rabi oscillation decoherence method [218, 219], which is close to the Doppler cooling limit of $T = 0.53$ mK. Sideband cooling is performed on the axial mode and $\overline{n}_{\text{axial}} = 0.1$ is typically achieved as measured by the peak height comparison method [129]. The results show that the motional state of the ion after sideband cooling is found to be $\overline{n}$=0.1, which corresponds to a temperature of 16.7±2.3 μK.

Sideband cooling of a molecular ion is achieved in a similar fashion as sideband cooling of a single ion. $^{40}CaH^+$ is prepared by loading two ions inside the trap and Doppler cooling them. H_2 gas is introduced into the chamber via a leak valve, which

reacts with one of the ions in the trap. This is shown on the EMCCD camera by a dark spot where the previously fluorescing ion was located. The non-reactant ion does not change position indicative of the presence of another non-fluorescing ion in the trap. The identity of the molecular ion is confirmed using the method described in a previous experiment [206]. The sideband cooling scheme proceeds by first Doppler cooling the crystal for 500 μs with the 397 nm laser detuned 10 MHz from resonance and then continuously exciting with the 729 nm laser alternating between the red first order COM and BM sidebands for 6 ms with the 854 nm laser on. Each cooling cycle is preceded by a spin polarization phase on the $S_{1/2}$ (m = +1/2)$\longrightarrow$$D_{5/2}$ (m = -3/2) transition to prepare the ion in the $S_{1/2}$ (m= -1/2) Zeeman state. Spin polarization is interleaved with the cooling and repeated every 100 μs. After cooling, we probe the two-ion crystal with the same technique used to measure motional sidebands. The average motional quanta after cooling is determined through the ratio of the heights of the red and blue sidebands [129].

The ion crystal occasionally suffers from collisions with residual background gas. Collisions during the sideband cooling procedure will melt the crystal and result in temperatures far above the Doppler cooling limit. Cooling lasers close to resonance may not completely bring the crystal back to temperatures near the Doppler limit within the normal cooling period. Collision events are detected by observing below normal fluorescence during the regular Doppler cooling stage. After detection of a collision, a short frequency chirped Doppler cooling pulse is applied that recrystallizes the ion chain and achieves the desired initial temperature for performing sideband cooling. We discard the electron shelving data recorded coincident with the collision event from out final data set.

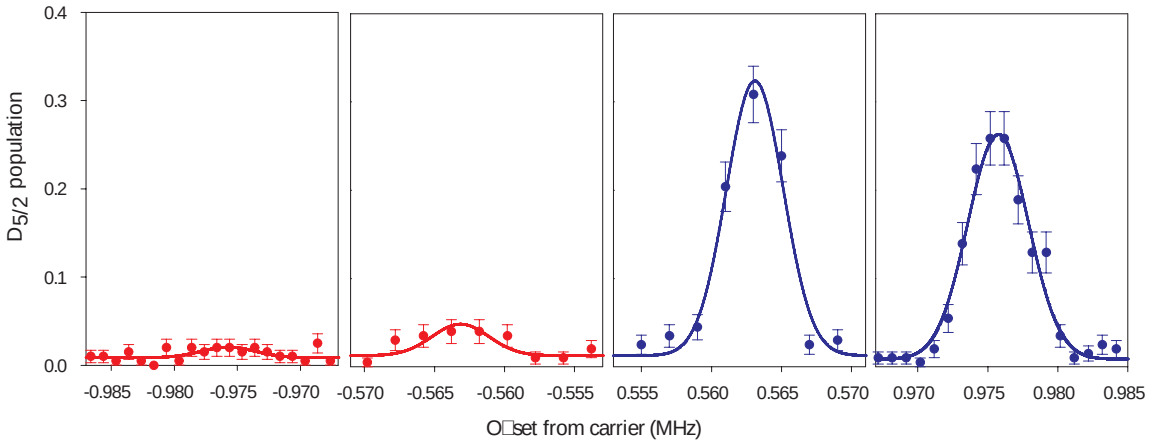

Figure 43: Measurement of the $S_{1/2}$ (m = -1/2)$\longrightarrow$$D_{5/2}$ (m = -5/2) first-order axial sidebands for the $^{40}Ca^{+}$- $^{40}CaH^{+}$ crystal by electron shelving. Red and blue sidebands are fit to a Gaussian of the same width but variable amplitude. Comparison of sideband heights yields an average mode occupation of $\overline{n}_{\mathrm{COM}} = 0.13 \pm 0.03$ for the center of mass mode and $\overline{n}_{\mathrm{BM}} = 0.05 \pm 0.02$ for the breathing mode.

Our molecular ion results are presented in Fig. 43. After sideband cooling, we observe that the red peak height is greatly suppressed relative to the blue peak height. Peak height comparison reveals $\overline{n}_{\mathrm{COM}} = 0.13 \pm 0.03$ and $\overline{n}_{\mathrm{BM}} = 0.05 \pm 0.02$. To determine the temperature, we match the expected occupation of the oscillator as a function of temperature with the measured occupation. We find $T_{\mathrm{COM}} = 12.47 \pm 0.03$ μK and $T_{\mathrm{BM}} = 15.36 \pm 0.01$ μK, which is more than a factor of 3 below the Doppler cooling limit. The presented data is typical and similar results were seen even when imperfect compensation resulted in a shifted breathing mode frequency [74, 206]. Ground state cooling of the motion in three dimensions was not achieved due to an unusually high radial heating rate. We were only able to cool to $\overline{n}_{\mathrm{radial}} = 1$ corresponding to 30% population in the ground state. This could be due to residual micromotion or stronger coupling between the fluctuating electric fields and the radial direction.

The sideband cooling results are an important step towards the implementation of quantum logic spectroscopy [31] or photon-recoil spectroscopy [217]. These techniques are limited by trap heating which acts as unwanted background that could mask the signal. For our current experiment, we measure a single ion background heating rate of 0.1 quanta/ms comparable with other experiments in similar scale traps [220]. The heating rate of the atomic and molecular ion on the center of mass mode was 0.3 quanta/ms. If this mode is used for spectroscopy, the heating rate provides an idea of how quickly the molecular ion must absorb or scatter photons to have a detectable signal.

6.3 Conclusions and future outlook

We have presented the first measurements on the vibrational spectra of sympathetically laser-cooled molecular ion $^{40}CaH^+$. Guided by theoretical calculations, we utilized a broadband mode-locked Ti:Sapph laser and a CW laser to resonantly dissociate the trapped $^{40}CaH^+$. Since the molecular ion had an internal temperature equilibrated with black body radiation, many rotational levels are thermally populated. The broadband laser effectively addressed all these rotational levels allowing only the vibrational structure to be probed. Furthermore, we cooled the ion down to its motional ground state inside the trap, which makes it possible to perform high precision measurements. We propose to study the electronic spectra of $^{40}CaH^+$ using the heating of narrow transitions of ground state cooled molecular ion, a method we call QSHS. For precision measurements, it is ideal to have the internal population of the molecule in the rovibrational ground state. For $^{40}CaH^+$, the vibrational population is already in the ground state, while the rotational states are still in equilibrium with black body radiation. Cooling the rotational motion can be done in several ways. Several groups have utilized optical pumping [66, 67], which has a disadvantage of requiring lasers that are deep IR, which may not be commercially available.

In addition, the technique requires detailed knowledge of the transitions involved. An alternative is to use collisions with cold gases to lower the internal temperature. This has been demonstrated with a magneto-optical trap (MOT) and a helium cryogenic trap [70, 73]. An advantage of these techniques is the applicability to a wide range of molecular ions without the need for detailed spectroscopic knowledge of those molecules. In the Brown lab, the construction and implementation of a helium buffer gas cryogenic cooling has been demonstrated on a chain of calcium ions [221]. The next step is to sympathetically rotationally cool $^{40}CaH^+$ with a helium buffer gas. The Brown lab is also interested in directly laser cooling a molecular ion. To date, direct laser cooling of a molecular ion has not been demonstrated. Few candidates have been proposed as ideal for direct laser cooling experiment, BH^+, AlH^+, and SrO^+ [44, 45]. For this experiment, we propose to cool BH^+ [13, 44, 222, 223]. Direct laser-cooling of molecules requires diagonal Franck-Condon factors, which would require fewer re-pump laser in order to reach the translationally cold limit. Direct laser cooling of molecular ions reduces unwanted Stark shifts introduced by the atomic cooling lasers, which would allow for higher precision measurements.

APPENDIX A

ANCILLARY MATERIAL

The table below shows the some physical properties of the transitions in $^{40}Ca^{+}$ ion.

Table 5: A table showing the physical properties of Ca^+. λ is the wavelength of the transition, f is the oscillator strength, $\tau(s)$ is the lifetime of the transition, dipole describes the permanent dipole moment of the transition, A_{fi} is the transition probability and BR is the branching ratio. The figures are taken from Refs. [408–414, 418–428]

Transition	λ(nm)	f	$\tau(s)$	dipole(quadrupole*)	A_{fi} $\times 10^6(s^{-1})$	BR
$4\ ^2S_{1/2} \leftrightarrow 4^2P_{3/2}$	393.63	0.62	7.4×10^{-9}	2.898	135.0	0.9347
$4\ ^2S_{1/2} \leftrightarrow 4^2P_{1/2}$	396.7	0.32	7.5×10^{-9}	4.099	132.33	0.9373
$4\ ^2P_{1/2} \leftrightarrow 3^2D_{3/2}$	866.214		0.094×10^{-6}	4.28	8.97	0.0626
$4\ ^2P_{3/2} \leftrightarrow 3^2D_{3/2}$	850	0.0088	0.9×10^{-6}	1.93	0.955	0.00661
$4\ ^2P_{3/2} \leftrightarrow 3^2D_{5/2}$	854.2089	0.053	0.1×10^{-6}	5.78	8.48	0.0587
$4\ ^2S_{1/2} \leftrightarrow 3^2D_{5/2}$	729		0.994	9.740*	(2.1×10^{-1})	
$4\ ^2S_{1/2} \leftrightarrow 3^2D_{3/2}$	732		1.111	7.939*	(2.1×10^{-1})	

Table 6: Fundamental physical constants used in this thesis. The values were taken from [430].

Fundamental constant	Symbol	Value
Speed of light in vacuum	c	299 792 458 m s^{-1}
Planck constant	h	6.62606957×10^{-34} J s
Reduced Planck constant	$\hbar$	$1.054571726\times10^{-34}$ J s
Proton-electron mass ratio	$m_p/m_e(\mu)$	1836.15267245
Fine-structure constant	α	$7.297\ 352\ 5698\times10^{-3}$
Electron mass	m_e	9.10938291×10^{-34} kg
Permittivity of free space	ε_0	$8.854187817\times10^{-12}$ F/m
Proton mass	m_p	$1.672621777\times10^{-27}$ kg
Elementary charge	e or q	$1.602176565\times10^{-19}$ C
Boltzmann constant	k_B	$1.380\ 6488\ \times10^{-23}$ J K^{-1}

Bibliography

[1] Herzberg, G., *Molecuar Spectra and Molecular Structure I. Spectra of Diatomic Molecules*. D. Van Nostrand Company, Inc., second ed., 1950.

[2] Oka, T., "Interstellar H_3^+," *Chem. Rev.*, vol. 113, pp. 8738–8761, 2013.

[3] Peik, E., "Fundamental constants and units and the search for temporal variations," *Nuc. Phys. B - Proc. Supp.*, vol. 203-204, pp. 18–32, 2010.

[4] Yamada, K. and Winnewisser, G., *Interstellar Molecules: Their Laboratory and Interstellar Habitat*. New York: Springer-Verlag Berlin Heidelberg, 2011.

[5] Spitzer, L., *Physical Process in the Interstellar Medium*. New York: Wiley-Interscience, 1978.

[6] Verschuur, G. and Kellermann, K., *Galactic and Extra-Galactic Radio Astronomy*. Berlin: Springer, 1988.

[7] Lockwood, A. C., Johnson, J. A., Bender, C. F., Carr, J. S., Barman, T., Richert, A. J. W., and Blake, G. A., "Near-ir direct detection of water vapor in tau bo$\ddot{O}$tis b," *Astrophys. J.*, vol. 783, p. L29, 2014.

[8] Hibbitts, C. a., Grieves, G. a., Poston, M. J., Dyar, M. D., Alexandrov, a. B., Johnson, M. a., and Orlando, T. M., "Thermal stability of water and hydroxyl on the surface of the Moon from temperature-programmed desorption measurements of lunar analog materials," *Icarus*, vol. 213, pp. 64–72, 2011.

[9] Klemperer, W., "Interstellar chemistry," *Proc. Natl. Acad. Sci. U. S. A.*, vol. 103, p. 12232, 2006.

[10] Swings, P. and Rosenfeld, L., "CH radical in space," *Astrophys. J.*, vol. 86, p. 483, 1937.

[11] Adams, W., "CH^+ ion in space," *Pub. Astr. Soc. Pac.*, vol. 93, p. 11, 1941.

[12] Sinha, K. and Tripathi, B. M., "On ionized molecules in solar atmosphere," *Bull. Astro. Soc. Ind.*, vol. 18, pp. 33–78, 1990.

[13] Challacombe, C. and Almy, G., "On the analysis of molecular $^3\Pi$ states with application of AlH, OH^+, and BH," *Phys. Rev.*, vol. 51, p. 930, 1937.

[14] Monterio, T. S., Danby, G., Cooper, I. L., Dickinson, A. S., and Lewis, E. L., "Broadening of the Ca^+ and Mg^+ resonance lines by collision with atomic hydrogen," *J. Phys. B: At. Mol. Opt. Phys.*, vol. 21, p. 4165, 1988.

[15] Dutta, C. M., Oubre, C., Nordlander, P., Kimura, M., and Dalgarno, a., "Charge-transfer cross sections in collisions of ground-state Ca and H^+," *Phys. Rev. A*, vol. 73, pp. 1–7, 2006.

[16] Herzberg, G., "Introduction to molecular ion spectroscopy," in *Molecular Ions: Spectroscopy, Structure, and Chemistry* (Miller, T. A. and Bondybey, V. E., eds.), p. 1, New York: North-Holland Publishing Company, 1983.

[17] Canuto, S., Castro, M. A., and Sinha, K., "Theoretical determination of the spectroscopic constants of CaH^+," *Phys. Rev. A*, vol. 48, pp. 2461–2463, 1993.

[18] Allen, C., *Astrophysical Quantities*. The Athlone Press, 3rd ed., 1973.

[19] Duncan, M. A., "Spectroscopy of metal ion complexes: gas-phase models for solvation.," *Annu. Rev. Phys. Chem.*, vol. 48, pp. 69–93, 1997.

[20] Schilling, J. B., Goddard III, W. A., and Beauchamp, J. L., "Theoretical studies of transition-metal hydrides. 2. CaH^+ through ZnH^+," *J. Phys. Chem.*, vol. 91, p. 5616, 1987.

[21] Aymar, M. and Dulieu, O., "The electronic structure of the alkaline-earth-atom (Ca, Sr, Ba) hydride molecular ions," *J. Phys. B: At. Mol. Opt. Phys.*., vol. 45, p. 215103, 2012.

[22] Habli, H., Dardouri, R., Oujia, B., and Gadea, F. X., "*Ab initio* adiabatic and diabatic energies and dipole moments of the CaH^+ molecular ion," *J. Phys. Chem.. A*, vol. 115, pp. 14045–14053, 2011.

[23] Boutalib, A., Daudey, J., and Mouhtadi, M. E., "Theoretical study of the lowest electronic states of CaH and CaH^+ molecules," *Chem. Phys.*, vol. 167, pp. 111–120, 1992.

[24] Abe, M., Moriwaki, Y., Hada, M., and Kajita, M., "*Ab initio* study on potential energy curves of electronic ground and excited states of $^{40}CaH^+$ molecule," *Chem. Phys. Lett.*, vol. 521, pp. 31–35, 2012.

[25] Abe, M., Kajita, M., Hada, M., and Moriwaki, Y., "*Ab initio* study on vibrational dipole moments of XH^+ molecular ions: X = ^{24}Mg, ^{40}Ca, ^{64}Zn, ^{88}Sr, ^{114}Cd, ^{138}Ba,^{174}Yb and ^{202}Hg," *J. Phys. B: At. Mol. Opt. Phys.*, vol. 43, p. 245102, 2010.

[26] Webb, J., Flambaum, V., Churchill, C., Drinkwater, M., and Barrow, J., "Search for time variation of the fine structure constant," *Phys. Rev. Lett.*, vol. 82, pp. 884–887, 1999.

[27] Webb, J., Murphy, M., Flambaum, V., Dzuba, V., Barrow, J., Churchill, C., Prochaska, J., and Wolfe, a., "Further evidence for cosmological evolution of the fine structure constant," *Phys. Rev. Lett.*, vol. 87, p. 091301, 2001.

[28] Schiller, S. and Korobov, V., "Tests of time independence of the electron and nuclear masses with ultracold molecules," *Phys. Rev. A*, vol. 71, p. 032505, 2005.

[29] Demille, D., Sainis, S., Sage, J., Bergeman, T., Kotochigova, S., and Tiesinga, E., "Enhanced sensitivity to variation of me/mp in molecular spectra," *Phys. Rev. Lett.*, vol. 100, p. 043202, 2008.

[30] Quinn, T. and Burnett, K., "Introduction: The fundamental constants of physics, precision measurements and the base units of the SI," *Philos. Trans. A. Math. Phys. Eng. Sci.*, vol. 363, pp. 2101–4, 2005.

[31] Rosenband, T., Hume, D. B., Schmidt, P. O., Chou, C. W., Brusch, a., Lorini, L., Oskay, W. H., Drullinger, R. E., Fortier, T. M., Stalnaker, J. E., Diddams, S. a., Swann, W. C., Newbury, N. R., Itano, W. M., Wineland, D. J., and Bergquist, J. C., "Frequency ratio of Al^+ and Hg^+ single-ion optical clocks; metrology at the 17th decimal place," *Science*, vol. 319, pp. 1808–12, 2008.

[32] Kajita, M., "Prospects of detecting me/mp variance using vibrational transition frequencies of $^2\Sigma$-state molecules," *Phys. Rev. A*, vol. 77, p. 012511, 2008.

[33] Kajita, M., "Sensitive measurement of mp/me variance using vibrational transition frequencies of cold molecules," *New J. Phys.*, vol. 11, p. 055010, 2009.

[34] Sturm, S., Köhler, F., Zatorski, J., Wagner, a., Harman, Z., Werth, G., Quint, W., Keitel, C. H., and Blaum, K., "High-precision measurement of the atomic mass of the electron," *Nature*, vol. 506, pp. 467–70, 2014.

[35] Curtis, L. J. and Erman, P., "Distortion effects in measurements of long optical lifetimes," *J.the Optical Society of America.*, vol. 67, p. 1218, 1977.

[36] Fortman, S. M., Medvedev, I. R., Neese, C. F., and Lucia, F. C. D., "How complete are astrophysical catalogs for the millimeter and submillimeter spectral region?," *Astrophys. J. Lett.*, vol. 725, p. L11, 2010.

[37] Wester, R., "Radiofrequency multipole traps: Tools for spectroscopy and dynamics of cold molecular ions," *J. Phys. B: At. Mol. Opt. Phys.*, vol. 42, p. 154001, 2009.

[38] Roth, B. and Schiller, S., "Sympathetically cooled molecular ions: From principles to first applications," in *Cold Molecules: Theory, Experiments, Applications* (Krems, R. V., Friedrich, B., and Stwalley, W., eds.), Boca Raton: Taylor and Francis Group, 1st ed., 2009.

[39] Corder, C., Arnold, B., and Metcalf, H., "Laser Cooling without Spontaneous Emission," *Phys. Rev. Lett*, vol. 114, p. 043002, 2015.

[40] Shuman, E., Barry, J., and DeMille, D., "Laser cooling of a diatomic molecule," *Nature*, vol. 467, pp. 820–823, 2010.

[41] Zhelyazkova, V., Cournol, A., Wall, T. E., Matsushima, A., Hudson, J. J., Hinds, E. A., Tarbutt, M. R., and Sauer, B. E., "Laser cooling and slowing of CaF molecules," *Phys. Rev. A*, vol. 89, p. 053416, 2014.

[42] Gao, Y. and Gao, T., "Laser cooling of the alkaline-earth-metal monohydrides: Insights from an *ab initio* theory study," *Phys. Rev. A*, vol. 90, p. 052506, 2014.

[43] Hummon, M. T., Yeo, M., Stuhl, B. K., Collopy, A. L., Xia, Y., and Ye, J., "2D magneto-pptical trapping of diatomic molecules," *Phys. Rev. Lett.*, vol. 110, p. 143001, 2013.

[44] Nguyen, J. H. V., Viteri, C. R., Hohenstein, E. G., Sherrill, C. D., Brown, K. R., and Odom, B., "Challenges of laser-cooling molecular ions," *N. J. Phys.*, vol. 13, p. 063023, 2011.

[45] Nguyen, J. and Odom, B., "Prospects of doppler cooling of three-electronic-level molecules," *Phys. Rev. A*, vol. 83, p. 053404, 2011.

[46] Lara, M., Bohn, J. L., Potter, D., Soldán, P., and Hutson, J. M., "Ultracold Rb-OH collisions and prospects for sympathetic cooling," *Phys. Rev. Lett.*, vol. 97, p. 183201, 2006.

[47] Harmon, T. J., Moazzen-Ahmadi, N., and Thompson, R. I., "Instability heating of sympathetically-cooled ions in a linear Paul trap," *Phys. Rev. A*, vol. 67, p. 013415, 2003.

[48] Alekseev, V. a., Krylova, D. D., and Letokhov, V. S., "Sympathetic cooling of two trapped ions," *Phys. Scr.*, vol. 51, pp. 368–372, 2006.

[49] Oshima, Y. and Moriwakil, Y., "Sympathetic cooling of ions in an RF trap," *Prog. Crystal. Growth. and Charact.*, vol. 33, pp. 405–408, 1996.

[50] Drewsen, M., "Ion Coulomb crystals," *Phys. B*, vol. 460, pp. 105–113, 2015.

[51] Kielpinski, D., King, B., Myatt, C., Sackett, C., Turchette, Q., Itano, W., Monroe, C., Wineland, D., and Zurek, W., "Sympathetic cooling of trapped ions for quantum logic," *Phys. Rev. A*, vol. 61, p. 032310, 2000.

[52] Hasegawa, T. and Shimizu, T., "Limiting temperature of sympathetically cooled ions in a radio-frequency trap," *Phys. Rev. A*, vol. 67, p. 013408, 2003.

[53] Mølhave, K. and Drewsen, M., "Formation of translationally cold MgH^+ and MgD^+ molecules in an ion trap," *Phys. Rev. A*, vol. 62, p. 011401, 2000.

[54] Zygelman, B., Lucic, Z., and Hudson, E. R., "Cold ion-atom chemistry driven by spontaneous radiative relaxation: A case study for the formation of the $YbCa^+$ molecular ion," *J. Phys. B: At. Mol. Opt. Phys.*, vol. 47, p. 015301, 2014.

[55] Gingell, A. D., Bell, M. T., Oldham, J. M., Softley, T. P., and Harvey, J. N., "Cold chemistry with electronically excited Ca^+ Coulomb crystals," *J. Chem. Phys.*, vol. 133, p. 194302, 2010.

[56] Bell, M. T., Gingell, A. D., Oldham, J. M., Softley, T. P., and Willitsch, S., "Ion-molecule chemistry at very low temperatures: Cold chemical reactions between Coulumb-crystallized ions and velocity-selected neutral molecules," *Faraday Discussions*, vol. 142, pp. 73–91, 2009.

[57] Chang, Y.-P., Dugocki, K., Küpper, J., Rösch, D., Wild, D., and Willitsch, S., "Specific chemical reactivities of spatially separated 3-aminophenol conformers with cold Ca^+ ions," *Science*, vol. 342, pp. 98–101, 2013.

[58] Wellers, C., Borodin, A., Vasilyev, S., Offenberg, D., and Schiller, S., "Resonant IR multi-photon dissociation spectroscopy of a trapped and sympathetically cooled biomolecular ion species," *Phys. Chem. Chem. Phys.*, vol. 13, pp. 18799–809, 2011.

[59] Højbjerre, K., Offenberg, D., Bisgaard, C., Stapelfeldt, H., Staanum, P., Mortensen, a., and Drewsen, M., "Consecutive photodissociation of a single complex molecular ion," *Phys. Rev. A*, vol. 77, p. 030702(R), 2008.

[60] Rolland, D., Specht, A. a., Blades, M. W., and Hepburn, J. W., "Resonance enhanced multiphoton dissociation of polycyclic aromatic hydrocarbons cations in an RF ion trap," *Chem. Phys. Lett.*, vol. 373, pp. 292–298, 2003.

[61] Koelemeij, J., Roth, B., Wicht, A., Ernsting, I., and Schiller, S., "Vibrational Spectroscopy of HD^+ with 2-ppb Accuracy," *Phys. Rev. Lett.*, vol. 98, p. 173002, 2007.

[62] Shen, J., Borodin, A., Hansen, M., and Schiller, S., "Observation of a rotational transition of trapped and sympathetically cooled molecular ions," *Phys. Rev. A*, vol. 85, p. 032519, 2012.

[63] Bressel, U., Borodin, A., Shen, J., Hansen, M., Ernsting, I., and Schiller, S., "Manipulation of individual hyperfine states in cold trapped molecular ions and application to HD^+ frequency metrology," *Phys. Rev. Lett.*, vol. 108, p. 183003, 2012.

[64] Roth, B., Koelemeij, J., Daerr, H., and Schiller, S., "Rovibrational spectroscopy of trapped molecular hydrogen ions at millikelvin temperatures," *Phys. Rev. A*, vol. 74, p. 040501, 2006.

[65] Bertelsen, A., Jørgensen, S., and Drewsen, M., "The rotational temperature of polar molecular ions in Coulomb crystals," *J. Phys. B: At. Mol. Opt. Phys.*, vol. 39, pp. L83–L89, 2006.

[66] Staanum, P. F., Højbjerre, K., Skyt, P. S., Hansen, A. K., and Drewsen, M., "Rotational laser cooling of vibrationally and translationally cold molecular ions," *Nat. Phys.*, vol. 6, pp. 271–274, 2010.

[67] Schneider, T., Roth, B., Duncker, H., Ernsting, I., and Schiller, S., "All-optical preparation of molecular ions in the rovibrational ground state," *Nat. Phys.*, vol. 6, pp. 275–278, 2010.

[68] Champenois, C., Hagel, G., Knoop, M., Houssin, M., Zumsteg, C., Vedel, F., and Drewsen, M., "Two-step Doppler cooling of a three-level ladder system with an intermediate metastable level," *Phys. Rev. A*, vol. 77, pp. 1–7, 2007.

[69] Deb, N., Heazlewood, B. R., Bell, M. T., and Softley, T. P., "Blackbody-mediated rotational laser cooling schemes in MgH^+, DCl^+, HCl^+, LiH and CsH," *Phys. Chem. Chem. Phys.*, vol. 15, pp. 14270–81, 2013.

[70] Hansen, a. K., Versolato, O. O., Kosowski, L., Kristensen, S. B., Gingell, A., Schwarz, M., Windberger, A., Ullrich, J., López-Urrutia, J. R. C., and Drewsen, M., "Efficient rotational cooling of Coulomb-crystallized molecular ions by a helium buffer gas," *Nature*, vol. 508, pp. 76–9, 2014.

[71] Lien, C.-Y., Williams, S. R., and Odom, B., "Optical pulse-shaping for internal cooling of molecules," *Phys. Chem. Chem. Phys.*, vol. 13, pp. 18825–9, 2011.

[72] Manai, I., Horchani, R., Lignier, H., Pillet, P., Comparat, D., Fioretti, A., and Allegrini, M., "Rovibrational cooling of molecules by optical pumping," *Phys. Rev. Lett.*, vol. 109, p. 183001, 2012.

[73] Rellergert, W. G., Sullivan, S. T., Schowalter, S. J., Kotochigova, S., Chen, K., and Hudson, E. R., "Evidence for sympathetic vibrational cooling of translationally cold molecules," *Nature*, vol. 495, pp. 490–4, 2013.

[74] Barrett, M. D., DeMarco, B., Schaetz, T., Leibfried, D., Britton, J., Chiaverini, J., Itano, W. M., Jelenkovic, B., Jost, J. D., Langer, C., Rosenband, T., and Wineland, D. J., "Sympathetic cooling of $^9Be^+$ and $^{24}Mg^+$ for quantum logic," *Phys. Rev. A*, vol. 68, p. 042302, 2003.

[75] Drullinger, R. E., Wineland, D. J., and Bergquist, J. C., "High-resolution optical spectra of laser cooled ions," *Appl. Phys.*, vol. 22, pp. 365–368, 1980.

[76] Imajo, H., Hayasaka, K., Ohmukai, R., Tanaka, U., Watanabe, M., and Urabe, S., "High-resolution ultraviolet spectra of sympathetically-laser-cooled Cd^+ ions," *Phys. Rev. A*, vol. 53, pp. 122–125, 1996.

[77] Thompson, R. C., "Precision measurement aspects of ion traps," *Meas. Sci. Technol.*, vol. 1, pp. 93–105, 1999.

[78] Carrignton, A. and Thrush, B. A., *Spectroscopy of Molecular ions*. New York: The Royal Society, 1988.

[79] Polfer, N. C. and Oomens, J., "Reaction products in mass spectrometry elucidated with infrared spectroscopy.," *Phys. Chem. Chem. Phys.*, vol. 9, pp. 3804–3817, 2007.

[80] Polfer, N. C., "Infrared multiple photon dissociation spectroscopy of trapped ions," *Chem. Soc. Rev.*, vol. 40, pp. 2211–2221, 2011.

[81] Oomens, J., Sartakov, B. G., Meijer, G., and von Helden, G., "Gas-phase infrared multiple photon dissociation spectroscopy of mass-selected molecular ions," *Int. J. Mass. Spec.*, vol. 254, pp. 1–19, 2006.

[82] Pribble, R. N. and Zwier, T. S., "Probing hydrogen bonding in benzene-$(water)_n$ clusters using resonant ion-dip IR spectroscopy," *Faraday Discuss.*, vol. 97, p. 229, 1994.

[83] Pribble, R. N., Garrett, A. W., Haber, K., and Zwier, T. S., "Resonant ion-dip infrared spectroscopy of benzene–H_2O and benzene-HOD," *J. Chem. Phys.*, vol. 103, p. 531, 1995.

[84] Brathwaite, A. D. and Duncan, M. A., "Infrared photodissociation spectroscopy of saturated group IV (Ti, Zr, Hf) metal carbonyl cations," *J. Phys. Chem. A*, vol. 117, pp. 11695–11703, 2013.

[85] Stearns, J. a., Mercier, S., Seaiby, C., Guidi, M., Boyarkin, O. V., and Rizzo, T. R., "Conformation-specific spectroscopy and photodissociation of cold, protonated tyrosine and phenylalanine," *J. Am. Chem. Soc.*, vol. 129, pp. 11814–11820, 2007.

[86] Metcalf, H. J. and Straten, P. v. d., *Laser Cooling and Trapping*. Springer-Verlag New York, Inc., 1999.

[87] Berkeland, D. J., Miller, J. D., Bergquist, J. C., Itano, W. M., and Wineland, D. J., "Minimization of ion micromotion in a Paul trap," *J. App. Phys.*, vol. 83, p. 5025, 1998.

[88] Bernath, P., *Spectra of Atoms and Molecules*. New York: Oxford University Press, USA, 1995.

[89] Crosser, M. S., Scott, S., Clark, A., and Wilt, P. M., "On the magnetic field near the center of Helmholtz coils," *Rev. Sci. Inst.*, vol. 81, p. 084701, 2010.

[90] Drakoudis, a., Sollner, M., and Werth, G., "Instabilities of ion motion in a linear Paul trap," *Int. J. Mass. Spec.*, vol. 252, pp. 61–68, 2006.

[91] Šašura, M. and Bužek, V., "Cold trapped ions as quantum information processors," *J. Mod. Opt.*, vol. 49, pp. 1593–1647, 2002.

[92] Sauter, T., Blatt, R., Neuhauser, W., and Toschek, P., "Quantum jumps observed in the fluorescence of a single ion," *Opt. Comm.*, vol. 60, pp. 287–292, 1986.

[93] Wuerker, R. F., Shelton, H., and Langmuir, R. V., "Electrodynamic containment of charged particles," *J. App. Phys.*, vol. 30, p. 342, 1959.

[94] Wineland, D. J. and Wayne, M., "Laser cooling," *Phys. Today*, vol. 40, pp. 156–162, 1987.

[95] Paul, W., "Electromagnetic traps for charged and neutral particles," *Rev. Mod. Phys.*, vol. 62, p. 535, 1990.

[96] Itano, W. M. and Wineland, D. J., "Laser cooling of atoms," *Phys. Rev. A*, vol. 20, p. 1521, 1979.

[97] Hendricks, R. J., Sørensen, J. L., Champenois, C., Knoop, M., and Drewsen, M., "Doppler cooling of calcium ions using a dipole-forbidden transition," *Phys. Rev. A*, vol. 77, p. 021401(R), 2007.

[98] Willitsch, S., "Coulomb-crystallised molecular ions in traps: Methods, applications, prospects," *Int. Rev. Phys. Chem.*, vol. 31, pp. 175–199, 2012.

[99] Mendoča, J. T. and Terčas, H., *Physics of Ultra-Cold Matter:Atomic Clouds, Bose-Einstein Condensates and Rydberg Plasmas*. Springer Series on Atomic, Optical, and Plasma Physics Vol 70, New York: Springer New York, 2013.

[100] Eschner, J., Morigi, G., Schmidt-Kaler, F., and Blatt, R., "Laser cooling of trapped ions," *J. Opt. Soc. Am. B*, vol. 20, pp. 1003–1015, 2003.

[101] Itano, W. M. and Wineland, D. J., "Laser cooling of ions stored in harmonic and Penning traps," *Phys. Rev. A*, vol. 25, pp. 35–54, 1982.

[102] Meekhof, D. M., Monroe, C., King, B. E., Itano, W. M., and Wineland, D. J., "Generation of nonclassical motional states of a trapped atom," *Phys. Rev. Lett.*, vol. 76, pp. 1796–1799, 1996.

[103] Staanum, P. F., Hoejbjerre, K., Wester, R., and Drewsen, M., "Probing isotope effects in chemical reactions using single ions," *Phys. Rev. Lett.*, vol. 100, p. 243003, 2008.

[104] Rohde, H., Gulde, S. T., Roos, C. F., Barton, P. A., Leibfried, D., Eschner, J., Schmidt-Kaler, F., and Blatt, R., "Sympathetic ground-state cooling and coherent manipulation with two-ion crystals," *J. Opt. B: Quant. Sem. Opt.*, vol. 3, p. S34, 2001.

[105] Neuhauser, W., Hohenstatt, M., Toschek, P., and Dehmelt, H., "Localized visible Ba^+ mono-ion oscillator," *Phys. Rev. A*, vol. 22, p. 1137, 1980.

[106] Madej, A. A. and Sankey, J. D., "Single, trapped Sr^+ atom: Laser cooling and quantum jumps by means of the 4d $^2D_{5/2}$-5s$^2S_{1/2}$ transition.," *Opt. Lett.*, vol. 15, p. 634, 1990.

[107] Lehmitz, H., Hattendorf-Ledwoch, J., Blatt, R., and Harde, H., "Population trapping in excited yb ions," *Phys. Rev. Lett.*, vol. 62, pp. 2108–2111, 1989.

[108] Bergquist, J. C., Hulet, R. G., Itano, W. M., and Wineland, D. J., "Observation of quantum jumps in a single atom," *Phys. Rev. Lett.*, vol. 57, pp. 1699–1702, 1986.

[109] Blinov, B. B., Moehring, D. L., Duan, L., and Monroe, C., "Observation of entanglement between a single trapped atom and a single photon," *Nature*, vol. 428, pp. 153–157, 2004.

[110] Balzer, C., Braun, A., Hannemann, T., Paape, C., Ettler, M., Neuhauser, W., and Wunderlich, C., "Electrodynamically trapped Yb^+ ions for quantum information processing," *Phys. Rev. A*, vol. 73, pp. 1–4, 2006.

[111] Hoyt, C. W., Barber, Z. W., Oates, C. W., Fortier, T. M., Diddams, S. A., and Hollberg, L., "Observation and absolute frequency measurements of the $^1S_0$-$^3P_0$ optical clock transition in neutral ytterbium," *Phys. Rev. Lett.*, vol. 95, p. 083003, 2005.

[112] McLoughlin, J. J., Nizamani, A. H., Siverns, J. D., Sterling, R. C., Hughes, M. D., Lekitsch, B., Stein, B., Weidt, S., and Hensinger, W. K., "Versatile ytterbium ion trap experiment for operation of scalable ion trap chips with motional heating and transition frequency measurements," *Phys. Rev. A*, vol. 83, p. 013406, 2010.

[113] Meyer, H. M., Steiner, M., Ratschbacher, L., Zipkes, C., and Michael, K., "Laser spectroscopy and cooling of Yb^+ ions on a deep-UV transition," *Phys. Rev. A*, vol. 85, p. 012502, 2012.

[114] Yu, N. and Maleki, L., "Lifetime measurements of the $4f^{14}5d$ metastable states in single ytterbium ions," *Phys. Rev. A*, vol. 61, p. 022507, 2000.

[115] Taylor, P., Roberts, M., Gateva-Kostova, S. V., Clarke, R. B. M., Barwood, G. P., Rowley, W. R. C., and Gill, P., "Investigation of the

$^2S_{1/2}-^2D_{5/2}$ clock transition in a single ytterbium ion," *Phys. Rev. A*, vol. 56, pp. 2699–2704, 1997.

[116] Alt, W., "An objective lens for efficient fluorescence detection of single atoms," *Opt. Int. J. Ligh. Elec. Opt.*, vol. 113, pp. 142–144, 2002.

[117] Olmschenk, S., Younge, K. C., Moehring, D. L., Matsukevich, D., Maunz, P., and Monroe, C., "Manipulation and detection of a trapped Yb^+ ion hyperfine qubit," *Phys. Rev. A*, vol. 76, p. 052314, 2007.

[118] Bauch, A., Schnier, D., and Tamm, C., "Collisional population trapping and optical de-excitation of ytterbium ions in a radiofrequency trap," *J. Mod. Opt.*, vol. 39, pp. 389–401, 1992.

[119] Itano, W. M., "Bragg diffraction from crystallized ion plasmas," *Science*, vol. 279, pp. 686–689, 1998.

[120] Roberts, M., Taylor, P., Gateva-Kostova, S. V., Clarke, R. B. M., Rowley, W. R. C., and Gill, P., "Measurement of the $^2S_{1/2}-^2D_{5/2}$ clock transition in a single $^{171}Yb^+$ ion," *Phys. Rev. A*, vol. 60, pp. 2867–2872, 1999.

[121] Schmidt, P. O., Rosenband, T., Langer, C., Itano, W. M., Bergquist, J. C., and Wineland, D. J., "Spectroscopy using quantum logic," *Science*, vol. 309, pp. 749–52, 2005.

[122] Leibrandt, D. R., Labaziewicz, J., Vuletic, V., and Chuang, I. L., "Cavity sideband cooling of a single trapped ion," *Phys. Rev. Lett.*, vol. 103, p. 103001, 2009.

[123] Monroe, C., Meekhof, D. M., King, B. E., Jefferts, S. R., Itano, W. M., Wineland, D. J., and Gould, P., "Resolved-sideband Raman cooling of a bound atom to the 3D zero-point energy," *Phys. Rev. Lett.*, vol. 75, pp. 4011–4014, 1995.

[124] Kowalewski, M., Morigi, G., Pinkse, P. W. H., and De Vivie-Riedle, R., "Cavity sideband cooling of trapped molecules," *Phys. Rev. A*, vol. 84, p. 033408, 2011.

[125] München, L. M. U., Schwedes, C., Becker, T., Von Zanthier, J., Walther, H., and Peik, E., "Laser sideband cooling with positive detuning," *Phys. Rev. A*, vol. 69, p. 053412, 2004.

[126] Schliesser, A., Rivière, R., Anetsberger, G., Arcizet, O., and Kippenberg, T. J., "Resolved sideband cooling of a micromechanical oscillator," *Nat. Phys.*, vol. 4, pp. 415 – 419, 2007.

[127] Teufel, J. D., Donner, T., Li, D., Harlow, J. W., Allman, M. S., Cicak, K., Sirois, A. J., Whittaker, J. D., Lehnert, K. W., and Simmonds, R. W., "Sideband cooling micromechanical motion to the quantum ground state," *Nature*, vol. 475, pp. 359–363, 2011.

[128] Morigi, G., Eschner, J., and Keitel, C., "Ground state laser cooling using electromagnetically induced transparency," *Phys. Rev. Lett.*, vol. 85, pp. 4458–61, 2000.

[129] Poulsen, G., *Sideband cooling of atomic and molecular ions*. PhD thesis, University of Aarhus, 2011.

[130] Wineland, D., Itano, W. M., Bergquist, J., Bollinger, J. J., and Prestage, J. D., "Spectroscopy of stored atomic ions," *Phys. Rev. Lett.*, vol. 54, 1985.

[131] Drewsen, M., Mortensen, A., Martinussen, R., Staanum, P., and Sørensen, J. L., "Non-destructive identification of cold and extremely localized single molecular ions," *Phys. Rev. Lett.*, vol. 93, p. 243201, 2004.

[132] Baba, T. and Waki, I., "Laser-cooled fluorescence mass spectrometry using laser-cooled barium ions in a tandem linear ion trap," *J. App. Phys.*, vol. 89, p. 4592, 2001.

[133] Ostendorf, a., Zhang, C., Wilson, M., Offenberg, D., Roth, B., and Schiller, S., "Sympathetic cooling of complex molecular ions to millikelvin temperatures," *Phys. Rev. Lett.*, vol. 97, p. 243005, 2006.

[134] Demtröder, W., *Molecular Physics: Theoretical Principles and Experimental Methods*. Wiley-VCH Verlag GmbH & Co. KGaA, 2003.

[135] Demtröder, W., *Atoms, Molecules and Photons: An Introduction to Atomic-, Molecular- and Quantum Physics*. Springer, 2011.

[136] Svanberg, S., *Atomic and Molecular Spectroscopy:Basic Aspects and Practical Applications*. Springer Series on Atomic, Optical, and Plasma Physics Vol. 6, New York: Springer New York, 2001.

[137] Barklem, P. S. and O'Mara, B. J., "The broadening of strong lines of Ca^+, Mg^+ and Ba^+ by collisions with neutral hydrogen atoms," *Mon. Not. R. Astron. Soc.*, vol. 300, p. 863, 1998.

[138] Kimura, N., Okada, K., Takayanagi, T., Wada, M., Ohtani, S., and Schuessler, H., "Sympathetic crystallization of CaH^+ produced by a laser-induced reaction," *Phys. Rev. A*, vol. 83, p. 033422, 2011.

[139] McFarland, R. H., Schlachter, A. S., Stearns, J. W., Liu, B., and Olson, R. E., "D^- production by charge transfer of (0.3 –3)-keV D^+ in thick alkaline-earth vapor targets: Interaction energies for CaH^+, CaH, and CaH^-," *Phys. Rev. A*, vol. 26, pp. 775–785, 1982.

[140] Schilling, J. B., Goddard III, W. A., and Beauchamp, J. L., "Theoritical studies of transition-metal hydrides. 1. bond energies for MH^+ with M= Ca, Sc, Ti, V, Cr, Mn, Fe, Co, Ni, Cu, and Zn," *J. Am. Chem. Soc.*, vol. 108, pp. 582–584, 1986.

[141] Kajita, M. and Moriwaki, Y., "Proposed detection of variation in mp/me using a vibrational transition frequency of a CaH^+ ion," *J. Phys. B: At. Mol. Opt. Phys.*, vol. 42, p. 154022, 2009.

[142] Fuentealba, P. and Reyes, O., "Pseudopotential calculations on the ground state of the alkaline-earth monohydride ions," *Mol. Phys.*, vol. 62, pp. 1291–1296, 1987.

[143] Habli, H., Ghalla, H., Oujia, B., and Gadéa, F., "*Ab initio* study of spectroscopic properties of the calcium hydride molecular ion," *Eur. Phys. J. D*, vol. 64, pp. 5–19, 2011.

[144] Kim, K. H., Lee, S. h., Lee, Y. S., and Jeung, G.-H., "Potential energy surfaces for the photochemical reactions $Ca^* + H_2 \rightarrow CaH + H$," *J. Chem. Phys.*, vol. 116, p. 589, 2002.

[145] Chen, L., Hsiao, M.-K., Chang, Y.-L., and Lin, K.-C., "Reaction dynamics of $Ca(4s3d\ ^1D_2)+CH_4 \rightarrow CaH(X^2\Sigma^+)+CH_3$: Reaction pathway and energy disposal for the CaH product.," *J. Chem. Phys.*, vol. 124, p. 024304, 2006.

[146] Chen, J.-j., Song, Y.-w., Lin, K.-c., and Hung, Y.-m., "Reaction pathway and energy disposal of the CaH product in the reaction of $Ca(4s4p\ ^1P_1)+CH_4 \rightarrow CaH(X^2\Sigma^+) + CH_3$," *J. Chem. Phys.*, vol. 118, p. 4983, 2003.

[147] Chang, Y.-l., Chen, L., Hsiao, M.-k., Chen, J.-j., and Lin, K.-c., "Reaction pathway for the nonadiabatic reaction of $Ca(4s3d\ ^1D) + H_2 \rightarrow CaH\ (X\ ^2\Sigma^+) + H$," *J. Chem. Phys.*, vol. 122, p. 084315, 2005.

[148] Liu, D.-K. and Lin, K.-C., "Nascent Rotational Distributions of MgH in Reaction of $Mg(4s\ ^1S_0)$ with H_2 and HD," *J. Chinese Chem. Soc.*, vol. 44, pp. 463–468, 1997.

[149] Liu, D.-k., Lin, K.-c., and Chen, J.-j., "Reaction dynamics of Mg ($4\ ^1S_0$, 3^1D_2) with H_2: Harpoon-type mechanism for highly excited states," *J. Chem. Phys.*, vol. 113, pp. 5302–5310, 2000.

[150] Wang, M., Wang, M., Sun, X., Sun, X., Bian, W., Bian, W., Sih, T., and Sih, T., "Quasiclassical trajectory study of $Mg(3s3p\ ^1P_1) + H_2$ reaction on fitted *ab initio* surfaces," *J. Phys. Chem. A*, vol. 103, pp. 7938–7948, 1999.

[151] Lin, K.-C. and González Ureña, A., "Dynamical and stereodynamical studies of alkaline-earth atommolecule reactions," *Int. Rev. Phys. Chem.*, vol. 26, pp. 289–352, 2007.

[152] Hohenstein, E. private communication, 2010.

[153] Le Roy, R. J., "Level 8.0: A computer program for solving the radial Schrødinger equation for boundand quasibound levels," tech. rep., University of Waterloo, 2007.

[154] Hudson, E. private communication, 2014.

[155] Biraben, F., Cagnac, B., and Grynberg, G., "Experimental evidence of two-photon transition without Doppler broadening," *Phys. Rev. Lett.*, vol. 32, p. 643, 1974.

[156] Gord, J. R., Garrett, A. W., Bandy, R. E., and Zwier, T. S., "REMPI fragmentation as a probe of hydrogen bonding in aromatic-X clusters," *Chem. Phys. Lett.*, vol. 171, pp. 443–450, 1990.

[157] Gasmi, K., Al-tuwirqi, R. M., Skowronek, S., Telle, H. H., and Urena, A. G., "Rotationally resolved (1+1′) resonance-enhanced multiphoton ionization (REMPI) of CaR (R=H, D) in supersonic beams : CaR X $^2\Sigma^+$ (υ =0)→ CaR* $B^2\Sigma^+$ (υ =0,1)→ CaR$^+$ X$^1\Sigma^+$," *J. Phys. Chem. A*, vol. 107, pp. 10960–10968, 2003.

[158] de Vries, M. S. and Hobza, P., "Gas-phase spectroscopy of biomolecular building blocks," *Ann. Rev. Phys. Chem.*, vol. 58, pp. 585–612, 2007.

[159] Mller, C., Klppel-Riech, M., Schrder, F., Schroeder, J., and Troe, J., "Fluorescence and REMPI spectroscopy of jet-cooled isolated 2-phenylindene in the S_1 state," *J. Phys. Chem. A*, vol. 110, pp. 5017–5031, 2006.

[160] Chen, Y.-t., "Molecular Rydberg states and ionization energy studied by two-photon resonant ionization spectroscopy," *J. Chin. Chem. Soc.*, vol. 49, pp. 703–722, 2002.

[161] Kimura, K., "Development of laser photoelectron spectroscopy based on resonantly enhanced multiphoton ionization," *J. Elec. Spec. Rel. Phen.*, vol. 100, pp. 273–296, 1999.

[162] Ito, M., "Two-colour dip spectroscopy of jet-cooled molecules," *Int. Rev. Phys. Chem.*, vol. 8, pp. 147–169, 1989.

[163] Syage, J. a. and Wessel, J. E., "Resonance ion dissociation spectroscopy of naphthalene ions prepared in a supersonic expansion," *J.Chem. Phys.*, vol. 87, pp. 3313–3320, 1987.

[164] Weinkauf, R., Walter, K., Boesl, U., and Schlag, E., "Mass-selected molecular spectra: (1+1)-photodissociation spectroscopy of CH_3I^+ and CD_3I^+," *Chem. Phys. Lett.*, vol. 141, pp. 267–276, 1987.

[165] Walter, K., Weinkauf, R., Boesl, U., and Schlag, E. W., "Molecular ion spectroscopy: Mass selected, resonant two-photon dissociation spectra of CH_3I^+ and CD_3I^+," *J.Chem. Phys.*, vol. 89, p. 1914, 1988.

[166] Eyler, J. R., "Infrared multiple photon dissociation spectroscopy of ions in Penning traps," *Mass Spec. Rev.*, vol. 28, pp. 448–467, 2009.

[167] Tran, V. Q., Karr, J.-P., Douillet, A., Koelemeij, J. C. J., and Hilico, L., "Two-photon spectroscopy of trapped HD^+ ions in the Lamb-Dicke regime," *Phys. Rev. A*, vol. 88, p. 033421, 2013.

[168] Ni, K.-K., Loh, H., Grau, M., Cossel, K. C., Ye, J., and Cornell, E. a., "State-specific detection of trapped HfF^+ by photodissociation," *J. Mol. Spec.*, vol. 300, pp. 12–15, 2014.

[169] Frohlich, D. and Sondergeld, M., "Experimental techniques in two-photon spectroscopy," *J. Phys. E*, vol. 10, p. 761, 1977.

[170] Tsuchiya, Y., Fujii, M., and Ito, M., "Electronic spectra of isolated cations in supersonic jets by mass-selected ion-dip spectroscopy. Cations of benzene, p-difluorobenzene, and 1,3,5-trifluorobenzene," *J. Chem. Phys.*, vol. 90, p. 6965, 1989.

[171] Walter, K., Boesl, U., and Schlag, E., "Molecular ion spectroscopy: Resonance-enhanced multiphoton dissociation spectra of the fluorobenzene cation," *Chem. Phys. Lett.*, vol. 162, pp. 261–268, 1989.

[172] Walter, K., Weinkauf, R., Boesl, U., and Schlag, E., "Spectroscopy of the benzene cation: Resonance enhanced multiphoton dissociation spectra of the $\beta \rightarrow$ X transition," *Chem. Phys.*, vol. 155, p. 8, 1989.

[173] Cheng, P. Y., Willey, K. F., Salcido, J. E., and Duncan, M. A., "Resonance-enhanced photodissociation spectroscopy of mass-selected metal cluster cations," *Int. J. Mass. Spec. Ion. Pro.*, vol. 102, pp. 67–80, 1990.

[174] Saigusa, H. and Lim, E. C., "Photodissociation spectra of naphthalene cluster ions $(C_{10}H_8)_n^+$, n=2-7: evidence for dimer core structure and comparison with neutral clusters," *J. Phys. Chem.*, vol. 98, pp. 13470–13475, 1994.

[175] Ripoche, X., Dimicoli, I., Le Calve, J., Piuzzi, F., and Botter, R., "Resonance-enhanced multiphoton dissociation spectroscopy of the forbidden $\tilde{B} \leftarrow \tilde{X}$ transition of the gas phase chlorobenzene cation," *Chem. Phys.*, vol. 124, pp. 305–313, 1988.

[176] Watson, C. H., Zimmerman, J. A., Bruce, J. E., and Eyler, J. R., "Resonance-enhanced two-laser infrared multiple photon dissociation of gaseous ions," *J. Phys. Chem.*, vol. 95, pp. 6081–6086, 1991.

[177] Boyarkin, O. V., Kowalczyk, M., and Rizzo, T. R., "Collisionally enhanced isotopic selectivity in multiphoton dissociation of vibrationally excited CF_3H," *J. Chem. Phys.*, vol. 118, p. 93, 2003.

[178] Madsen, J. a. and Brodbelt, J. S., "Comparison of infrared multiphoton dissociation and collision-induced dissociation of supercharged peptides in ion traps," *J. Am. Soc. Mass Spec.*, vol. 20, pp. 349–58, 2009.

[179] Shapiro, M., "Theory of one- and two-photon dissociation with strong laser pulses," *J. Chem. Phys.*, vol. 101, p. 3844, 1994.

[180] Kondo, A. and Meath, W., "On the dynamics of pulsed and continuous wave laser-molecule interactions and the effects of permanent dipoles," *Mol. Phys.*, vol. 74, pp. 113–119, 1991.

[181] Lin, S., Fujuimura, Y., and Neusser, H.J.and Schlag, E., *Multiphoton Spectroscopy of Molecules*. Orlando,FL: Academic Press, Inc, 1984.

[182] Shapiro, M., "Associtaion, dissociation, and the acceleration and supression of reactions by laser pulses," in *Advances in Chemical Physics* (Progogine, I. and Rice, S., eds.), vol. 114, p. 123, New York: John Wiley and Sons Inc., 2000.

[183] Wieman, C. E. and Hollberg, L., "Using diode lasers for atomic physics," *Rev. Sci. Inst.*, vol. 62, pp. 1–20, 1991.

[184] McCarron, D. J., "A guide to acousto-optic modulators," tech. rep., Durham University Joinint Quantum Center, 2007.

[185] Trebino, R., Baltuska, A., Peshnichnikov, M., and Wiersma, D. A., "Measuring ultrashort pulses in the single-cycle regime: Frequency-resolved optical gating," in *Few-Cycle Pulse Generation and its Applications* (Kaertner, F., ed.), Topics in Applied Physics (Book 95), New York: Springer-Verlag, 2004.

[186] Rhodes, M., Steinmeyer, G., and Trebino, R., "Standards for ultrashort-laser-pulse-measurement techniques and their consideration for self-referenced spectral interferometry.," *Appl. Opt.*, vol. 53, pp. D1–D11, 2014.

[187] Goeders, J. E., *Resolved sideband spectroscopy for the detection of weak optical transitions*. PhD thesis, Georgia Institute of Technology, 2013.

[188] Clark, C. R., Goeders, J. E., Dodia, Y. K., Viteri, C. R., and Brown, K. R., "Detection of single-ion spectra by Coulomb-crystal heating," *Phys. Rev. A*, vol. 81, p. 043428, 2010.

[189] Rugango, R., Goeders, J. E., Dixon, T. H., Gray, J. M., Khanyile, N. B., Shu, G., Clark, R. J., and Brown, K. R., "Sympathetic cooling of molecular ion motion to the ground state," *New J. Phys.*, vol. 17, p. 035009, 2015.

[190] Furukawa, T., Nishimura, J., Tanaka, U., and Urabe, S. *Jap. J. App. Phys.*, vol. 44, p. 7619, 2005.

[191] Siverns, J. D., Simkins, L. R., Weidt, S., and Hensinger, W. K., "On the application of radio frequency voltages to ion traps via helical resonators," *App. Phys. B*, vol. 107, pp. 921–934, 2012.

[192] Dai, D. P., Xia, Y., Yin, Y. N., Yang, X. X., Fang, Y. F., Li, X. J., and Yin, J. P., "A linewidth-narrowed and frequency-stabilized dye laser for application in laser cooling of molecules," *Opt. Exp.*, vol. 22, p. 28645, 2014.

[193] Riedle, E., Ashworth, S. H., Farrell, J. T., and Nesbitt, D. J., "Stabilization and precise calibration of a continuous-wave difference frequency spectrometer by use of a simple transfer cavity," *Rev. Sci. Inst.*, vol. 65, pp. 42–48, 1994.

[194] Doret, S. C., "Transfer cavity / stabilized hene based laser. frequency stabilization." 2011.

[195] Uetake, S., Matsubara, K., Ito, H., Hayasaka, K., and Hosokawa, M., "Frequency stability measurement of a transfer-cavity-stabilized diode laser by using an optical frequency comb," *App. Phys. B: Las. Opt.*, vol. 97, pp. 413–419, 2009.

[196] Cutler, L. and Searle, C., "Some aspects of the theory and measurement of frequency fluctuations in frequency standards," *Proc. IEEE*, vol. 54, pp. 136–154, 1966.

[197] Allan, D. W., "Atomic frequency standards," *Proc. IEEE*, vol. 54, pp. 221–230, 1966.

[198] Carr, L. D., DeMille, D., Krems, R. V., and Ye, J., "Cold and ultracold molecules: Science, technology and applications," *New J. Phys.*, vol. 11, p. 055049, 2009.

[199] Dulieu, O., Krems, R., Weidemüller, M., and Willitsch, S., "Physics and chemistry of cold molecules," *Phys. Chem. Chem. Phys.*, vol. 13, pp. 18703–4, 2011.

[200] Willitsch, S., Bell, M. T., Gingell, A. D., and Softley, T. P., "Chemical applications of laser- and sympathetically-cooled ions in ion traps," *Phys. Chem. Chem. Phys.*, vol. 10, pp. 7200–10, 2008.

[201] Tong, X., Wild, D., and Willitsch, S., "Collisional and radiative effects in the state-selective preparation of translationally cold molecular ions in ion traps," *Phys. Rev. A*, vol. 83, p. 023415, 2011.

[202] Seck, C. M., Hohenstein, E. G., Lien, C.-y., Stollenwerk, P. R., and Odom, B. C., "Rotational state analysis of AlH^+ by two-photon dissociation," *J. Mol. Spec.*, vol. 300, p. 108, 2014.

[203] Germann, M., Tong, X., and Willitsch, S., "Observation of electric-dipole-forbidden infrared transitions in cold molecular ions," *Nat. Phys.*, vol. 10, pp. 1745–2473, 2014.

[204] Sainis, S., Sage, J., Tiesinga, E., Kotochigova, S., Bergeman, T., and DeMille, D., "Detailed spectroscopy of the $Cs_2 a^3\Sigma_u^+$ state and implications for measurements sensitive to variation of the electron-proton mass ratio," *Phys. Rev. A*, vol. 86, p. 022513, 2012.

[205] Baron, J., Campbell, W. C., DeMille, D., Doyle, J. M., Gabrielse, G., Gurevich, Y. V., Hess, P. W., Hutzler, N. R., Kirilov, E., Kozyryev, I., O'Leary, B. R., Panda, C. D., Parsons, M. F., Petrik, E. S., Spaun, B., Vutha, a. C., and West, a. D., "Order of magnitude smaller limit on the electric dipole moment of the electron," *Science*, vol. 343, pp. 269–72, 2014.

[206] Goeders, J. E., Clark, C. R., Vittorini, G., Wright, K., Viteri, C. R., and Brown, K. R., "Identifying single molecular ions by resolved sideband measurements.," *J. Phys. Chem. A*, vol. 117, pp. 9725–31, 2013.

[207] Rizzo, T. R., Stearns, J. a., and Boyarkin, O. V., "Spectroscopic studies of cold, gas-phase biomolecular ions," *Int. Rev. Phys. Chem.*, vol. 28, pp. 481–515, 2009.

[208] Schneider, C., Schowalter, S. J., Chen, K., Sullivan, S. T., and Hudson, E. R., "Laser-cooling-assisted mass spectrometry," *Phys. Rev. Applied*, vol. 2, p. 034013, 2014.

[209] Tong, X., Nagy, T., Reyes, J. Y., Germann, M., Meuwly, M., and Willitsch, S., "State-selected ion-molecule reactions with Coulomb-crystallized molecular ions in traps," *Chem. Phys. Lett.*, vol. 547, pp. 1–8, 2012.

[210] Hansen, A. K., Sorensen, M. a., Staanum, P. F., and Drewsen, M., "Single-ion recycling reactions," *Angewandte Chemie*, vol. 51, pp. 7960–2, 2012.

[211] Lien, C., Seck, C.M., L. Y., Nguyen, J., Tabor, D. A., and Odom, B. C., "Broadband optical cooling of molecular rotors from room temperature to the ground state," *Nat. Comm.*, vol. 5, p. 4783, 2014.

[212] Schmidt, P., Rosenband, T., Koelemeij, J., Hume, D., Itano, W., Bergquist, J., and Wineland, D., "Spectroscopy of atomic and molecular ions using quantum logic," *Aip Conf. Proc.*, vol. 1, pp. 305–312, 2006.

[213] Dian, B. C., Longarte, A., and Zwier, T. S., "Conformational dynamics in a dipeptide after single-mode vibrational excitation," *Science*, vol. 296, pp. 2369–2373, 2002.

[214] Vigren, E., *Dissociative recombination of organic molecular ions of relevance for interstellar clouds and Titian's upper atmosphere*. PhD thesis, 2010.

[215] Peik, E., "Logical spectroscopy," *Science*, vol. 309, p. 710, 2005.

[216] Mur-Petit, J., García-Ripoll, J. J., Pérez-Ríos, J., Campos-Martínez, J., Hernández, M. I., and Willitsch, S., "Temperature-independent quantum logic for molecular spectroscopy," *Phys. Rev. A*, vol. 85, p. 022308, 2012.

[217] Wan, Y., Gebert, F., Wäbbena, J. B., Scharnhorst, N., Amairi, S., Leroux, I. D., Hemmerling, B., Lärch, N., Hammerer, K., and Schmidt, P. O., "Precision spectroscopy by photon-recoil signal amplification," *Nat. Comm.*, vol. 5, p. 3096, 2014.

[218] Roos, C., Rohde, H., Gulde, S., Mundt, A., Reymond, G., Lederbauer, M., Eschner, J., Schmidt-Kaler, F., Leibfried, D., and Blatt, R., "Towards quantum information with trapped calcium ions," *2000 IEEE International Symposium on Circuits and Systems. Emerging Technologies for the 21st Century. Proceedings (IEEE Cat No.00CH36353)*, p. 240, 2000.

[219] Shu, G., Vittorini, G., Buikema, A., Nichols, C. S., Volin, C., Stick, D., and Brown, K. R., "Heating rates and ion-motion control in a y-junction surface-electrode trap," *Phys. Rev. A*, vol. 89, p. 062308, 2014.

[220] Roos, C., Zeiger, T., Rohde, H., Nägerl, H. C., Eschner, J., Leibfried, D., Schmidt-Kaler, F., and Blatt, R., "Quantum state engineering on an optical transition and decoherence in a Paul trap," *Phys. Rev. Lett.*, vol. 83, pp. 4713–4716, 1999.

[221] Vittorini, G., Wright, K., Brown, K. R., Harter, A. W., and Doret, S. C., "Modular cryostat for ion trapping with surface-electrode ion traps," *Rev. Sci. Instrum.*, vol. 84, p. 043112, 2013.

[222] Gilkison, A., Viteri, C., and Grant, E., "Coupling of Electron Orbital Motion with Rotation in the High Rydberg States of BH," *Phys. Rev. Lett.*, vol. 92, p. 173005, 2004.

[223] Shi, D.-h., Liu, H. U. I., Zhang, J.-p., Sun, J.-f., Liu, Y.-f., and Zhu, Z.-l., "Spectroscopic investigations on BH^+ ion using MRCI method and correlation-consistent sextuple basis set augmented with diffuse functions," *Int. J. Quant. Chem.*, vol. 111, pp. 2171–2179, 2011.

[224] Chang, Y.-P., Dugocki, K., Küpper, J., Rösch, D., Wild, D., and Willitsch, S., "Specific chemical reactivities of spatially separated 3-aminophenol conformers with cold Ca^+ ions," *Science*, vol. 342, pp. 98–101, 2013.

[225] Chou, C. W., Hume, D. B., Koelemeij, J. C. J., Wineland, D. J., and Rosenband, T., "Frequency comparison of two high-accuracy Al^+ optical clocks," *Phys. Rev. Lett.*, vol. 104, p. 070802, 2010.

[226] Page, A. J. and von Nagy-Felsobuki, E. I., "*Ab initio* electronic and rovibrational structure of Mg_2^{2+}," *Chem. Phys.*, vol. 351, pp. 37–45, 2008.

[227] Cha, C., Weinkauf, R., and Boesl, U., "Laser spectroscopy of molecular ions: The $\tilde{A}\rightarrow\tilde{X}$ transition of the acetylene radical cation," *J. Chem. Phys.*, vol. 103, p. 5224, 1995.

[228] Bartana, A., Koslof, R., and Tannor, D. J., "Laser cooling of molecules by dynamically trapped states," *Chem. Phys.*, vol. 267, pp. 195–207, 2001.

[229] Heijnsbergen, D. V., Jaeger, T. D., Helden, G. V., Meijer, G., and Duncan, M., "The infrared spectrum of Al^+ benzene in the gas phase," *Chem. Phys. Lett.*, vol. 364, pp. 345–351, 2002.

[230] Banerjee, S., Bhattacharyya, S. S., and Saha, S., "Non-adiabatic effects on resonance-enhanced two-photon of H_2," *Phys. Rev. A*, vol. 49, p. 1836, 1994.

[231] Doyle, J., Friedrich, B., Krems, R. V., and Masnou-Seeuws, F., "Editorial: Quo vadis, cold molecules?," *Euro. Phys. J. D*, vol. 31, pp. 149–164, 2004.

[232] Lauder, M., Knight, P., and Greenland, P., "Pulse-shape effects in intense-field laser excitation of atoms," *Int. J. Opt.*, vol. 33, pp. 1231–1252, 1986.

[233] Weiner, A. M., "Femtosecond pulse shaping using spatial light modulators," *Rev. Sci. Inst.*, vol. 71, p. 1929, 2000.

[234] Assion, a., Baumert, T., Bergt, M., Brixner, T., Kiefer, B., Seyfried, V., Strehle, M., and Gerber, G., "Control of chemical reactions by feedback-optimized phase-shaped femtosecond laser pulses," *Science*, vol. 282, pp. 919–22, 1998.

[235] Tague, T. J. and Andrews, L., "Reactions of pulsed-laser evaporated boron atoms with hydrogen. Infrared spectra of boron hydride intermediate species in solid argon," *J. Am. Chem. Soc.*, vol. 116, pp. 4970–4976, 1994.

[236] Drewsen, M., "Cooling, identification and spectroscopy of super-heavy element ions," *Euro. Phys. J. D*, vol. 45, pp. 125–127, 2007.

[237] Herskind, P., Dantan, A., Langkilde-Lauesen, M. B., Mortensen, A., Sorensen, J. L., and Drewsen, M., "Loading of large ion Coulomb crystals into a linear Paul trap incorporating an optical cavity for cavity QED studies," *App. Phys. B*, vol. 93, pp. 373–379, 2008.

[238] Härter, a., Krükow, a., Deiss, M., Drews, B., Tiemann, E., and Denschlag, J. H., "Population distribution of product states following three-body recombination in an ultracold atomic gas," *Nat. Phys.*, vol. 9, pp. 512–517, 2013.

[239] Chatel, B., Degert, J., Stock, S., and Girard, B., "Competition between sequential and direct paths in a two-photon transition," *Phys. Rev. A*, vol. 68, p. 041402, 2003.

[240] Wineland, D., Monroe, C., Leibfried, D., King, B. E., and Meekhof, D. M., "Experimental issues in coherent quantum-state manipulation of trapped atomic ions," *J. Res. Natl. Inst. Stand. Tech.*, vol. 103, p. 259, 1998.

[241] Goulay, F., Osborn, D. L., Taatjes, C. a., Zou, P., Meloni, G., and Leone, S. R., "Direct detection of polyynes formation from the reaction of ethynyl radical (C_2H) with propyne (CH_3-C≡CH) and allene (CH_2=C=CH_2)," *Phys. Chem. Chem. Phys.*, vol. 9, pp. 4291–300, 2007.

[242] Turulski, J. and Niedzielskib, J., "The classical Langevin rate constant for ion/molecule capture: When, if at all, is it constant?," *Int. J. Mass. Spec. Ion Proc.*, vol. 139, pp. 155–162, 1994.

[243] Barrow, J. D., "Varying constants," *Phil. Trans. Roy. Soc. Lond.*, vol. A363, pp. 2139–2153, 2005.

[244] Chwalla, M. M., *Precision spectroscopy with $^{40}Ca^+$ ions in a Paul trap*. PhD thesis, MIT, 2009.

[245] Kolodziejski, L., "Sensitive, 3D micromotion compensation in a surface-electrode ion trap," Master's thesis, 2013.

[246] Larson, D. J., Bergquist, J., Bollinger, J. J., Itano, W. M., and Wineland, J., "Sympathetic cooling of trapped ions: A laser-cooled two-species nonneutral ion plasma," *Phys. Rev. Lett.*, vol. 57, p. 70, 1986.

[247] Sofikitis, D., Weber, S., Fioretti, A., Horchani, R., Allegrini, M., Chatel, B., Comparat, D., and Pillet, P., "Molecular vibrational cooling by optical pumping with shaped femtosecond pulses," *New J. Phys.*, vol. 11, p. 055037, 2009.

[248] Mortensen, A., Lindballe, J. J. T., Jensen, I. S., Staanum, P., Voigt, D., and Drewsen, M., "Isotope shifts of the $4S^2\ ^1S_0 \rightarrow 4s5p^1P_1$ transition and hyperfine splitting of the $4s5p^1P_1$ state in calcium," *Phys. Rev. A*, vol. 69, p. 042502, 2004.

[249] Gudeman, C. and Saykallyn, R., "Velocity modulation infrared laser spectroscopy of molecular ions," *Ann. Rev. Phys. Chem.*, vol. 35, pp. 387–418, 1984.

[250] Vogelius, I. S., Madsen, L. B., and Drewsen, M., "Rotational cooling of molecular ions through laser-induced coupling to the collective modes of a two-ion Coulomb crystal," *J. Phys. B: At. Mol. Opt. Phys.*, vol. 39, pp. S1267–S1280, 2006.

[251] Flambaum, V. V., "Variation of fundamental constants: Theory and observations," *Int.J.Mod.Phys.*, vol. A22, pp. 4937–4950, 2007.

[252] Grynberg, G. and Cagnac, B., "Doppler-free multiphotonic spectroscopy," *Rep. Prog.Phys.*, vol. 40, pp. 791–841, 1977.

[253] Uzan, J.-p., "Varying constants, gravitation and cosmology," *Liv. Rev. Rel.*, vol. 14, pp. 1–145, 2011.

[254] Brewer, R. G., Mooradian, A., and Stoicheff, B. P., "The early days of precision laser spectroscopy," *Phys. Today*, vol. 60, pp. 49–55, 2007.

[255] Drever, R. W. P., Hall, J. L., Kowalski, F. V., Hough, J., Ford, G. M., Munley, a. J., and Ward, H., "Laser phase and frequency stabilization using an optical resonator," *App. Phys. B: Phot. Las. Chem.*, vol. 31, pp. 97–105, 1983.

[256] Bauschlicher, C. W., Langhoff, S. R., and Taylor, P. R., "On the dissociation energy of BH," *J. Chem. Phys.*, vol. 93, p. 502, 1990.

[257] Berry, K. R. and Duncan, M. A., "Photoionization spectroscopy of LiMg," *Chem. Phys. Lett.*, vol. 279, pp. 44–49, 1997.

[258] Niederhausen, T., Thumm, U., and Martin, F., "Laser-controlled vibrational heating and cooling of oriented H_2^+ molecules," *J. Phys. B: At. Mol. Opt. Phys.*, vol. 45, p. 105602, 2012.

[259] Berengut, J. C. and Flambaum, V. V., "Manifestations of a spatial variation of fundamental constants on atomic clocks, Oklo, meteorites, and cosmological phenomena," *Europhys. Lett.*, vol. 97, p. 20006, 2010.

[260] Ricardo Viteri, C., Gilkison, A. T., Rixon, S. J., and Grant, E. R., "Rovibrational characterization of $X^2\Sigma^+$ $^{11}BH^+$ by the extrapolation of photoselected high Rydberg series in ^{11}BH," *J. Chem. Phys.*, vol. 124, p. 144312, 2006.

[261] Hasegawa, T., "Sympathetic cooling of a mass-mismatched two-ion chain in a double-well trap potential," *Phys. Rev. A*, vol. 83, p. 053407, 2011.

[262] Karr, J.-P., Douillet, a., and Hilico, L., "Photodissociation of trapped H_2^+ ions for REMPD spectroscopy," *App. Phys. B*, vol. 107, pp. 1043–1052, 2011.

[263] Kajita, M., Gopakumar, G., Abe, M., and Hada, M., "Sensitivity of vibrational spectroscopy of optically trapped SrLi and CaLi molecules to variations in mp/me," *J. Phys. B: At. Mol. Opt. Phys.*, vol. 46, p. 025001, 2013.

[264] Ottinger, C., "Chemiluminescent ionmolecule reactions B^++H_2," *J. Chem. Phys.*, vol. 74, p. 928, 1981.

[265] Schiller, S., Bakalov, D., and Korobov, V., "Simplest molecules as candidates for precise optical clocks," *Phys. Rev. Lett.*, vol. 113, p. 023004, 2014.

[266] Roos, C. F., *Controlling the quantum state of trapped ions*. PhD thesis, University of Innsbruck, 2000.

[267] Højbjerre, K., *Experiments with cold trapped molecular ions*. PhD thesis, University of Aarhus, 2009.

[268] Ozeri, R., "The trapped-ion qubit tool box," *Contemporary Physics*, vol. 52, pp. 531–550, 2011.

[269] Hornekær, L., *Single and multi-species Coulomb ion crystals: structures, dynamics and sympathetic cooling*. PhD thesis, University of Aarhus, 2000.

[270] Schnell, M. and Meijer, G., "Cold molecules: preparation, applications, and challenges," *Angewandte Chemie*, vol. 48, pp. 6010–31, 2009.

[271] Friedrich, B. and Doyle, J. M., "Why are cold molecules so hot?," *Chem. Phys. Phys. Chem.*, vol. 10, pp. 604–23, 2009.

[272] Chakrabarty, S., Holz, M., Campbell, E. K., Banerjee, A., Gerlich, D., and Maier, J. P., "A novel method to measure electronic spectra of cold molecular ions," *J. Phys. Chem. Lett.*, vol. 4, pp. 4051–4054, 2013.

[273] Korobenko, A., Milner, A. A., Hepburn, J. W., and Milner, V., "Rotational spectroscopy with an optical centrifuge," *Phys. Chem. Chem. Phys.*, vol. 16, pp. 4071–4076, 2014.

[274] Rosmus, P. and Meyer, W., "PNOCI and CEPA studies of electron correlation effects. IV. Ionization energies of the first and second row diatomic hydrides and the spectroscopic constants of their ions," *J. Chem. Phys.*, vol. 66, p. 13, 1977.

[275] Grieman, F. J., Mahan, B. H., O'Keefe, A., and Winn, S., "Laser-induced fluorescence of trapped molecular ions: The $CH^+ A^1\Pi \rightarrow X^1\Sigma^+$ system," *Faraday Discuss. Chem. Soc.*, vol. 71, p. 191, 1981.

[276] Matsubara, K., Li, Y., Kajita, M., Hayasaka, K., Hosokawa, M., and Urabe, S., "Single Ca^+ ion trapping toward precise frequency measurement of the $4^2S_{1/2} \leftrightarrow 3^2D_{5/2}$ transition," *Proc. 2005 IEEE Int. Freq. Control Symp. Expo. 2005*, vol. 4, pp. 616–622, 2005.

[277] Rosch, D., Willitsch, S., Chang, Y.-P., and Kupper, J., "Chemical reactions of conformationally selected 3-aminophenol molecules in a beam with Coulomb-crystallized Ca^+ ions," *J. Chem. Phys.*, vol. 140, p. 124202, 2014.

[278] Vogelius, I. S., Madsen, L. B., and Drewsen, M., "Blackbody-radiation-assisted laser cooling of molecular ions," *Phys. Rev. Lett.*, vol. 89, p. 173003, 2002.

[279] Gordv, W., "Microwave spectroscopy," *Rev. Sci. Inst.*, vol. 20, p. 668, 1948.

[280] Wineland, D. J., Itano, W. M., and Bergquist, J. C., "Absorption spectroscopy at the limit: Detection of a single atom," *Optics Lett.*, vol. 12, pp. 389–91, 1987.

[281] Kajita, M., Abe, M., Hada, M., and Moriwaki, Y., "Estimated accuracies of pure XH^+ (X: even isotopes of group II atoms) vibrational transition frequencies: Towards the test of the variance in mp/me," *J. Phys. B: At. Mol. Opt. Phys.*, vol. 44, p. 025402, 2011.

[282] Bertelsen, A., Vogelius, I. S., Jørgensen, S., Kosloff, R., and Drewsen, M., "Photo-dissociation of cold MgH^+ ions," *Euro. Phys. J. D*, vol. 31, pp. 403–408, 2004.

[283] Baba, T. and Waki, I., "Sympathetic cooling rate of gas-phase ions in a radio-frequency-quadrupole ion trap," *App. Phys. B: Las. Opt.*, vol. 74, pp. 375–382, 2002.

[284] Kowalewski, M., Kahra, S., Leschhorn, G., and Sch, T., "Femtosecond pump-probe spectroscopy for single trapped molecular ions," *EPJ Web of Conferences*, vol. 41, p. 02028, 2013.

[285] Pomerantz, A. E. and Zare, R. N., "Doppler-free multi-photon ionization: a proposal for enhancing ion images," *Chem. Phys. Lett.*, vol. 370, pp. 515–521, 2003.

[286] Vogelius, I. S., Madsen, L. B., and Drewsen, M., "Rotational cooling of molecules using lamps," *J. Phys. B: At. Mol. Opt. Phys.*, vol. 37, p. 5, 2004.

[287] VanDevender, a. P., Colombe, Y., Amini, J., Leibfried, D., and Wineland, D. J., "Efficient fiber optic detection of trapped ion fluorescence," *Phys. Rev. Lett.*, vol. 105, p. 023001, 2010.

[288] Chen, K., Schowalter, S., Kotochigova, S., Petrov, A., Rellergert, W., Sullivan, S., and Hudson, E., "Molecular-ion trap-depletion spectroscopy of $BaCl^+$," *Phys. Rev. A*, vol. 83, p. 030501, 2011.

[289] Viteri, C. R., Gilkison, A. T., and Grant, E. R., "The np Rydberg series of boron monohydride: l-uncoupling and Rydberg electron interactions with the rovibrational motion of the ion core," *J. Chem. Phys.*, vol. 136, p. 214312, 2012.

[290] Truppe, S., Hendricks, R. J., Tokunaga, S. K., Lewandowski, H. J., Kozlov, G., Henkel, C., Hinds, E. A., and Tarbutt, M. R., "A search for varying fundamental constants using hertz-level frequency measurements of cold CH molecules," *Nat. Comm.*, vol. 4, pp. 1–8, 2013.

[291] Murphy, M. T., Flambaum, V. V., and Henkel, C., "Strong limit on a variable proton-to-electron mass ratio from molecules in the distant universe," *Science*, vol. 320, pp. 1611–1613, 2008.

[292] Krems, R. V., "Cold controlled chemistry," *Phys. Chem. Chem. Phys.*, vol. 10, pp. 4079–92, 2008.

[293] Uzan, J.-p., "The fundamental constants and their variation: observational and theoretical status," *Rev. Mod. Phys.*, vol. 75, p. 403, 2003.

[294] Vargas-mart, M. and Arturo, Z., "Ion-laser interactions: The most complete solution," *Physics Reports*, vol. 513, pp. 229–261, 2012.

[295] Breckenridge, W., Umemoto, H., and Wang, J.-H., "Initial internal energy distributions of CdH (CdD) produced in the reaction of Cd(5s5p $^3P_1$) with H_2, D_2, and HD," *Chem. Phys. Lett.*, vol. 123, p. 23, 1986.

[296] Cooper, D. L. and Richards, W. G., "Spin splitting in BH^+," *J. Phys. B: At. Mol. Opt. Phys.*, vol. 14, pp. L217–L130, 1981.

[297] Antoine, R., Doussineau, T., Dugourd, P., and Calvo, F., "Multiphoton dissociation of macromolecular ions at the single-molecule level," *Phys. Rev. A*, vol. 87, p. 013435, 2013.

[298] Crabtree, K. N., Hodges, J. N., Siller, B. M., Perry, A. J., Kelly, J. E., Jenkins, P. a., and McCall, B. J., "Sub-Doppler mid-infrared spectroscopy of molecular ions," *Chem. Phys. Lett.*, vol. 551, pp. 1–6, 2012.

[299] Tarbutt, M. R., Hudson, J. J., Sauer, B. E., and Hinds, E. A., *Cold Molecules: Theory, Experiment, Applications*. CRC Press, 2009.

[300] Roth, B., Ostendorf, a., Wenz, H., and Schiller, S., "Production of large molecular ion crystals via sympathetic cooling by laser-cooled Ba^+," *J. Phys. B: At. Mol. Opt. Phys.*, vol. 38, pp. 3673–3685, 2005.

[301] Murad, E., "Abstraction reactions of Ca^+ and Sr^+ ions," *J. Chem. Phys.*, vol. 78, p. 6611, 1983.

[302] Margolis, H. S., "Spectroscopic applications of femtosecond optical frequency combs," *Chem. Soc. Rev.*, vol. 41, pp. 5174–84, 2012.

[303] Hall, F. H. J. and Willitsch, S., "Millikelvin reactive collisions between sympathetically cooled molecular ions and laser-cooled atoms in an ion-atom hybrid trap," *Phys. Rev. Lett.*, vol. 109, p. 233202, 2012.

[304] Poirier, R. a., Peterson, M. R., and Menzinger, M., "An *ab initio* study of the reaction Be(^{3}P) +H_2($^1\Sigma_g^+$) → BeH($^2\Sigma^+$)+H(^{2}S)," *J. Chem. Phys.*, vol. 78, p. 4592, 1983.

[305] Gua, S., Li, G.-Z., and Marshall, A. G., "Effect of ion-neutral collision mechanism on the trapped-ion equation of motion: A new mass spectral line shape for high-mass trapped ions," *Int. J. Mass. Spec. Ion Proc.*, vol. 168, pp. 185–193, 1997.

[306] Gilkison, a. T., Viteri, C. R., and Grant, E. R., "Spectroscopic experiments on autoionization and neutral fragmentation in the high-Rydberg states of BH," *J. Phys.: Conf. Ser.*, vol. 4, pp. 261–266, 2005.

[307] Calmet, X. and Fritzsch, H., "The cosmological evolution of the nucleon mass and the electroweak coupling constants," *Eur.Phys.J*, vol. C24, pp. 639–642, 2002.

[308] Haeffner, H., Roos, C. F., and Blatt, R., "Quantum computing with trapped ions," *Physics Reports*, vol. 469, pp. 155–203, 2008.

[309] Roth, B., Koelemeij, J., Schiller, S., Hilico, L., Karr, J.-p., Korobov, V., and Bakalov, D., "Precision spectroscopy of molecular hydrogen ions: Towards frequency metrology of particle masses," *Lecture Notes in Physics*, vol. 745, pp. 205–232, 2008.

[310] Salomaaf, R. and Stenholm, S., "Two-photon spectroscopy: Effects of a resonant intermediate state," *J. Phys. B: At., Mol., Opt. Phys.*, vol. 8, p. 1795, 1975.

[311] Landa, H., Drewsen, M., Reznik, B., and Retzker, A., "Modes of oscillation in radiofrequency Paul traps," *New J. Phys.*, vol. 14, p. 093023, 2012.

[312] Mokhberi, a. and Willitsch, S., "Sympathetic cooling of molecular ions in a surface-electrode ion trap," *Phys. Rev. A*, vol. 90, p. 023402, 2014.

[313] Weiner, A. M., "Femtosecond optical pulse shaping and processing," *Prog. Quant. Elect.*, vol. 19, pp. 161–237, 1995.

[314] Aikawa, K., Akamatsu, D., Hayashi, M., Oasa, K., Kobayashi, J., Naidon, P., Kishimoto, T., Ueda, M., and Inouye, S., "Coherent transfer of photoassociated molecules into the rovibrational ground state," *Phys. Rev. Lett.*, vol. 105, p. 203001, 2010.

[315] Georgiadis, R. and Armentrout, P. B., "Kinetic energy dependence of the reactions of Ca^+ and Zn^+ with H_2, D_2, and HD. Effect of empty vs full d orbitals," *J. Phys. Chem*, vol. 92, pp. 7060–7067, 1988.

[316] Dantan, A., Marler, J. P., Albert, M., Guénot, D., and Drewsen, M., "Non-invasive vibrational mode spectroscopy of ion Coulomb crystals through resonant collective coupling to an optical cavity field," *Phys. Rev. Lett.*, vol. 105, p. 4, 2010.

[317] Reich, D. M. and Koch, C. P., "Cooling molecular vibrations with shaped laser pulses: Optimal control theory exploiting the timescale between coherent excitation and spontaneous emission," *New J. Phys.*, vol. 15, p. 125028, 2013.

[318] Gerlich, D., "The production and study of ultra-cold molecular ions," in *Low temperatures and cold molecules* (Smith, I., ed.), pp. 295–344, Singapore: World Scientific Publishing Co. Pte. Ltd, 2008.

[319] Schauer, M., Danielson, J., Nguyen, A. T., Wang, L. B., Zhao, X., and Torgerson, J., "Collisional population transfer in trapped Yb^+ ions," *Phys. Rev. A*, vol. 79, p. 062705, 2009.

[320] Wang, J.-h. and Breckenridge, W., "Initial internal energy distributions of ZnH (ZnD) produced in the reaction of Zn(4s4p3P,) with H_2, D_2 AND HD," *Chem. Phys. Lett.*, vol. 123, p. 17, 1986.

[321] Huang, C., Li, W., Kim, M. H., and Suits, A. G., "Two-color reduced-Doppler ion imaging," *J. Chem. Phys.*, vol. 125, p. 121101, 2006.

[322] Bowe, P., Hornekær, L., Brodersen, C., Drewsen, M., Hangst, J. S., and Schiffer, J., "Sympathetic crystallization of trapped ions," *Phys. Rev. Lett.*, vol. 82, pp. 2071–2074, 1999.

[323] Comparat, D., "A Study of molecular cooling via Sisyphus processes," *Phys. Rev. A*, vol. 89, p. 043410, 2014.

[324] Hall, F. H., Eberle, P., Hegi, G., Raoult, M., Aymar, M., Dulieu, O., and Willitsch, S., "Ion-neutral chemistry at ultralow energies: dynamics of reactive collisions between laser-cooled Ca^+ ions and Rb atoms in an ion-atom hybrid trap," *Mol.Phys.*, vol. 111, pp. 2020–2032, 2013.

[325] Dupr, J., Meyer, C., Cedex, O., Fayt, A., and Lele-sadi, M., "Two-photon transitions in 10μm sub-Doppler laser-Stark spectroscopy of CD_3C," *Int. J. Inf. Mill. Wav.*, vol. 8, p. 901, 1987.

[326] Steane, A. M. and Lucas, D. M., "Quantum computing with trapped ions , atoms and light," *Fort. Phys.*, pp. 1–17, 2008.

[327] Staanum, P., Hojbjerre, K., and Drewsen, M., *Sympathetically-Cooled Single Ion Mass Spectrometry.* Boca Raton: Taylor and Francis Group, 2010.

[328] Bethlem, H. L., Kajita, M., Sartakov, B., Meijer, G., and Ubachs, W., "Prospects for precision measurements on ammonia molecules in a fountain," *Euro. Phys. J.: Spec. Top.*, vol. 163, pp. 55–69, 2008.

[329] Simon, A., Jones, W., Ortega, J.-m., Boissel, P., and Ma, P., "Infrared multiphoton dissociation spectroscopy of gas-phase," *J. Am. Chem. Soc.*, pp. 11666–11674, 2004.

[330] Blickensderfer, R. P., Jordan, K. D., Adams, N., and H., B. W., "Complexes of Be $(2s2p^3P,^1P)$and Mg$(3s3p^3P,^1P)$ with H_2. Implications for the Mg(^1P) + H_2 $\rightarrow$ MgH$(^2\Sigma)$+H(^2S) reaction," *J. Phys. Chem*, vol. 86, pp. 1930–1932, 1982.

[331] Ryjkov, V., Zhao, X., and Schuessler, H., "Sympathetic cooling of fullerene ions by laser-cooled Mg^+ ions in a linear RF trap," *Phys. Rev. A*, vol. 74, p. 023401, 2006.

[332] Beloy, K., Kozlov, M. G., Borschevsky, a., Hauser, a. W., Flambaum, V. V., and Schwerdtfeger, P., "Rotational spectrum of the molecular ion NH^+ as a probe for α- and me/mp variation," *Phys. Rev. A*, vol. 83, pp. 1–7, 2011.

[333] Staanum, P., Jensen, I. S., Martinussen, R. G., Voigt, D., and Drewsen, M., "Lifetime measurement of the metastable 3d $^2D_{5/2}$ state in the $^{40}Ca^+$ ion using the shelving technique on a few-ion string," *Phys. Rev. A*, vol. 69, p. 032503, 2004.

[334] Herskind, P. F., Dantan, A., Albert, M., Marler, J. P., and Drewsen, M., "Positioning of the rf potential minimum line of a linear Paul trap with micrometer precision," *J. Phys. B: At. Mol. Opt. Phys.*, vol. 42, p. 154008, 2009.

[335] Lehmann, J. C., "Recent developments in the spectroscopy of small molecules," *Rep. Prog. Phys.*, vol. 41, p. 1610, 1978.

[336] Vogelius, I., Madsen, L., and Drewsen, M., "Rotational cooling of heteronuclear molecular ions with $^1\Sigma$, $^2\Sigma$, $^3\Sigma$, and $^2\Pi$ electronic ground states," *Phys. Rev. A*, vol. 70, p. 053412, 2004.

[337] Chen, K.-m. and Yeung, E. S., "Rovibronic two-photon transitions of symmetric top molecules," *J. Chem. Phys.*, vol. 69, p. 43, 1978.

[338] Klein, R., "*Ab initio* calculations of low lying states of the BH^+ and AlH^+ ions," *J. Chem. Phys.*, vol. 77, p. 3559, 1982.

[339] Schiller, S., Roth, B., Lewen, F., Ricken, O., and Wiedner, M. C., "Ultra-narrow-linewidth continuous-wave THz sources based on multiplier chains," *App. Phys. B*, vol. 95, pp. 55–61, 2008.

[340] Maier, J. P. and Willitsch, S., "Spectroscopy and chemical dynamics," *CHIMIA Int. J. Chem.*, vol. 64, pp. 855–858, 2010.

[341] Bauer, S., Herzberg, G., and Johns, J., "The absorption spectrum of BH and BD in the vacuum ultraviolet," *J. Mol. Spec.*, vol. 13, pp. 25–280, 1964.

[342] Prestage, J. D., Tjoelker, R. L., and Maleki, L., "Atomic clocks and variations of the fine structure constant," *Phys. Rev. Lett.*, vol. 74, p. 3511, 1995.

[343] Okada, K., Wada, M., Takayanagi, T., Ohtani, S., and Schuessler, H. a., "Characterization of ion Coulomb crystals in a linear Paul trap," *Phys. Rev. A*, vol. 81, p. 013420, 2010.

[344] Macke, B. and Legrand, J., "Two photon coherence and pumping in infrared Doppler free molecular spectroscopy," *Opt. Comm.*, vol. 32, p. 174, 1980.

[345] Viteri, C. R., Gilkison, A. T., and Grant, E. R., "Dynamics of dissociative recombination versus electron ejection in single rovibronic resonances of BH," *J. Chem. Phys.*, vol. 126, p. 084301, 2007.

[346] Florez, H. M., Cruz, L. S., Miranda, M. H. G. D., Oliveira, R. A. D., Martinelli, M., and Felinto, D., "Power-broadening-free correlation spectroscopy in cold atoms," *Phys. Rev. A*, vol. 88, p. 033812, 2013.

[347] Viteau, M., Chotia, A., Allegrini, M., Bouloufa, N., Dulieu, O., Comparat, D., and Pillet, P., "Optical pumping and vibrational cooling of molecules," *Science*, vol. 321, pp. 232–4, 2008.

[348] Eichelberger, B. R., Snow, T. P., and Bierbaum, V. M., "Collision rate constants for polarizable ions," *J. Am. Soc. Mass Spec.*, vol. 14, pp. 501–5, 2003.

[349] Wunderlich, C. and Balzer, C., "Quantum measurements and new concepts for experiments with trapped ions," *Adv. At. Mol. Opt. Phys.*, vol. 49, pp. 295–376, 2003.

[350] Lomsadze, B., Fehrenbach, C. W., and DePaola, B. D., "Measurement of ionization in direct frequency comb spectroscopy," *J. App. Phys.*, vol. 113, p. 103105, 2013.

[351] Dooley, P., "Molecular imaging using femtosecond laser pulses," *thesis*.

[352] Allouche, A. R. and Aubert-Frecon, M., "Theoretical study of the low-lying electronic states of the CaLi molecule," *Chem. Phys. Lett.*, vol. 222, pp. 524–528, 1994.

[353] Mulliken, R. S., "The low electronic states of simple heteropolar diatomic molecules. I. General survey," *Phys. Rev.*, vol. 50, pp. 1017–1027, 1936.

[354] Moffitt, W., "Atoms in molecules and crystals," *Proc. Roy. Soc. Lond.. Series A, Math. Phys. Sc.*, vol. 210, pp. 245–268, 1951.

[355] Phillips, J. C., "Ionicity of the chemical bond in crystals," *Rev. Mod. Phys.*, vol. 42, pp. 317–356, 1970.

[356] Roos, C. F., Riebe, M., Häffner, H., Hänsel, W., Benhelm, J., Lancaster, G. P. T., Becher, C., Schmidt-Kaler, F., and Blatt, R., "Control and measurement of three-qubit entangled states.," *Science*, vol. 304, pp. 1478–80, 2004.

[357] Rosenband, T., Schmidt, P., Hume, D., Itano, W. M., Fortier, T., Stalnaker, J., Kim, K., Diddams, S., Koelemeij, J., Bergquist, J., and Wineland, D. J., "Observation of the $^1S_0 - ^3P_0$ Clock Transition in $^{27}Al^+$," *Phys. Rev. Lett.*, vol. 98, p. 220801, 2007.

[358] Wineland, D. J., Monroe, C., Itano, W. M., Leibfried, D., King, B. E., and Meekhof, D. M., "Experimental issues in coherent quantum-state manipulation of trapped atomic ions," *J. Res. Nat. Inst. of St. Tech.*, vol. 103, 1997.

[359] Dalleska, N. F., Crellin, K. C., and Armentrout, P. B., "Reactions of alkaline earth ions with hydrogen, deuterium, and hydrogen deuteride," *J. Phys. Chem.*, vol. 97, pp. 3123–3128, 1993.

[360] Jung, K., Yoshida, T., and Hasegawa, S., "Hydrogen compounds formation of calcium in an ICP-DRC-MS," *J. Anal. At. Spectrom.*, vol. 27, p. 131, 2012.

[361] Margolis, H. S., "Frequency metrology and clocks," *J. Phys. B: At. Mol. Opt. Phys.*, vol. 42, p. 154017, 2009.

[362] Schmidt, T. W. and Sharp, R. G., "The optical spectroscopy of extraterrestrial molecules," *Aust. J. Chem.*, vol. 58, pp. 69–81, 2005.

[363] Maier, J. P., "Approaches to spectroscopic characterization of cations," *Int. J. Mass Spectrom. Ion Process.*, vol. 104, pp. 1–22, 1991.

[364] Korolkov, M. and Paramonov, G., "Vibrationally state-selective electronic excitation of diatomic molecules by ultrashort laser pulses," *Phys. Rev. A*, vol. 57, pp. 4998–5001, 1998.

[365] Brodbelt, J. S. and Wilson, J., "Infrared multiphoton dissociation in quadrupole ion traps," *Mass Spec. Rev.*, vol. 28, pp. 390–424, 2009.

[366] Boesl, U., "Multiphoton excitation and mass-selective ion detection for neutral and ion spectroscopy," *J. Phys. Chem.*, vol. 95, pp. 2949–2962, 1991.

[367] Wessel, J. E. and Syage, J. a., "Excitonic interactions in naphthalene clusters," *J. Phys. Chem.*, vol. 94, pp. 737–747, 1990.

[368] Celii, F. G. and Maier, J. P., "Stimulated-emission pumping spectroscopy of molecular ions," *J. Opt. Soc. Ame. B*, vol. 7, p. 1944, 1990.

[369] Singh, P. C., Shen, L., Kim, M. H., and Suits, A. G., "Photodissociation and photoelectron imaging of molecular ions: probing multisurface and multichannel dynamics," *Chem. Sci.*, vol. 1, p. 552, 2010.

[370] Rohde, F., Almendros, M., Schuck, C., Huwer, J., Hennrich, M., and Eschner, J., "A diode laser stabilization scheme for $^{40}Ca^{+}$ single ion spectroscopy," *J. Phys. B: At. Mol. Opt. Phys.*, vol. 43, p. 115401, 2010.

[371] Blatt, R. and Wineland, D., "Entangled states of trapped atomic ions," *Nature*, vol. 453, p. 1008, 2008.

[372] DeMille, D., "Quantum computation with trapped polar molecules," *Phys. Rev. Lett.*, vol. 88, p. 067901, 2002.

[373] Krems, R., Bretonisch, F., and Stwalley, W. C., *Cold Molecules: Theory, Experiment, Applications*. CRC Press, 2009.

[374] Ghosh, K. P., *Ion Traps*. Oxford University Press, Inc., 1995.

[375] Wang, Y., Gebert, F., Wübbena, J. B., Scharnhorst, N., Amairi, S., Leroux, I. D., Hemmerling, B., Lörch, N., Hammerer, K., and Schmidt, P. O., "Precision spectroscopy by photon-recoil signal amplification," *Nature Comm.*, vol. 5, p. 3096, 2014.

[376] Berkeland, D., "Linear paul trap for strontium ions," *Rev. Sci. Inst.*, vol. 73, p. 2856, 2002.

[377] Nagerl, H. C., Roos, C., Leibfried, D., Rohde, H., Thalhammer, G., Eschner, J., Schmidt-Kaler, F., and Blatt, R., " Investigating a qubit candidate: Spectroscopy on the $S_{1/2}$ to $D_{5/2}$ transition of a trapped calcium ion in a linear Paul trap," *Phys. Rev. A*, vol. 61, 2000.

[378] Tong, X., Winney, A. H., and Willitsch, S., "Sympathetic cooling of molecular ions in selected rotational and vibrational states produced by threshold photoionization," *Phys. Rev. Lett.*, vol. 105, p. 143001, 2010.

[379] Okada, K., Suganuma, T., Furukawa, T., Takayanagi, T., Wada, M., and Schuessler, H. A., "Cold ion polar-molecule reactions studied with a combined Stark-velocity-filter ion-trap apparatus," *Phys. Rev. A*, vol. 87, p. 043427, 2013.

[380] Blythe, P., Roth, B., Fröhlich, U., Wenz, H., and Schiller, S., "Production of ultracold trapped molecular hydrogen ions," *Phys. Rev. Lett.*, vol. 95, p. 183002, 2005.

[381] Boyarkin, O. V., Mercier, S. R., Kamariotis, A., and Rizzo, T. R., "Electronic spectroscopy of cold, protonated tryptophan and tyrosine," *J. Am. Chem. Soc.*, vol. 128, pp. 2816–2817, 2006.

[382] Wübbena, J. B., Amairi, S., Mandel, O., and Schmidt, P. O., "Sympathetic cooling of mixed-species two-ion crystals for precision spectroscopy," *Phys. Rev. A*, vol. 85, p. 043412, 2012.

[383] Shi, M., Herskind, P. F., Drewsen, M., and Chuang, I. L., "Microwave quantum logic spectroscopy and control of molecular ions," *New J. Phys.*, vol. 15, p. 113019, 2013.

[384] Hume, D. B., Chou, C. W., Leibrandt, D. R., Thorpe, M. J., Wineland, D. J., and Rosenband, T., "Trapped-ion state detection through coherent motion," *Phys. Rev. Lett.*, vol. 107, p. 243902, 2011.

[385] Lin, Y.-W., Williams, S., and Odom, B. C., "Resonant few-photon excitation of a single-ion oscillator," *Phys. Rev. A*, vol. 87, p. 011402, 2013.

[386] Loh, H., Cossel, K. C., Grau, M. C., Ni, K.-K., Meyer, E. R., Bohn, J. L., Ye, J., and Cornell, E. A., "Precision spectroscopy of polarized molecules in an ion trap," *Science*, vol. 342, pp. 1220–1222, 2013.

[387] Danzl, J. G., Mark, M. J., Haller, E., Gustavsson, M., Hart, R., Aldegunde, J., Hutson, J. M., and Naegerl, H.-C., "Quantum gas of rovibronic ground-state molecules in an optical lattice," *Nat. Phys.*, vol. 6, pp. 265–270, 2009.

[388] Thompson, R. J., Klipstein, W. M., Seidel, D. J., Kohel, J., and Maleki, L., "The laser cooling and atomic physics (LCAP) program at JPL," *AIP Conf. Proc.*, vol. 504, p. 655, 2000.

[389] Heavner, T. P., "A laser-cooled atomic clock in space," *AIP Conf. Proc.*, vol. 691, pp. 691–694, 2000.

[390] Ye, J., Blatt, S., Boyd, M. M., Foreman, S. M., Hudson, E. R., Ido, T., Lev, B., Ludlow, A. D., Sawyer, B. C., Stuhl, B., and Zelevinsky, T., "Precision measurement based on ultracold atoms and cold molecules," *AIP Conf. Proc.*, vol. 869, pp. 80–91, 2006.

[391] Menotti, C., Lewensteint, M., Lahaye, T., and Pfau, T., *Dipolar interaction in ultra-cold atomic gases*, vol. 970. 2008.

[392] Schowalter, S. J., Chen, K., Rellergert, W. G., Sullivan, S. T., and Hudson, E. R., "An integrated ion trap and time-of-flight mass spectrometer for chemical and photo-reaction dynamics studies," *Rev. Sci. Inst.*, vol. 83, p. 043103, 2012.

[393] Puri, P., Schowalter, S. J., Kotochigova, S., Petrov, A., and Hudson, E. R., "Action spectroscopy of $SrCl^+$ using an integrated ion trap time-of-flight mass spectrometer," *J. Chem. Phys.*, vol. 141, p. 014309, 2014.

[394] Sullivan, S. T., Rellergert, W. G., Kotochigova, S., Chen, K., Schowalter, S. J., and Hudson, E. R., "Trapping molecular ions formed via photo-associative ionization of ultracold atoms," *Phys. Chem. Chem. Phys.*, vol. 13, p. 18859, 2011.

[395] James, D. F. V., "Quantum dynamics of cold trapped ions with application to quantum computation," *App. Phys. B: Las. Opt.*, vol. 66, p. 20, 1997.

[396] Drewsen, M., Jensen, I., Lindballe, J., Nissen, N., Martinussen, R., Mortensen, a., Staanum, P., and Voigt, D., "Ion Coulomb crystals: A tool for studying ion processes," *Int. J. Mass Spec.*, vol. 229, pp. 83–91, 2003.

[397] Itano, W. M., Bergquist, J. C., Bollinger, J. J., and Wineland, D. J., "Cooling methods in ion traps," *Phys. Scripta*, vol. T59, pp. 106–120, 2007.

[398] Herschbach, D., "Molecular collisions, from warm to ultracold," *Faraday Discussions*, vol. 142, pp. 93–111, 2009.

[399] Drewsen, M. and Brøner, a., "Harmonic linear Paul trap: Stability diagram and effective potentials," *Phys. Rev. A*, vol. 62, pp. 1–4, 2000.

[400] Koo, K., Sudbery, J., Segal, D. M., and Thompson, R. C., "Doppler cooling of Ca^+ ions in a Penning trap," *Phys. Rev. A*, vol. 69, p. 043402, 2004.

[401] Marciante, M., Champenois, C., Pedregosa-Gutierrez, J., Calisti, a., and Knoop, M., "Parallel ion strings in linear multipole traps," *Phys. Rev. A*, vol. 83, p. 021404(, 2011.

[402] Stenholm, S., "The semiclassical theory of laser cooling," *Rev. Mod. Phys.*, vol. 58, pp. 699–739, 1986.

[403] Myatt, C. J., Burt, E. A., Ghrist, R. W., Cornell, E. A., and Wieman, C. E., "Production of two overlapping Bose-Einstein condensates by sympathetic cooling," *Phys. Rev. Lett.*, vol. 78, pp. 586–589, 1997.

[404] Truscott, A. G., Strecker, K. E., McAlexander, W. I., Partridge, G. B., and Hulet, R. G., "Observation of Fermi pressure in a gas of trapped atoms," *Science*, vol. 291, pp. 2570–2572, 2001.

[405] Asvany, O., Ricken, O., Müller, H. S. P., Wiedner, M. C., Giesen, T. F., and Schlemmer, S., "High-resolution rotational spectroscopy in a cold ion trap: H_2D^+ and D_2H^+," *Phys. Rev. Lett.*, vol. 100, pp. 13–16, 2008.

[406] Okada, K., Wada, M., Boesten, L., Nakamura, T., Katayama, I., and Ohtani, S., "Acceleration of the chemical reaction of trapped Ca^+ ions with H_2O molecules by laser excitation," *J. Phys. B At. Mol. Opt. Phys.*, vol. 36, pp. 33–46, 2003.

[407] Sheridan, K., Lange, W., and Keller, M., "All-optical ion generation for ion trap loading," *Appl. Phys. B*, vol. 104, pp. 755–761, 2011.

[408] Huang, Y., Liu, P., Bian, W., Guan, H., and Gao, K., "Evaluation of the systematic shifts and absolute frequency measurement of a single Ca^+ ion frequency standard," *Appl. Phys. B*, vol. 114, pp. 189–201, 2014.

[409] Gao, K., "Optical frequency standard based on a single $^{40}Ca^+$," *Chinese Sci. Bull.*, vol. 58, pp. 853–863, 2013.

[410] Wolf, A. L., Van Den Berg, S. A., Gohle, C., Salumbides, E. J., Ubachs, W., and Eikema, K. S. E., "Frequency metrology on the 4s $^2S_{1/2} \leftrightarrow 4p^2P_{1/2}$ transition in $^{40}Ca^+$ for a comparison with quasar data," *Phys. Rev. A*, vol. 78, p. 032511, 2008.

[411] Guan, H., Shao, H., Qian, Y., Huang, Y., Liu, P.-L., Bian, W., Li, C.-B., Sahoo, B. K., and Gao, K.-L., "Combined experimental and theoretical probe of the lifetime of the 3d $^2D_{5/2}$ state in $^{40}Ca^+$," *Phys. Rev. A*, vol. 91, p. 022511, 2015.

[412] Huang, Y., Cao, J., Liu, P., Liang, K., Ou, B., Guan, H., Huang, X., Li, T., and Gao, K., "Hertz-level measurement of the $^{40}Ca^+$ $4s\ ^2S_{1/2}$-$3d\ ^2D_{5/2}$ clock transition frequency with respect to the SI second through the Global Positioning System," *Phys. Rev. A*, vol. 85, p. 030503, 2012.

[413] Safronova, U. I. and Safronova, M. S., "Blackbody radiation shift, multipole polarizabilities, oscillator strengths, lifetimes, hyperfine constants, and excitation energies in Ca^+," *Phys. Rev. A*, vol. 83, p. 012503, 2011.

[414] Wolf, A. L., Van Den Berg, S. A., Ubachs, W., and Eikema, K. S. E., "Direct frequency comb spectroscopy of trapped ions," *Phys. Rev. Lett.*, vol. 102, p. 223901, 2009.

[415] Ramm, M., Pruttivarasin, T., Kokish, M., Talukdar, I., and Häffner, H., "Precision measurement method for branching fractions of excited $P_{1/2}$ states applied to $^{40}Ca^+$," *Phys. Rev. Lett.*, vol. 111, p. 023004, 2013.

[416] Gallagher, A., "Oscillator strengths of Ca II, Sr II, and Ba II," *Phys. Rev.*, vol. 157, pp. 24–30, 1967.

[417] Sahoo, B. K., Das, B. P., and Mukherjee, D., "Relativistic coupled-cluster studies of ionization potentials, lifetimes, and polarizabilities in singly ionized calcium," *Phys. Rev. A*, vol. 79, p. 052511, 2009.

[418] Kjeldsen, H., Folkmann, F., Innocenti, F., Zuin, L., and Hansen, J., "Observation and interpretation of the metastable $3p^6$ 3d Ca^+ ion spectrum in the 3p excitation region," *J. Phys. B At. Mol. Opt. Phys.,*, vol. 35, p. L375, 2002.

[419] Knoop, M., Vedel, M., and Vedel, F., "Lifetime, collisional-quenching and j-mixing of metastable $3D$ levels of Ca^+," *Phys. Rev. A*, vol. 52, pp. 3763–3770, 1995.

[420] Tang, Y. B., Qiao, H. X., Shi, T. Y., and Mitroy, J., "Dynamic polarizabilities for the low-lying states of Ca^+," *Phys. Rev. A*, vol. 87, p. 042517, 2013.

[421] Kreuter, a., Becher, C., Lancaster, G. P. T., Mundt, a. B., Russo, C., Häffner, H., Roos, C., Hänsel, W., Schmidt-Kaler, F., Blatt, R., and Safronova, M. S., "Experimental and theoretical study of the 3d ^{2}D-level lifetimes of $^{40}Ca^+$," *Phys. Rev. A*, vol. 71, p. 032504, 2005.

[422] Champenois, C., Houssin, M., Lisowski, C., Knoop, M., Hagel, G., Vedel, M., and Vedel, F., "Evaluation of the ultimate performances of a Ca^+ single-ion frequency standard," *Phys. Lett. Sect. A Gen. At. Solid State Phys.*, vol. 331, pp. 298–311, 2004.

[423] Gerritsma, R., Kirchmair, G., Zähringer, F., Benhelm, J., Blatt, R., and Roos, C. F., "Precision measurement of the branching fractions of the 4p $^2P_{3/2}$ decay of Ca II," *Eur. Phys. J. D*, vol. 50, pp. 13–19, 2008.

[424] Emmoth, B., Braun, M., Bromanderl, J., and Martinson, I., "Lifetimes of excited levels in Ca I-Ca III," *Phys. Scr.*, vol. 12, pp. 75–79, 1975.

[425] SafronovaU.I. and SafronovaM.S., "Excitation energies, E1, M1, and E2 transition rates, and lifetimes in Ca^+, Sr^+, Cd^+, Ba^+, and Hg^+," *Can. J. Phys.*, vol. 89, pp. 465–472, 2011.

[426] Andersen, T., Desesquelles, J., Jessen, K., and Sørensen, G., "Measurements of atomic lifetimes for neutral and ionized magnesium and calcium," *J. Quant. Spec. Radiat. Transf.*, vol. 10, pp. 1143–1150, 1970.

[427] Lidberg, J., Al-Khalili, A., Norlin, L.-O., Royen, P., Tordoir, X., and Mannervik, S., "Lifetimes of the metastable $3d^2D_{3/2}$ and $3d^2D_{5/2}$ levels in Ca^+ measured by laser probing of a stored ion beam," *J. Phys. B: At. Mol. Opt. Phys.*, vol. 32, pp. 757–767, 1999.

[428] Verner, D. A., Verner, E. M., and Ferland, G., "Atomic data for permitted resonance lines of atoms and ions from H to Si, and S, Ar, Ca and Fe," *At. Dat. Nucl. Dat. Tab.*, vol. 64, pp. 1–180, 1996.

[429] Raizen, M. G., Gilligan, J. M., Bergquist, J. C., Itano, W. M., and Wineland, D. J., "Ionic crystals in a linear Paul trap," *Phys. Rev. A*, vol. 45, pp. 6493–6501, 1992.

[430] Mohr, P. and Taylor, B. N., "Values of fundamental physical constants," in *NIST Reference on Constants, Units, and Uncertainty*, National Institute of Standards and Technology, 2011.